Calibration of a Space - Born Electron Telescope

Report on the calibrations performed with the
SIM 3 experiment of the COSPIN instrument
for the ULYSSES mission

written by

Bernd Iwers

AEG Aktiengesellschaft
Geschaeftsbereich Marine- und Sondertechnik
Fachbereich Raumfahrt
Industriestrasse 29
D-2000 Wedel/Holstein

under Werkvertrag 860232
for project ULYSSES grant
01 ON 078 Pos. 835

TABLE OF CONTENT

LIST OF TABLES

LIST OF FIGURES

1 Introduction

ULYSSES is the first mission, and the only mission in the foreseeable future, that will allow in-situ measurements in regions of the heliosphere far from the ecliptic plane. Never before has a man-made object ventured so far into an unexplored area of the heliosphere. Our knowledge gathered so far about cosmic rays is derived from ground based observations and - since 1957 - from a number of space-born instruments. Although some of these missions have ventured as far 'out' as Pioneer 10 (to a distance from the sun of about R = 40 AU) and as far 'in' as Helios 1 and 2 (as close as 0.29 AU to the sun), all these missions have been confined to a very narrow region of the heliosphere.

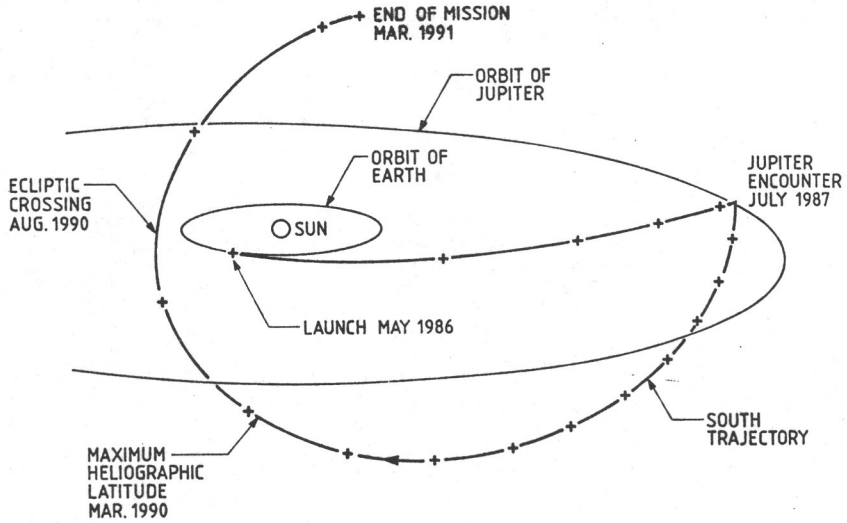

Figure 1-1 Nominal ULYSSES spacecraft trajectory for a launch in May 1986, viewed from 15° above the ecliptic plane. Tick marks are shown at 100-day intervals (Marsden et al., 1986)

With the ULYSSES mission, a first attempt is made to explore the region up to about 80° heliographic latitude. Fig. 1-1 shows a typical ULYSSES trajectory based on the originally planned launch date of May 1986, table 1-1 summarizes a typical time schedule for this launch. Since the Challenger accident of February 1986 and the subsequent halt of all shuttle launch activities, the launch has been postponed to October 1990. Table 1-2 (Marsden et al., 1986) shows a summary of the scientific payload and the prime scientific objectives of the ULYSSES mission.

Table 1-1 Nominal ULYSSES mission time

Event	Average time elapsed(month)	Calendar date
Launch	0	15 May 1986
Jupiter encounter	14	July 1987
First polar pass		
start	43	December 1989
max. latitude	45	February 1990
end	47	April 1990
Ecliptic crossing	49	July 1990
Second polar pass		
start	54	November 1990
max. latitude	56	January 1991
end	58	March 1991
End of mission	58	31 March 1991

The KET (Kiel Electron Telescope) - as part of the COSPIN consortium - is designed to measure electron fluxes in the energy range from 4 to 6000 MeV and to determine energy spectra in the range 8 - 500 MeV. It will also provide proton and α - particle measurements over a wide energy range. It consists of an entrance telescope to define the aperture and of a small light-weight calorimeter to measure electrons, surrounded by an anticoincidence (see chapter 2). Because of the long duration of the ULYSSES mission, careful thoughts have gone into the design of the instrument to assure reliability and continuous performance in the different environments (cruise phase, Jupiter encounter and solar polar phase) and over the complete mission time of almost 5 years.

Severe constraints in the available weight and power resulted in an ultra light-weight electron calorimeter which is nonetheless capable of measuring particles over a wide energy range. The design phase was accompanied by model calculations of the instrument response (Julliot 1980, 1985) to validate the detector and sensor design. After assembly the instrument(s) were calibrated using particles at several accelerators.

The most important aspects of these calibrations were

(1) to determine the response of the individual detectors as a function of particle and energy
(2) to determine the detection threshold of the individual detectors, especially the Cerenkov threshold of C1 and C2 (see chapter 2.2)
(3) to determine the energy thresholds for the coincidence countrate channels
(4) to provide correction tables for the countrate data (response matrix)
(5) to determine the electron detection efficiency of individual countrate channels and the complete instrument as a function of energy
(6) to determine the proton rejection rate for the electron channels
(7) to use the calibration data to verify and adjust the mathematical model of the instrument
(8) to determine the background in the various countrate channels due to the RTG

This report summarizes the calibration activities performed by the KET - group (Universität Kiel, CEN/Saclay and Universita di Milano) and the results of the data evaluation as they are available to date. Chapter 2 contains a brief description of the scientific objectives of the instrument and of the physical characteristics, in chapter 3 the various accelerators are described and a summary of the calibration history is given. Chapter 4 contains the results of the data evaluation as they are available to date, and chapter 5 discusses ways to retrieve the spectral information from the data.

Throughout this document data will be used and results will be quoted from a diploma thesis written, under the supervision by the author of this report, by Holger Sierks (1988) at the Institut für Kernphysik .

Table 1-2 Summary of scientific investigations and associated instrumentation for the ULYSSES spacecraft

Investigation	Principal Investigator	Measurement	Instrumentation
Magnetic Field **(HED)**	A. Balogh Imperial College, London	Spatial and temporal variations of the heliospheric and Jovian magnetic field in the range ±0.01 nT to ±44000 nT	Triaxial vector helium and fluxgate magnetometers
Solar-Wind **(BAM)**	S.J. Bame Los Alamos Nat. Lab.	Solar-wind ions between 257 eV/Q and 35 keV/Q; Solar-wind electrons be - tween 1 eV and 903 eV	Two electrostatic analyzers with channel electron multi- pliers (CEMs)
Solar-Wind Ion Composition **(GLG)**	G. Gloeckler Univ. Maryland J. Geiss Univ. Bern	Elemental and ionic-charge composition, temperature and mean velocity of solar - wind ions for speeds from 145 km/s (H^{+}) to 1352 km/s (Fe^{+8})	Electrostatic analyzer with time-of-flight and energy measurement
Low-Energy Ions and Electrons **(LAN)**	L. Lanzerotti Bell Laboratories	Energetic ions from 50 keV to 5 MeV; electrons from 30 keV to 300 keV	Two sensor heads with five solid state detector telescopes
Energetic-Part. Composition and Interstellar Gas **(KEP)**	E. Keppler MPI Lindau	Composition of energetic ions from 80 keV to 15 MeV/nuc; Interstellar neutral medium	Four solid-state detector telescopes LiF-coated conversion plates with channel electron multi- pliers
Cosmic Rays/ Solar Particles **(SIM)**	J.A. Simpson U. Chicago	Cosmic rays and energetic solar particles in the range 0.3-600 MeV/nuc; Electrons in the range 4-6000 MeV	Five solid-state detector telescopes, one double Cerenkov and semiconductor telescope
Unified Radio and Plasma Waves **(STO)**	R.G. Stone NASA/GSFC	Plasma waves; remote sensing of travelling solar radio bursts, and electron density Electric Field: Plasma waves: 0-60 kHz Radio receiver:1-940 kHz Magnetic Field:10-500 Hz	 72 m radial dipole antenna 7.5 m axial monopole antenna Two-axis search coil
Solar X-rays/ Cosmic Gamma Ray Bursts **(HUS)**	K. Hurley CESR Toulouse M. Sommer MPI Garching	Solar-flare X-rays and cosmic gamma - ray bursts in the energy range 5-150 keV	Two Si solid-state detectors Two CsI scintillation crystals
Cosmic Dust **(GRU)**	E Grün MPI, Heidelberg	Direct measurement of particulate matter in mass range 10^{-16} - 10^{-17} g	Multicoincindence impact detector with channeltron

2 Instrument Description

2.1 Scientific Objectives

The heliosphere is dominated by the radial outflow of the solar wind from the sun. This plasma flow is highly variable in time with high speed flow regions (streams) alternating with low speed streams. As the sun rotates, the high speed streams overtake the slow ones and extended stream-stream interaction regions develop near the ecliptic plane creating a very complex environment for the propagation of solar and galactic cosmic rays. These interactions should decrease with increasing heliographic latitude. Over the solar poles the solar wind flow is expected to be essentially parallel to the radial magnetic field, in contrast to the ecliptic plane where the field is wound in a tight spiral by the solar rotation. The radial field over the poles should provide more direct access for the low energy cosmic rays ($\leq$ 100 MeV/n) to the inner solar system than does the field near the ecliptic. Here the low energy galactic particles (E $\simeq$ 1 MeV) are effectively excluded from reaching the inner part of the heliosphere, the observed fluxes originate primarily from acceleration regions on the sun (flares) and from interplanetary space (shocks).

Until now, most spacecraft observations have been confined to the ecliptic plane and thus to a region from ℓ = +7.25° to ℓ = -7.25° in heliolatitude. The only exceptions are the Pioneer 11 and Voyager 1 spacecrafts, with Pioneer 11 having briefly reached a latitude of ℓ = 16° near R = 4 AU in 1976 (having since returned to latitudes above ℓ = 10° at R > 12 AU since 1982), and Voyager 1 having climbed to latitudes near ℓ = 30° at R > 15 AU following its flyby of Saturn. For relativistic cosmic rays, no significant latitude gradients have been observed from either Pioneer 11 (McKibben et al., 1979; Van Allen, 1980) or Voyager 1 (Decker et al., 1984). For protons in the energy range 30 - 70 MeV, McKibben et al. (1979) reported a marginally significant evidence for a positive (poleward increasing intensity) gradient of about 1%/degree. For the anomalous helium component in the energy range 11 - 70 MeV/n a positive gradient of 2-3%/degree was found with clear evidence. Webber et al. (1979) have found a positive latitude gradient of about 3%/degree for the anomalous oxygen component of 7.1 - 10.6 MeV/n from Voyager 1 data. For electrons no data exists to date.

The most important role for any new mission will therefore be to gather data. At present there is almost a complete lack of information concerning the conditions for modulation of cosmic rays at high latitudes.

The KET (Kiel Electron Telescope) has been specifically designed to measure with sufficient resolution the intensities, anisotropies, and energy spectra of energetic charged particles of galactic, solar, and planetary origin in the energy range of 1 - 2000 MeV/n for heavy particles (protons and alpha) and from 4 - 6000 MeV for electrons. The primary experimental goals of this instrument are to determine for particles of galactic origin (Simpson et al., 1983)

(a) the latitudinal range of shocks and other disturbances of the interplanetary medium which affect the level of modulation observed near the ecliptic plane,
(b) the nucleon/electron ratio as a function of latitude, as a critical diagnostic of the role of drifts in modulation,
(c) the interstellar spectra of electrons, protons, and helium over a large energy range and to measure
(d) the anomalous components as a function of latitude, to determine their region of acceleration and their manner of propagation in the heliosphere.

In addition the instrument will be used - albeit with a low energy resolution - to study

(a) the roles played by coronal vs. interplanetary processes in distributing solar-flare particles throughout the heliosphere,
(b) the roles played by storage, long-term coronal acceleration, and interplanetary acceleration for maintaining the intensity of low-energy particles,
(c) the variation with latitude of Forbush decreases and 27-day recurrent intensity decreases for high-energy particles ($E \simeq 100$ MeV) to determine the three-dimensional structure of shocks and co-rotating interaction regions,

(d) the distribution of jovian electrons with latitude to determine the extent and rapidity of latitudinal propagation in the heliosphere.

2.2 Sensor Description[1]

To reduce weight and complexity of the instrument the KET consists of two separate parts - SIM 3B (sensor) and SIM 3A (electronics compartment). Figure 2-1 shows a cross section of the sensor telescope. The detectors are arranged in the sensor in a way as to form a telescope for the detection of charged particles with the sensor functionally consisting of two parts, (1) an entrance telescope and (2) a calorimeter, surrounded by an anticoincidence plastic scintillator. The telescope has a full opening angle of $\phi = 44°$ for particles with sufficient energy to reach at least the D2 detector, the corresponding geometric factor is $G = 0.73$ cm^{2}sr ($G = 1.46$ cm^{2}sr in those coincidence channels, where particles entering from the rear side are also registered) - see chapter 4.2.2.1. Low energy protons and heavier particles, which do not reach D2, are registered with an auxiliary field of view with a full opening angle of $\phi = 106°$, the corresponding geometric factor is $G = 7.66$ cm^{2}sr. The instrument is mounted on the spacecraft platform to view perpendicular to the spacecraft spin axis (see figure 2-3).

The instrument incorporates several measuring techniques in order to identify the type of particles and their energies

- electron-photon cascades in a shower detector
- Cerenkov threshold
- dE/dx versus E
- discriminator settings.

---

[1] The numbers quoted in this paragraph reflect design criteria. The actual detector dimensions differ between the two instruments (see figure 2-1, figure 2-2 and chapter 4.2.2.1)

2.2.1 Entrance Telescope

The solid state detectors D1 and D2 together with the silica aerogel detector C1 constitute the entrance telescope. The solid state detectors are of the surface barrier type and are both 1 mm thick. Detector D1 has an active area of 750 mm^2, D2 has an active area of 500 mm^2. D2 defines, together with the aperture of the guard counter A, the acceptable entrance cone of the sensor for energetic particles. The third detector in this entrance telescope - C1 - is a cylindrical block of silica aerogel with a diameter of 40 mm and a height of 40 mm. This detector is used to select singly-charged particles of high velocity ($\beta > 0.951$) to discriminate between electrons and protons.

Velocity measurements of high-energy particles are made with Cerenkov detectors. If one wants to use such a detector to distinguish between electrons and protons over a large energy range, a very small value of the refractive index is needed. In the past only Cerenkov detectors using gas under pressure have been available, for a space born instrument such a detector would require a large amount of weight for the necessary pressure container and the gas supply and would require the use of thin and fragile windows to reduce the amount of mass in the acceptance cone of the instrument. Cantin et al. (1974) first described the use of aerogels of silica as a Cerenkov detector having refractive indices ranging from 1.01 to 1.10. The refractive index is a direct function of the density of the material and can be approximated by

$$d \simeq 4(n-1) \ [g/cm^3] \ \text{(Bourdinand et al., 1976).}$$

If the density is too low, the material becomes too brittle and fragile and is impossible to handle.

In the KET sensor the block of aerogel is placed in a diffusive box with the walls of the box covered by three layers (thickness $\simeq$ 450 µm) of white reflective material (Millipore[2]) and is viewed through a hole in the guard counter A by a high-sensitivity photomultiplier with a 1.5-inch photocathode. Al-

---

2 Millipore is a registered trademark of the Millipore Corporation

though the number of photoelectrons produced by silica aerogel of refractive index n = 1.055 in the range of the visible light is $n_e \simeq 100$ photons/cm, the overall yield of a diffusive box solution is rather low. This is mostly due to a substantial self-absorption of light inside the aerogel and the fact, that only a fraction of total light produced in the diffusive box is actually seen by the photocathode. Carlson et al. (1978) use the following formula to estimate the number of photoelectrons detected

$$n_e = \frac{n^2 - 1}{n^2} \, LK \, \frac{\varepsilon}{1-\eta(1-\varepsilon)}$$

where

- n_e : number of detected photoelectrons
- n : refractive index of the radiator medium, $n \simeq 1.05 - 1.06$
- L : particle trajectory length in the radiator medium, $L = 4$ cm
- K : constant describing the light collection efficiency of the arrangement. This constant depends on the self-absorption in the aerogel and the quantum efficiency of the photocathode. For a photomultiplier with a quantum efficiency $Q \simeq 20\%$ and a silica block of 4 cm thickness, K is approximately in the range, $K \simeq 35 - 42$
- ε : ratio of the photocathode area to the total internal area of the diffusive box used in KET for C1, $\varepsilon \simeq 0.08$
- η : reflection coefficient of the diffusive material (Millipore), $0.9 < \eta < 0.96$

Using these values and the expression given above one can compute the number of photoelectrons to be

$$6 < n_e < 12$$

in fairly good agreement with a value of 6-8 photoelectrons derived from measurements of μ-mesons.

To prevent particles from hitting the photomultiplier surface directly and thus simulating an aerogel detector response, a thin plastic scintillator S1 is directly coupled to the surface of PM1. A singly-charged minimum ionizing particle will give a discriminator signal in S1 a value of $6 \cdot \sigma$ above the signature of a relativistic alpha particle in C1.

2.2.2 The Calorimeter

The lead fluoride (PbF_2) Cerenkov detector C2 and the plastic scintillator S2 (NE 104) constitute the calorimeter part of the KET sensor. PbF_2 is a Cerenkov radiation emitting material with no detectable scintillation component in its radiation. During the design phase several materials were considered:

(a) Cerenkov detector versus anorganic scintillator (e.g. CsI). A scintillating material would be much more sensitive to the background radiation coming from the RTG, thus causing a very high count rate in this channel and reducing the life-time (fraction of time, during which the instrument is not busy and can detect wanted particles) of the instrument. Although a Cerenkov detector produces much less photons than a scintillator, it is much less sensitive to the γ-ray background of the RTG.

(b) Lead fluoride versus lead glass. Table 2-1 summarizes the physical properties of these materials. To cover the desired energy range for electrons, a detector having 2.5 radiation length was considered necessary for the instrument. Although PbF_2 is much more difficult to machine and is very brittle, a lead glass detector with the same radiation length would have been almost twice as large and about 50% heavier.

The conical shape of this detector is optimized for maximum light output. All sides of this detector are highly polished to use the effect of total internal reflection to increase light output. Light, which has left the detector at the conical side walls and the top, is scattered back into the crystal by the reflective material (Millipore) covering the inside walls of the C2 housing. The Cerenkov light of C2 is viewed through a hole in the S2 using a diffusive box design. The inside walls of this diffusive box are also covered with three layers of Millipore giving a coefficient of reflection of $k \simeq 0.96$. The light collection efficiency of the diffusive box is approx. 28% resulting, together with the quantum efficiency of the PM2 photocathode of $Q_E = 20\%$, in a signal for minimum ionizing heavy particles equivalent to $n_e = 16 - 20$ photoelectrons. The height of C2 is 22 mm giving a radiation length $r = 2.6$.

For low energy electrons entering C2 the ensueing electron-photon shower is completely absorbed in the detector. With increasing electron energies the shower is not fully absorbed in C2 anymore. The cup-shaped scintillator S2 is used to discriminate between particles and showers completely absorbed in C2 (absorption mode) and others which leave C2 (penetration mode). The shape of S2 has been optimized for light collection and uniformity and to allow for the detector to be viewed by only one small 1-inch photomultiplier. The surface of this scintillator has been highly polished to aid the total internal reflection of the photons. Only the edges have been covered with reflective paint to minimize light losses, the guard detector A has been surface treated the same way. The photomultipliers PM3 and PM4 are directly coupled to the scintillators with a thin layer of RTV[3] (silicon rubber) which is in adhesive contact to both the photocathode window and the scintillator surface.

Table 2-1 Physical properties of PbF_2 and Lead Glass

	Lead Fluoride	Lead Glass
Composition	100% PbF_2	31% SiO_2 65% PbO 3% K_2O 1% Sb_2O_3 + As_2O_3
Density	7.77 g/cm^3	5.1 g/cm^3
Refractive Index	1.78	1.81
<Z/A>	0.4078	0.4359
<I>	579.3 eV	362.3 eV
Radiation Length	0.85 cm	1.56 cm

[3] Rhodorsil RTV 141 is a two-component silicon rubber manufactured by Rhone-Poulenc Industries, Department Silicones.

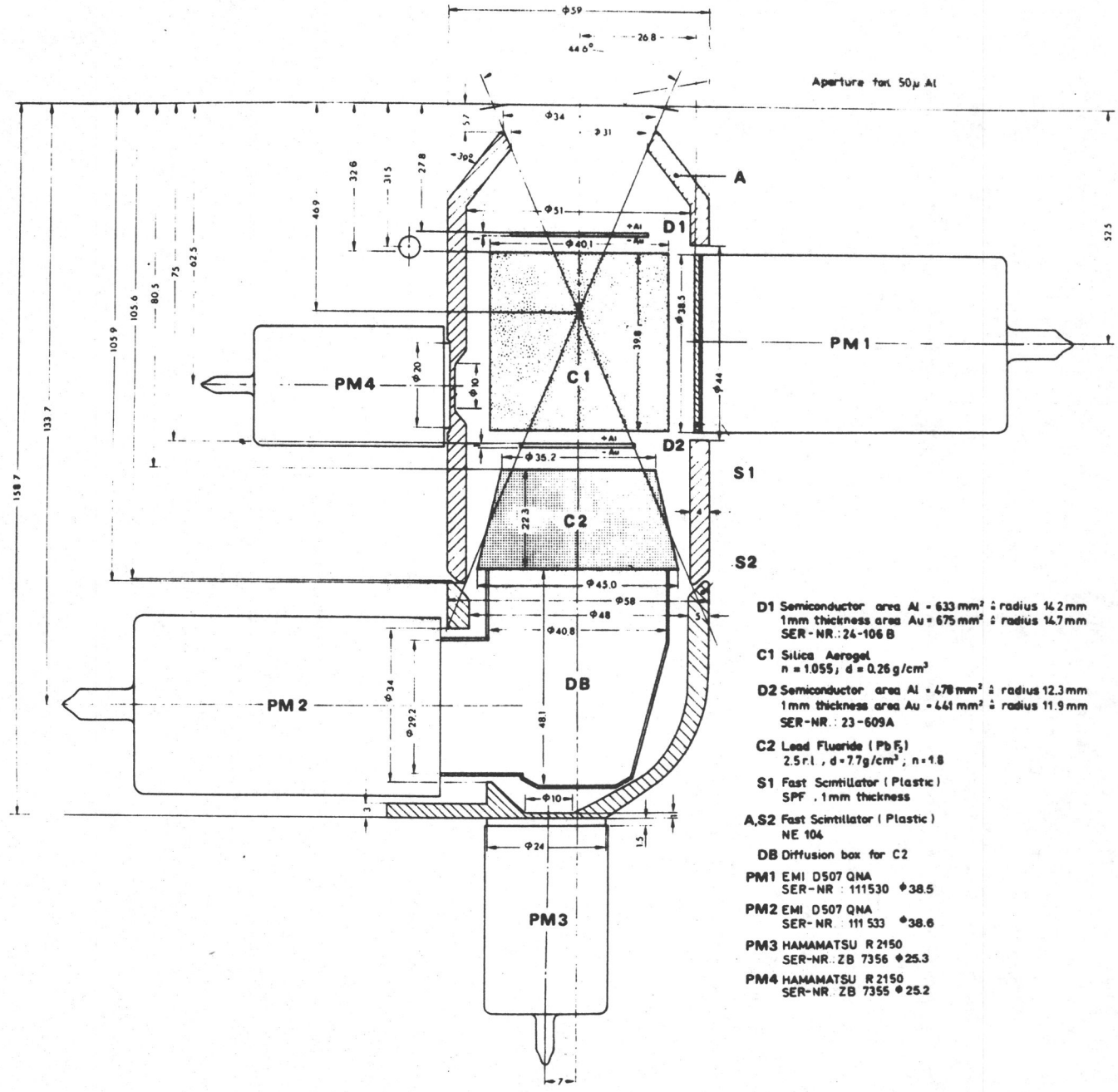

Figure 2-1 Detailed cross section of the KET - SFM sensor

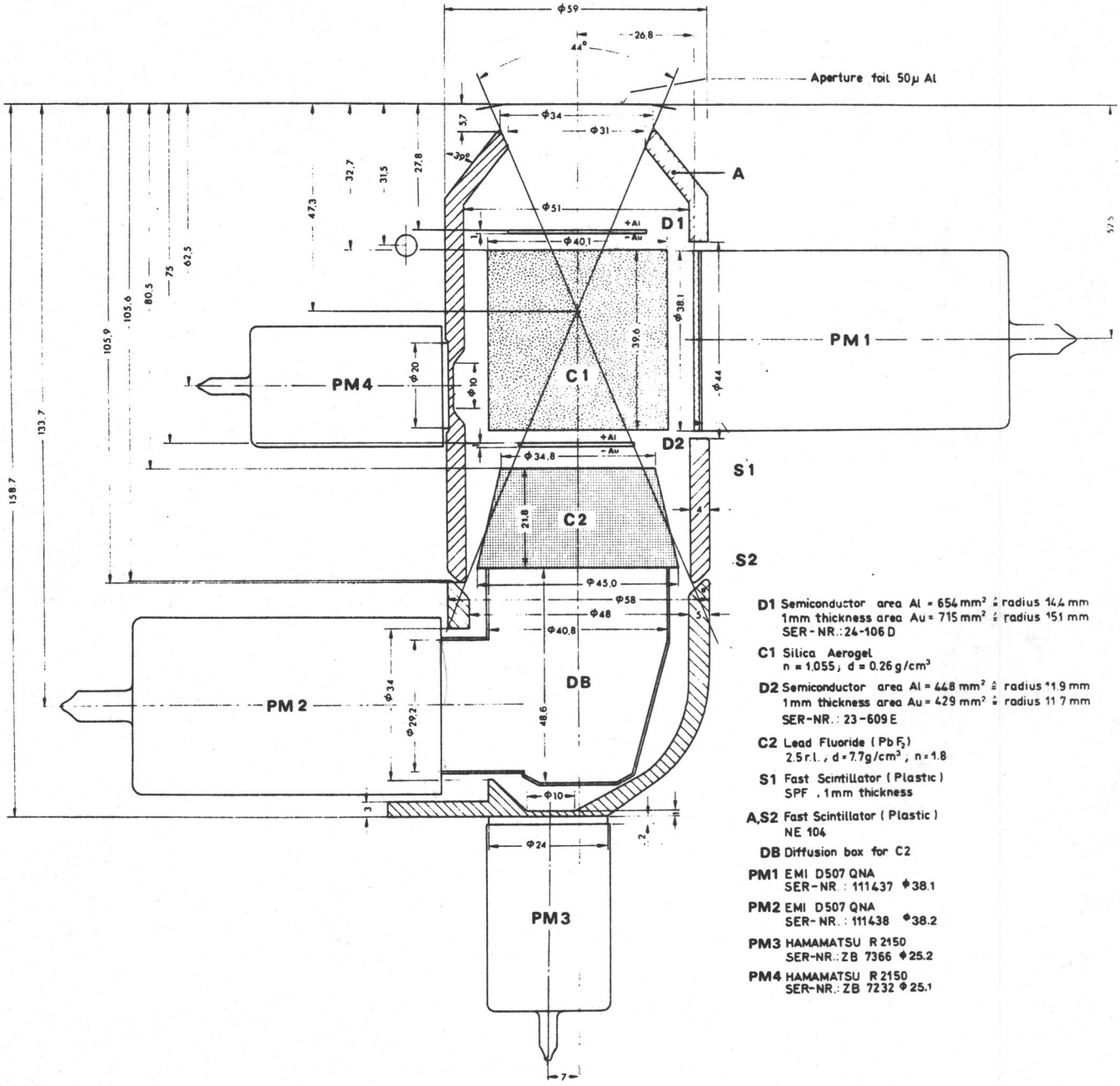

Figure 2-2 Detailed cross section of the KET - SFS sensor

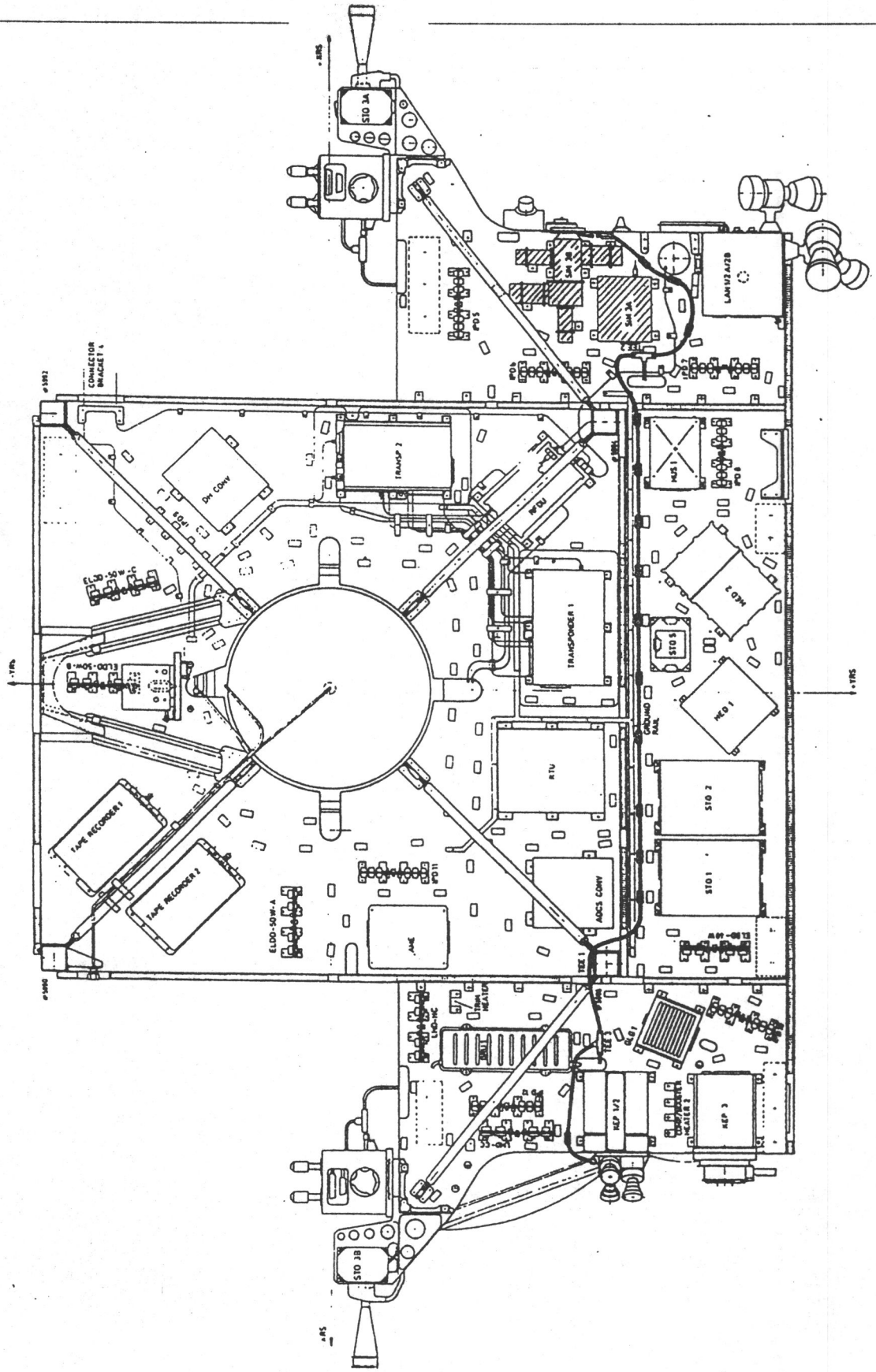

Figure 2-3 Location of SIM3 A and B on the spacecraft platform (ESA ISPM-PG-0132, Experiment Interface Document)

2.3 Analog Electronics

Fig. 2-4 shows a functional block diagram of the KET electronic. The purpose of the on-board electronics is to

(1) amplify the weak detector/photomultiplier signals,
(2) perform a pulse shaping function to reduce noise,
(3) count with small and known deadtime
- the rates of events exceeding the lowest threshold for the individual detectors,
- the rate of certain coincidence events meeting predetermined threshold and coincidence requirements,
- the rate of two selected event types in eight sector counters per S/C spin period,

(4) perform an analysis of the pulse height (amount of charge created) in each detector with sufficient resolution,
(5) provide a sequence of test pulses to the charge sensitive preamplifiers,
(6) provide the high voltages required for solid-state detector and photomultiplier operation,
(7) accumulate and format the rates and pulse-height information for transmittal to the COSPIN DPU,
(8) measure eight housekeeping informations to monitor performance of the instrument and to
(9) provide the electrical command, data, housekeeping, and power interface to the COSPIN DPU.

The electronic is functionally divided into two parts, (1) the analog electronics on six printed circuit boards and (2) the digital electronic on two boards.

The signals created by the passage of energetic charged particle in the six detectors/photomultipliers are fed via coaxial cables into associated charge sensitive preamplifiers (CSAs). Filter networks in each amplifier chain are used to limit the bandwidth of the signals (to reduce noise) and to form the CSA output pulses ('tail-pulse' with a rise time of 20 ns and a decay time of

60 µs) into bipolar pulses. After passage through the filter network the signals are split up into the discriminator branch and the PHA branch. Thirteen 'Zero-Crossing' amplitude discriminators provide input to a strobed coincidence network to determine the occurrence of any of fourteen types of coincidences (table 2-2). The zero-crossing technique makes the discrimination time independent of the pulse-height, so the strobe signal can have a short, fixed delay relative to the leading edge of the first contributing pulse resulting in a 'coincidence window' of less than 1 µs.

Table 2-3 shows the threshold parameters for all 13 thresholds for the Selected Flight Model (SFM), table 2-4 shows the same data for the Selected Flight Spare (SFS) model. The coincidence logic requires approx. 3 µs to test an 'event' for validity. In case a valid coincidence condition is detected, one of 14 prescalers is incremented and a PHA-start signal is generated which enables the peakdetectors (sample and hold circuit) and starts the pulse-height analysis cycle. An analog multiplexer connects the peakdetectors to a single 8-bit Analog Digital Converter (ADC) with a switchable time constant to account for the different dynamic ranges of the detector signals. These ranges have been set to correspond to the useful detector signal ranges and their energy resolution, and are : 1 - 2000 for the solid-state detectors D1 and D2, and 1 - 300 for the optical detectors C1, C2, and S2 of which only 1 - 200 is used for the C1. The A detector is used only in anticoincidence, the signal is therefore not pulse-height analyzed. A failure-mode reconfiguration circuit allows to logically disable any threshold in the coincidence logic (see below). This is necessary to account for noisy or dead detectors and to keep the instrument working, however, with reduced scientific output.

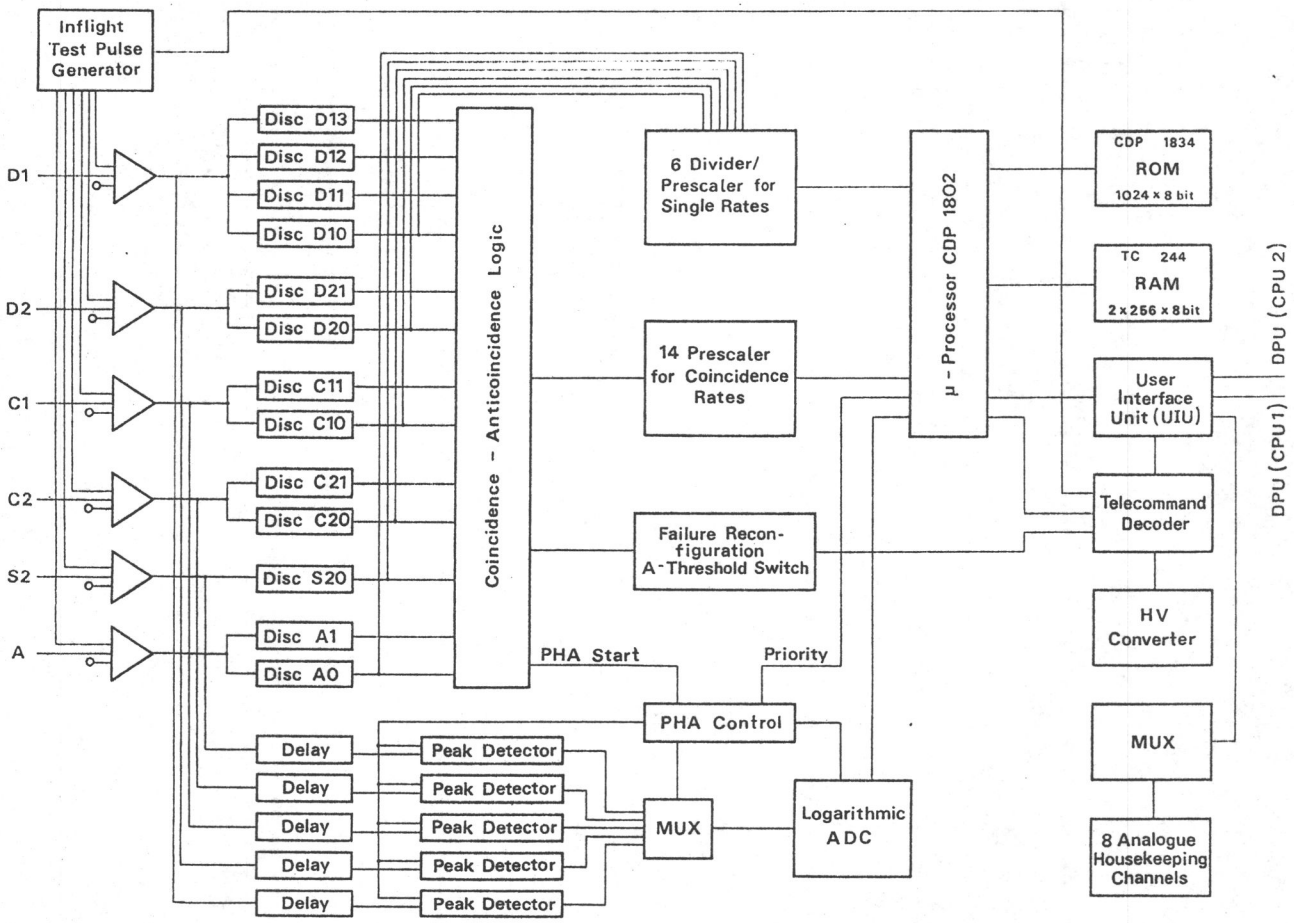

Figure 2-4 KET electronics functional block diagram

Table 2-2 KET - SFM countrate channels and coincidence conditions

Channel Acronym	Particle Type	Energy Range [MeV/nuc]	Coincidence Condition
P1	Proton	2.7 - 5.4	D11$\overline{\text{D12C10D20C20S20A0}}$
	Proton	23.1 - 34.1	
	Alpha	2.3 - 2.7	
P4	Proton	5.4 - 23.1	D12$\overline{\text{D13C10D20C20S20A0}}$
	Alpha	2.7 - 6.0	
	Alpha	20.4 - 34.2	
P32	Proton	34.1 - 116	D11$\overline{\text{D12C10D20C20S20A0}}$
P116	Proton	116 - 190	D10$\overline{\text{D12C10D20C20S20A0}}$
	Alpha	126 - 190	
P190	Proton	190 - 1880	D10$\overline{\text{D11C10D20D21C20C21S20A0}}$
P4000	Proton	> 1880	D10$\overline{\text{D11C10C11D20D21C20C21S20A0}}$
A4	Alpha	6.0 - 20.4	D13$\overline{\text{C10D20C20S20A0}}$
A32	Alpha	34.2 - 116	D12$\overline{\text{D13C10D21C20S20A0}}$
A116	Alpha	116 - 126	D12$\overline{\text{D13C10D21C20S20A0}}$
A190	Alpha	190 - 1880	D11$\overline{\text{D12C10D21C20S20A0}}$
A4000	Alpha	> 1880	D11$\overline{\text{D12C10C11D21C20S20A0}}$
E4	Electron	4 - 9	D10$\overline{\text{D11C10C11D20D21C20S20A0}}$
E12	Electron	9 - 500	D10$\overline{\text{D11C10C11D20D21C20S20A0}}$
E300	Electron	> 500	D10$\overline{\text{D11C10C11D20D21C20S20A0}}$/$\overline{\text{A1}}$

Table 2-3 KET - SFM discriminator thresholds

Channel	Level	U [mV]	PHA Ch. No.	Q [pAs]	E [MeV]	Nph
D1	q_{min}	2.10	-	.005	.110	-
	D10	3.46	18	.00824	.185	-
	D11	20.36	82	.0485	1.089	-
	D12	86.82	130	.207	4.643	-
	D13	394.16	181	.938	21.081	-
	q_{max}	4202.0	-	10.0	224.5	-
D2	q_{min}	2.00	-	.005	.112	-
	D20	3.38	31	.00845	.190	-
	D21	19.43	84	.0486	1.092	-
	q_{max}	3997.0	-	10.0	224.7	-
C1	q_{min}	10.96	-	.024	-	1.0
	C10	23.38	62	.0512	-	2.2
	C11	681.35	211	1.492	-	63.8
	q_{max}	2192.0	-	4.8	-	205.0
C2	q_{min}	20.0	-	.048	-	2.2
	C20	33.19	24	.0797	-	3.7
	C21	713.65	168	1.712	-	79.8
	q_{max}	6003.0	-	14.4	-	671.0
S2	q_{min}	20.5	-	.05	-	10.5
	S20	101.03	28	.247	-	51.7
	q_{max}	6135.0	-	15.0	-	3140.0
A	q_{min}	41.3	-	.0992	-	16.0
	A0	65.42	-	.157	-	25.2
	A1	1311.22	-	3.147	-	505.0
	q_{max}	2066.0	-	4.96	-	796.0

U = Amplitude of test-signal on CSA test input
PHA-Ch. = Result of analog-to-digital conversion of the test signal
Q = Charge (in pAs) equivalent to the test signal on CSA test input
E = Energy deposited in D1 and D2 equivalent to Q
Nph = Number of photoelectrons created at the photocathode equivalent to Q

Table 2-4 KET - SFS discriminator thresholds

Channel	Level	U [mV]	PHA Ch. No.	Q [pAs]	E [MeV]	Nph
D1	q_{min}	1.94	-	.005	.112	-
	D10	3.13	31	.0081	.181	-
	D11	18.54	85	.0478	1.075	-
	D12	82.80	133	.214	4.801	-
	D13	373.60	183	.964	21.660	-
	q_{max}	3875.0	-	10.0	224.7	-
D2	q_{min}	1.89	-	.005	.112	-
	D20	2.97	29	.00784	.176	-
	D21	18.28	84	.0483	1.085	-
	q_{max}	3785.0	-	10.0	224.6	-
C1	q_{min}	9.40	-	.024	-	0.7
	C10	20.02	61	.0511	-	1.5
	C11	603.23	212	1.538	-	54.9
	q_{max}	1883.0	-	4.8	-	171.0
C2	q_{min}	19.3	-	.048	-	0.9
	C20	25.23	24	.0626	-	1.2
	C21	687.77	168	1.706	-	33.1
	q_{max}	5805.0	-	14.4	-	279.0
S2	q_{min}	20.0	-	.05	-	14.5
	S20	61.66	25	.154	-	44.7
	q_{max}	6006.0	-	15.0	-	4354.0
A	q_{min}	39.5	-	.0992	-	14.0
	A0	60.94	-	.153	-	21.8
	A1	1263.44	-	3.159	-	450.2
	q_{max}	1984.0	-	4.96	-	707.0

U = Amplitude of test-signal on CSA test input
PHA-Ch. = Result of analog-to-digital conversion of the test signal
Q = Charge (in pAs) equivalent to the test signal on CSA test input
E = Energy deposited in D1 and D2 equivalent to Q
Nph = Number of photoelectrons created at the photocathode equivalent to Q

2.4 Digital Electronics

A microprocessor (µP) RCA CDP 1802 controls the internal data flow and I/O processing in the KET instrument. It is used to control the rate accumulation, to store the PHA data, to format and finally to send the scientific data to the COSPIN Data Processing Unit (DPU) via the User Interface Unit (UIU). To reduce the amount of hardware required for the 34 individual count rates, a mixed hardware/software solution has been used in the instrument.

- The signals of the lowest thresholds of all detectors are counted in dedicated hardware counters. These counters are read by the µP every 16 ms and accumulated in RAM memory.

- The coincidence rates are handled differently. A single 256x8 bit RAM is used as a prescaler. The coincidence logic creates an address for each valid event upon recognition, the RAM-byte corresponding to this address is then incremented by 1. The bytes pointing to the energy channels P1, P4, P190, P4000, A4, E4, and E12 are transferred to the µP every 16 ms, the content of the prescaler is added to the existing content of the scaler in the main memory (24 bit). For the channels P116, A32, A116, A190, A4000, and E300 no accumulation is performed. To account for the possible high fluxes in channel P1, the µP checks the carry bit of this counter every 1.6 ms and adds 255 to the P1 scaler if the carry bit was set.

In addition to the rates, up to 20 PHA-words will be stored per accumulation period (128 s average in tracking mode). A PHA-word (40 bit) consists of 4 out of 5 possible PHA results (4x8 bit), the remaining 8 bit contain the coincidence type information (4 bit), sector information for channel E4 (3 bit), and the priority flag (1 bit). In case 20 PHA events are already stored in memory, the µP switches to the next higher priority level. If another event is registered with a priority equal or higher than that of an already existing event, the new event replaces a previously stored event in memory. Up to a maximum number of ten events with higher priority can replace existing events. Table 2-5 gives the priority scheme for all coincidence channels.

Table 2-5 KET instrument PHA priority scheme

Priority Level	Coincidence Rate
0	P190, P4000, A190
1	P32, P116, A32, A116, A4000, E4
2	E300
3	E12

Fourteen telecommands are used to command the KET instrument, table 2-6 summarizes these commands. The failure mode telecommands allow to reconfiger the coincidence logic in case of a catastrophic detector failure or a failure in a discriminator circuit. Two types of failures are possible:

i) discriminator or detector are inoperative
ii) detector has become noisy and triggers the discriminator at a high frequency.

Both cases can be monitored on ground by checking the single detector rates. In case (i) all coincident data requiring this discriminator would be lost, in case (ii) an unacceptably large deadtime would be introduced in the coincidence logic. After the µP has received a failure mode command, two things happen:

i) the threshold is removed from the strobe generation,
ii) whenever an event is detected, a threshold signal is either generated or not depending on the type of event. Table 2-7 summarizes the effect of failure mode settings on the coincidence logic.

Table 2-6 KET telecommands

Telecommandbit							OFF/ON	Function
X	0	0	1	0	0	0	0/1	FM1 -D1-
X	0	0	1	0	0	1	0/1	FM2 -D2-
X	0	0	1	0	1	0	0/1	FM3 -C1-
X	0	0	1	0	1	1	0/1	FM4 -C2-
X	0	0	1	1	0	0	0/1	FM5 -S2-
X	0	0	1	1	0	1	0/1	FM6 -A-
X	0	0	0	0	0	0	0/1	A1
X	0	0	0	0	0	1	0/1	HV1
X	0	0	0	0	1	0	0/1	HV2
X	0	0	0	0	1	1	0/1	+ 10 V
X	0	1	0	X	0	0	0	HV2 - Step 0
					•	•	•	
X	0	1	0	X	1	1	1	HV2 - Step 7
X	1	0	0	X	X	X	X	Reset FM
X	1	0	1	X	X	X	0/1	IFTG
X	1	1	0	X	X	X	X	Reset µP

Also part of the electronics compartment is the HV - generator which supplies the voltage needed by the surface barrier detectors D1 and D2 and the photomultipliers PM1 through PM4. These voltages have to be switched on and off by separate telecommands, they do not rise with the normal switch-on procedure of the instrument. As a provision against aging of the photomultipliers or degradation of the optical detectors due to irradiation in the jovian environment, the HV can be set to any of 8 levels by telecommand. Nominal operating voltage is at step 2, the voltage can be adjusted upwards by as much as 40% and downwards by 10%.

To test the function of the instrument electronics, an In-Flight-Test-Generator (IFTG) can be switched on by telecommand. This IFTG circuit feeds a predefined sequence of test pulses to the CSA test inputs. This IFTG can perform a functional test only, no in-flight calibration can be performed.

Table 2-7 Effect of the FM-setting on the coincidence logic

Failure Mode	Effect
FM1	D10 is generated for all event types
FM2	D20 is generated for all event types
FM3	C10 is generated for P190, P4000, A190, A4000, E4, E12, E300
	$\overline{C10}$ is generated for P1, P4, P32, P116, A4, A32, A116
FM4	C20 is generated for P116, P190, P4000, A116, A190, A4000, E4, E12, E300
	$\overline{C20}$ is generated for P1, P4, P32, A4, A32
FM5	$\overline{S20}$ is generated for all event types
FM6	$\overline{A0}$ is generated for all event types

3 Calibration

To fully understand the data returned by a space born charged particle telescope requires complete knowledge of all instrument responses to all kinds of charged particles. This is particularly true for an instrument which is part of a mission to fly into so far unexplored regions of the heliosphere. It is not sufficient to just model the instrument response and calculate key parameters, the experimenter has to subject the instrument to the very kind of particles it will measure later in space. The calibration effort required to fully evaluate the response of the KET instrument to charged particles goes beyond that of conventional (dE/dx-E mode) charged particle detectors.

The instrument is primarily designed to measure electrons using a Cerenkov radiation emitting calorimetric detector, so the main emphasis during calibration was put on subjecting the instrument to as many electron energies as possible to determine the calorimeter signal and the efficiency of the detector assembly as a function of energy. To cover the wide range of energies, we went to three electron accelerators and one proton accelerator (see chapter 3.2). Time did not permit further calibration of the instrument, but the data collected should be sufficient to predict the instrument response and to interpret the flight data. The task of evaluating the data has just begun, some key parameters have been determined already but more work has yet to go into the detailed analysis especially with respect to energy spectrum retrieval and creation of response matrices for isotropically incident radiation (using the measurements of the instrument response as a function of the angle of incidence, i.e. the angle between the beam axis and the optical axis of the instrument). For a good calibration it is necessary to have beams with well defined energies containing only one kind of particle. Beams at high energy facilities contain, however, usually a number of parasitic particles like pions (Π) and μ-mesons, which are not found in space. These particles cannot always be easily identified from the data (or excluded from the beam by a trigger condition). In addition, unknown background radiation coming from the main beam structure, the targets, the extracted beam, the deflecting magnets, the beam halo, and the beam stops influence the instrument performance and restrict the data quality.

3.1 Calibration Set-Up

High energy accelerator facilities do not provide means to set up an instrument in vacuum due to the negligible energy loss the particles suffer in air and due to the fact, that the usual equipment is very large and does not require vacuum to operate. As a consequence, the beam location is usually not well defined. In most test areas the beam is only defined by two 'points', the beam window, a foil covering the end of the vacuum tube with a diameter of typical 10 - 20 cm, and the approximate location of the beam stop, which is usually some 10 m away from the beam window. The beam itself is frequently also not well defined, the cross section is very often not point-like but rather large and sometimes even elliptical. The cross section in the focal point of the proton beam at CERN for example was approx. 150 mm horizontally and approx. 40 mm vertically, with this area being defined by the points where the intensity had dropped from maximum in the center to a value of 1/e. Thus, placing an instrument with a full aperture opening of 31 mm into the center of the beam was a difficult task and consisted of two steps:

1) Find the geometrical location of the beam axis in the test area using the beam window and beam stop and set up a table in this location.
2) With the KET placed on the table search for the center of the beam by horizontal and vertical displacement of the table surface. Beam center is defined as the maximum ratio of KET counts to the counts of a fixed beam monitor.

To adjust the intensity of the beam and to restrict the beam diameter, lead collimators were used during most runs. These collimators increase the number of background particles, however, due to particle interaction on the inner walls of the collimator. The accelerator conditions - beam intensity and beam location vary with energy and machine condition - were not stable enough to make useful measurements without the use of collimators.

The KET was mounted on a platform allowing the instrument to be turned around the center of the aperture with a resolution of 1° for measurements of the instrument response as a function of the angle of incidence. The orientation of

the instrument axis to the beam axis for the angular measurements and the direction of displacement of the instrument axis with respect to the beam axis can be seen in figure 3-1.

To protect the KET against the unclean environment in the test areas, the instrument was kept in the Perspex transport box under constant dry nitrogen purge. To reduce particle scatter from the box walls, a foil covered window had been cut into the wall facing the aperture. The instrument was connected to the DPU-Simulator and the Remote Interface Unit (RIU). A set of 30 m long coax cables connected the RIU to the GSE in the experimenters area.

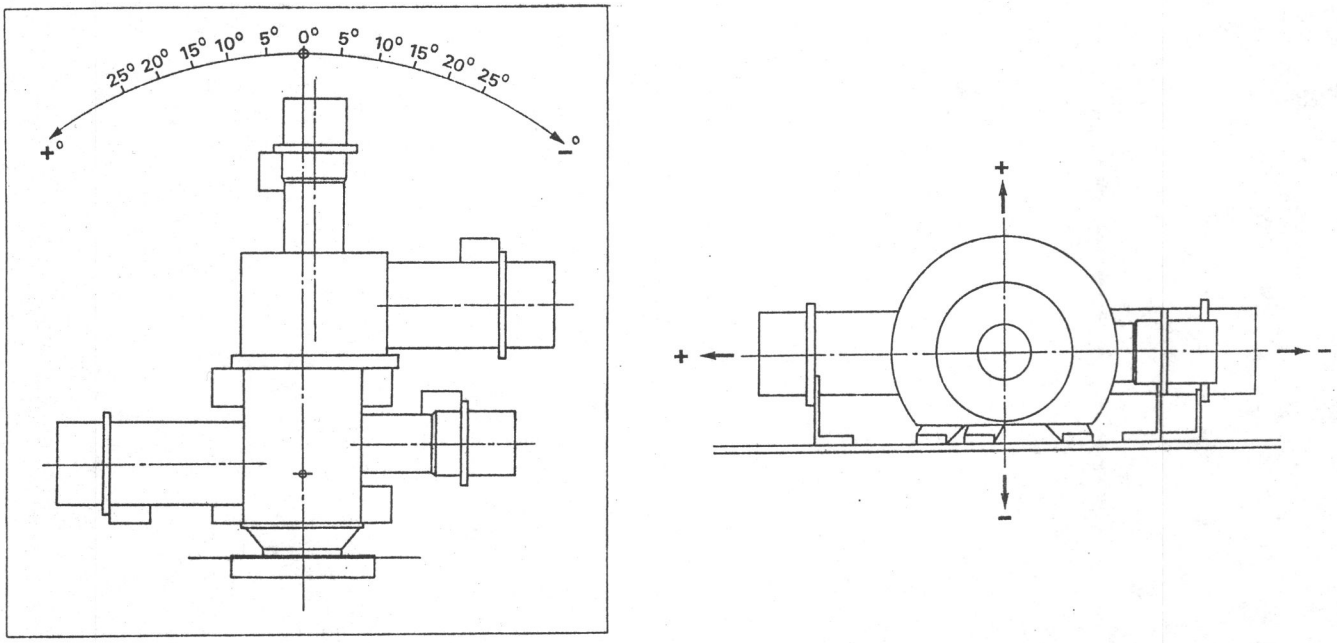

Figure 3-1 KET sensor axis and beam axis orientation during angular and displacement measurements

To monitor the beam intensity, a pair of crossed plastic scintillation detectors of size 1x1 cm^2 was placed in front of the KET. The photomultiplier signals were wired together in a coincidence unit and the number of coincidences counted to provide a beam reference for the KET count rates. Figure 3-2 shows a typical arrangement for these monitor detectors at the Universität Bonn ac

celerator. In an attempt to measure the electron detection efficiency of the KET, the coincidence signal was connected to the C1 test input for several runs, replacing the C1 detector signal. This method yielded useful results for electron energies above 500 MeV (see chapter 4.2.3), the amount of scatter introduced by these scintillation detectors at low energies resulted in too low efficiency values. Thus, at the very low energies at the ORME accelerator these beam monitors were not used.

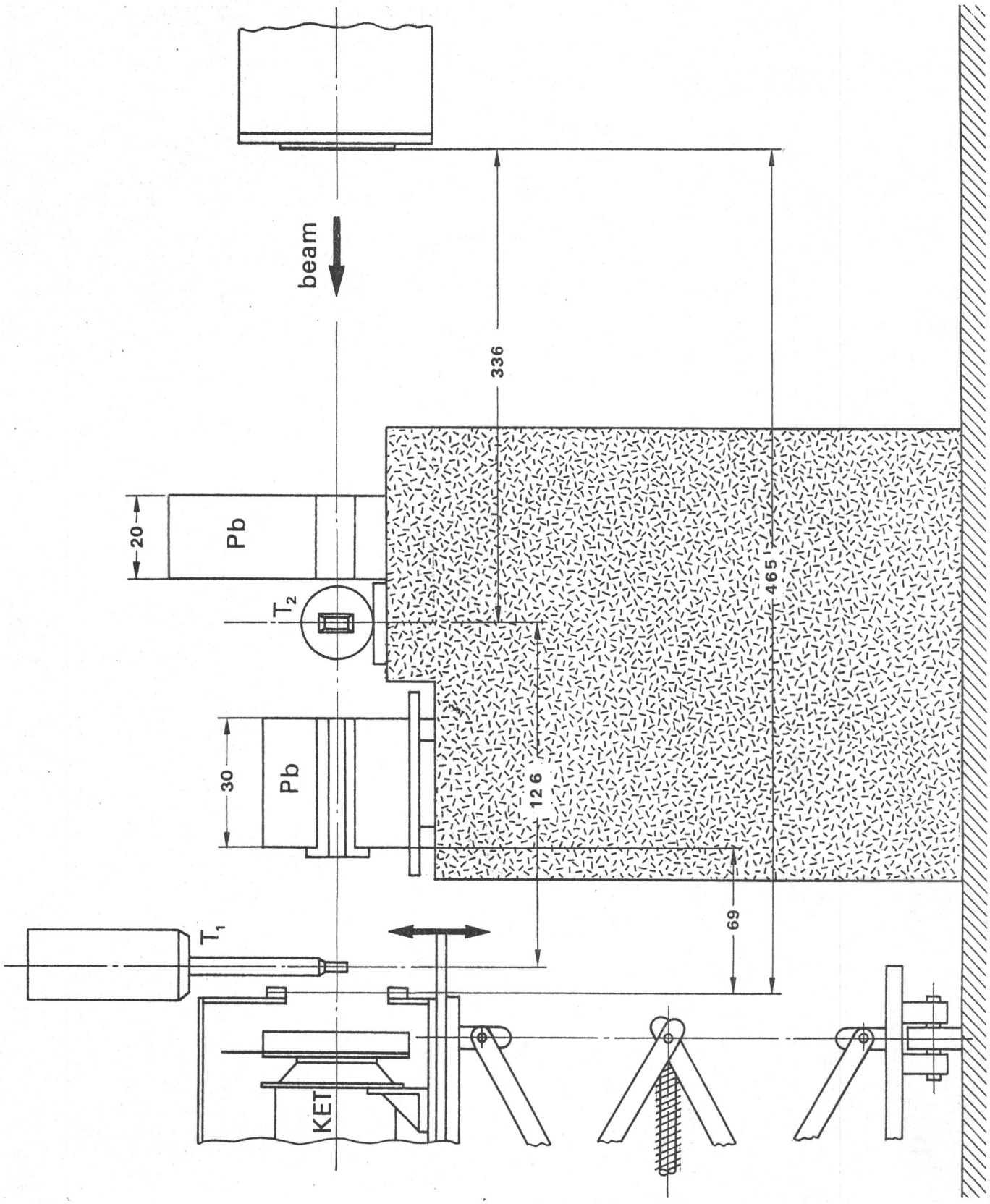

Figure 3-2 Set-Up of the monitor telescope (scintillation detectors T1 and T2) at the Universität Bonn 2.5 GeV Synchrotron accelerator site

3.2 Calibration History

Calibration of the KET instrument(s) took place from October 1982 to July 1985 at five different locations. Table 3-1 lists the personnel and the institutions involved in the calibration activities. Table 3-2 contains the history of the calibrations for the SFM, table 3-3 for the SFS.

Table 3-1 Personnel and institutions involved in KET calibrations

Institution	Personnel
Institut für Kernphysik, Universität Kiel	B. Iwers
	A. Kovacs-Birkas
	H. Kunow
	R. Müller-Mellin
	D. Müller
	E. Rode
	T. Schulz
	K. H. Stellmaschek
Service d'Astrophysique, Centre d'Etudes Nucleaires de Saclay	J. C. Curtois
	J. J. Engelmann
	A. Raviart
	A. Roy
	L. Treguer
Instituto di Fisica, Universita di Milano	C. Paizis

Table 3-2 Particle calibration history of KET - SFM

Year	Date	Facility*	Exposure
1984	Oct 22-23	ORME	e^+: 20 - 200 MeV
			Π^+: same momentum range
			μ^+: same momentum range
1984	Oct 28 - Nov 5	DESY	e^-: 300 - 5000 MeV
1985	Jan 21 - 27	BONN	e^-: 50 - 1200 MeV
1985	Mar 11 - 15	MOUND	RTG: γ-radiation
1985	Mar 26 - Apr 2	ORME	e^+: 7.5 - 200 MeV
			Π^+: same momentum range
			μ^+: same momentum range
1985	Apr 18 - 23	CERN/PS	p : 1 - 5 GeV/c
			e^+: same momentum range
			Π^+: same momentum range
			μ^+: same momentum range
1985	Aug 9 - 16	CERN/PS	p : 1 - 5 GeV/c
			e^+: same momentum range
			Π^+: same momentum range
			μ^+: same momentum range

*ORME DES MERISIERS : AL 600, Gif Sur Yvette
DESY : Deutsches Elektronen Synchrotron, Hamburg
- 7.5 GeV Synchrotron DESY I, Test-area F36
BONN : Physikalisches Institut, Universität Bonn
- 2.5 GeV Synchrotron
CERN/PS : Centre Europeenne pour la Recherche Nucleaire, Geneva - Testbeam T10, East Experiment Area
MOUND : Mound Laboratories, Monsanto Corp., Miamisburg/Ohio
- Radioisotope Thermal Generator

Table 3-3 Particle calibration history of KET - SFS

Year	Date	Facility*	Exposure
1982	Oct 12 - 14	JPL	SRTG: γ-radiation
1984	Nov 1 - 5	DESY	e^-: 200 - 5000 MeV
1985	Jan 27 - 30	BONN	e^-: 30 - 1200 MeV
1985	Mar 11 - 15	MOUND	RTG: γ-radiation
1985	Mar 21 - Apr 1	ORME	e^+: 7.5 - 175 MeV
			Π^+: same momentum range
			μ^+: same momentum range
1985	Aug 12 - 15	CERN/PS	p : 1 - 5 GeV/c
			e^+: same momentum range
			Π^+: same momentum range
			μ^+: same momentum range

*JPL : NASA/Jet Propulsion Laboratory, Pasadena
- Simulated Radioisotope Thermal Generator

DESY : Deutsches Elektronen Synchrotron, Hamburg
- 7.5 GeV Synchrotron DESY I, Test-area F36

BONN : Physikalisches Institut, Universität Bonn
- 2.5 GeV Synchrotron

ORME DES MERISIERS : AL 600, Gif Sur Yvette

CERN/PS : Centre Europeenne pour la Recherche Nucleaire, Geneva - Testbeam T10, East Experiment Area

MOUND : Mound Laboratories, Monsanto Corp., Miamisburg/Ohio
- Radioisotope Thermal Generator

3.3 Description of Runs and Accelerators

Tables 3-5 through 3-15 list in detail the calibration runs performed at the different accelerator sites with the two instruments together with the instrument conditions and the beam energies. The more than 600 runs documented in these tables all differ in at least one parameter

- particle type
- energy
- angle of incidence or displacement of axis
- instrument configuration (FM settings, high voltages)
- external trigger or not

The information in the tables is given as follows

Run Identification	Id number consists of the floppy number and the actual run number separated by a slash (/), e.g. 13/35. The floppies carry in addition labels: DKS for SFM and DKF for SFS.
Condition	Describes the KET condition:
HV	High voltage step number,
FM/A1	Number(s) of the detector(s) for which a failure mode has been set, A1 indicates that the high threshold for the A-detector discriminator has been chosen (default is A1:OFF)
ϕ	Angle of incidence [°] with the instrument turned in the horizontal plane. An angle of incidence in the vertical plane is noted in the 'Remark' column.
Δx	Displacement [mm] of instrument axis with respect to the beam axis in the horizontal plane. A vertical displacement is noted in the 'Remark' column.
Energy	Energy [MeV] of the particles entering the instrument.
Counts Beam	Number of particles registered by the beam monitor (scintillator T1T2).

Events PHA	Total number of events pulse-height analyzed by KET.
Beam	Energy [MeV] of the primary particle beam. Beam energy was changed during calibration at the Universität Bonn and at ORME DES MERISIERS.
Remark	Special remarks to particular runs and collimator information.

3.3.1 DESY

Tests for both instruments (SFM and SFS) were performed at DESY in testbeam area F36 (see figure 3-3) of the DESY I - Synchrotron from October 28 to November 5, 1984. Accelerator characteristics are summarized in table 3-4.

Particles injected by a linear accelerator (LINAC II) are accelerated up to the maximum energy in the synchrotron and extracted into the experiment beam(s) by a carbon-thread target. The high energy Bremsstrahlung-photons created on this target subsequently hit a conversion target. Two adjustable analyzing magnets are used to perform the energy and charge selection of the pair-production electrons created in the conversion target. Beam intensity can be controlled through the choice of the conversion target, collimators can be used to increase the energy resolution of the beam, which is generally of the order of 3%. Two locations were provided where lead collimators could be inserted into the beam, one directly behind the beam window and one in front of the last focussing magnet. The available collimators had a length of 300 mm and square cross sections of 1x1 mm^2, 3x3 mm^2, 5x5 mm^2 and 20x20 mm^2. The combination of collimators used for the different runs is given in the last column of table 3-5 and 3-6, which list the calibration runs for the SFM and the SFS respectively.

The angle of incidence listed in column 4 of table 3-5 shows the position of the instrument as defined in figure 3-1 and is consistent with all other listings in this report. The log book record differs from these values and is not correct.

Table 3-4 DESY accelerator characteristics

Maximum Energy	7.9 GeV Lab
Diameter of Ring	100 m
Number of beam magnets	48
Maximum Magnetic Field	0.79 Tesla
Number of HF-Accelerators	16
Maximum HF-Energy	1 MW
Vacuum	5•10(-7) Torr

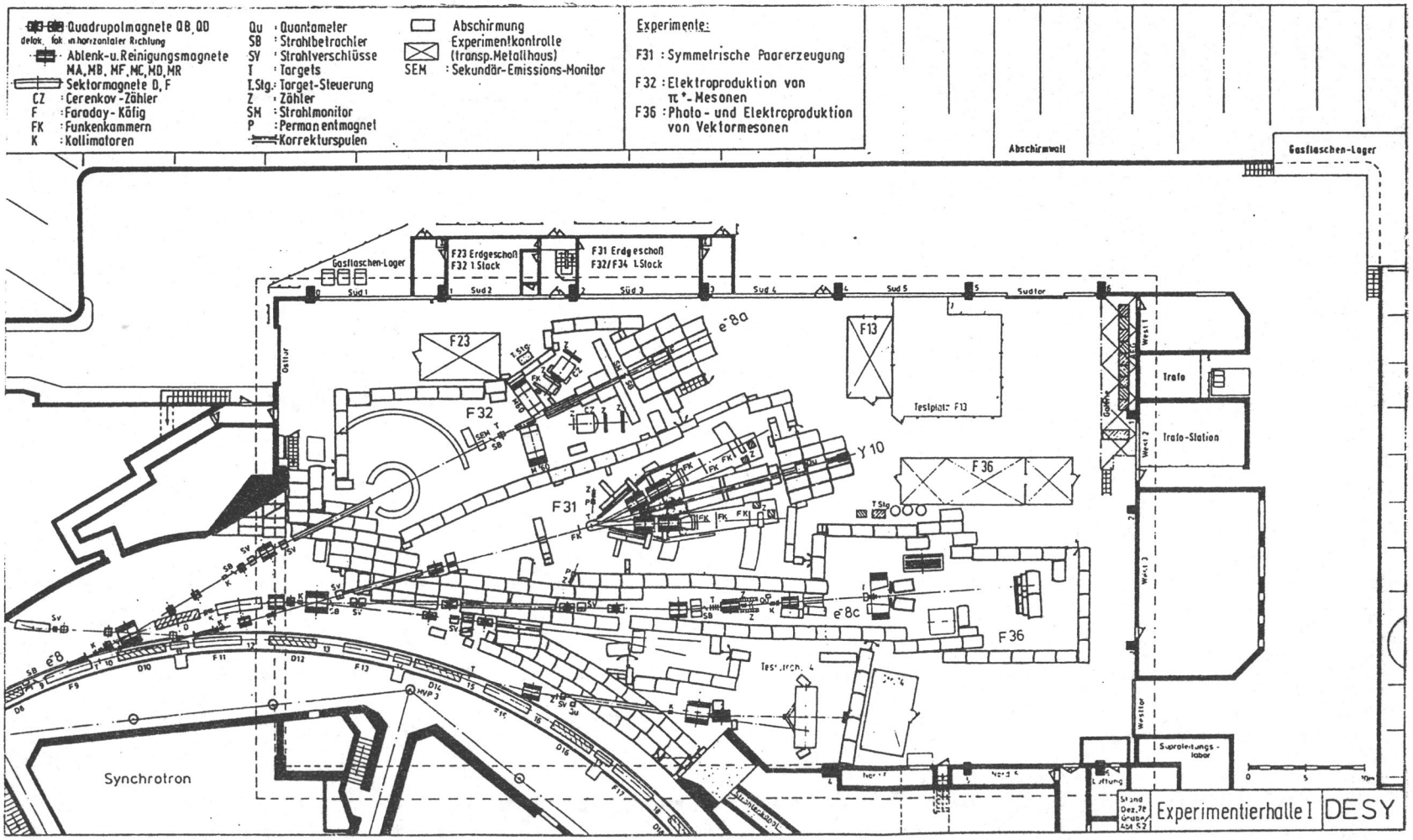

Figure 3-3 DESY experiment area F36

Table 3-5 Calibration runs of the KET - SFM at the DESY 7.9 GeV Synchrotron

Run Identification	Condition HV	FM/A1	ϕ	Δx	Energy [MeV]	Counts Beam	Events PHA	Remark
13/35,36	2	-	0	-	150	-	4994	
12/34	2	-	0	-	200	-	11320	
21/86	2	-	180	-	200	19489		No collimator, Floppy Disc missing
17/68	2	-	0	-	300	3886	1022	coll. 3x3 before magnet
13/37	2	-	0	-	500	-	4280	coll. 5x5 before magnet
18/70	0	-	0	-	500	6520	3590	coll. 3x3 before magnet
18/69	1	-	0	-	500	6180	3415	coll. 3x3 before magnet
12/33	2	-	0	-	500	-	0	No data in run, read error
11/28	2	-	0	-	750	-	6303	coll. 5x5
11/29	2	-	0	-	1000	-	7272	coll. 5x5
14/42	2	-	0	-	1000	8420	2040	coll. 3x3 before magnet
16/56	2	-	+5	-	1000	1929	2064	coll. 3x3 before magnet
16/55	2	-	+10	-	1000	6584	573	coll. 3x3 before magnet
16/57	2	-	+15	-	1000	5722	940	coll. 3x3 before magnet
15/52	2	-	+20	-	1000	55732	634	coll. 3x3 before magnet
15/53	2	6	+25	-	1000	13722	160	coll. 3x3 before magnet
15/54	2	A1	+25	-	1000	14200	226	coll. 3x3 before magnet
21/84	2	-	180	-	1000	63000	-	No collimator, Floppy Disc missing
14/43	2	-	-5	-	1000	8160	2140	coll. 3x3 before magnet
14/44	2	-	-10	-	1000	7600	1900	coll. 3x3 before magnet
14/45	2	-	-15	-	1000	5309	838	coll. 3x3 before magnet
14/46	2	-	-20	-	1000	19222	289	coll. 3x3 before magnet
14/47	2	A1	-20	-	1000	7388	793	coll. 3x3 before magnet
15/48	2	A1,5	-20	-	1000	9265	143	coll. 3x3 before magnet
15/49	2	A1	-25	-	1000	6049	64	coll. 3x3 before magnet
15/50	2	6	-25	-	1000	5969	100	coll. 3x3 before magnet
15/51	2	1,2,6	-90	-	1000	5004	760	coll. 3x3 before magnet
16/58	2	-	0	-	1000	3799	620	coll. 3x3 before magnet
17/65	2	-	0	+5	1000	8090	1260	coll. 3x3 before magnet
17/66	2	-	0	+10	1000	7966	1144	coll. 3x3 before magnet
17/67	2	-	0	+15	1000	8177	292	coll. 3x3 before magnet
16/59	2	-	0	-5	1000	4657	1693	coll. 3x3 before magnet
16/60	2	-	0	-10	1000	8240	1520	coll. 3x3 before magnet
16/61	2	-	0	-15	1000	6814	1600	coll. 3x3 before magnet
17/62	2	-	0	-20	1000	7663	1605	coll. 3x3 before magnet

Table 3-5 (contd) Calibration runs of the KET - SFM at the DESY 7.9 GeV Synchrotron

Run Identification	Condition HV	FM/A1	ϕ	Δx	Energy [MeV]	Counts Beam	Events PHA	Remark
17/63	2	-	0	-25	1000	10083	804	coll. 3x3 before magnet
17/64	2	-	0	-30	1000	8004	247	coll. 3x3 before magnet
18/71	0	-	0	-	1000	10050	2020	coll. 3x3 before magnet
18/72	0	-	0	+5	1000	6550	1200	Vertical Displacement, coll. 3x3
18/73	0	-	0	+10	1000	9400	1700	Vertical Displacement, coll. 3x3
18/74	0	-	0	+15	1000	7990	985	Vertical Displacement, coll. 3x3
18/75	0	-	0	-5	1000	7300	1340	Vertical Displacement, coll. 3x3
19/76	0	-	0	-10	1000	9400	1700	Vertical Displacement, coll. 3x3
19/77	0	-	0	-15	1000	7950	1473	Vertical Displacement, coll. 3x3
12/30	2	-	0	-	2000	-	6937	coll. 5x5, coll .3x3
13/38	2	-	0	-	2000	5500	3180	coll. 5x5, coll. 3x3
19/81	0	-	0	-	2000	2400	1603	coll. 1x1
19/80	0	5	0	-	2000	2365	1600	coll. 1x1
19/78	0	-	0	-	2000	16000	1580	High flux to test effect of high count-rates on PM-signals, coll. 3x3
19/79	0	5	0	-	2000	13000	1300	High flux to test effect of high count-rates on PM-signals, coll. 3x3
19/82	0	-	0	-	2000	327800	3640	High flux to test effect of high count-rates on PM-signals, no collimator, E300-counter overflow
12/31	2	-	0	-	3000	-	100	
14/41	2	-	0	-	3000	7320	2697	coll. 5x5, coll. 5x5
20/83	2	-	180	-	3000	209712	1285	Due to varying machine current, different combinations of collimators were used during this run: 1) coll. 3x3 + coll. 5x5 2) coll. 5x5 at 9:16h 3) coll. 3x3 at 9:26h
13/39	2	-	0	-	4000	5400	2567	coll. 5x5, coll. 3x3
13/40	2	-	0	-	5000	3100	1888	coll. 5x5, coll. 5x5
21/85	2	-	180	-	5000	47400	-	No collimator, Floppy Disc missing

Table 3-6 Calibration runs of the KET - SFS at the DESY 7.9 GeV Synchrotron

Run Identification	Condition HV	FM/A1	ϕ	Δx	Energy [MeV]	Counts Beam	Events PHA	Remark
28/1-30/13	2	-	0	-	1000	-	-	Use the instrument to find center of beam, coll. 3x3
32/22	2	-	0	-	150	1865	2701	no collimator
32/21	2	-	0	-	200	4225	2850	coll. 20x20
33/25,26	2	-	180	-	200	10200	818	no collimator
32/20	2	-	0	-	300	5150	4155	coll. 20x20
31/19	2	-	0	-	500	3295	2034	coll. 5x5
38/58	2	5	0	-	500	4310	2576	coll. 5x5
33/24	2	-	180	-	500	53325	3788	no collimator
37/53	0	-	0	-	500	501	302	coll. 3x3
37/54	0	-	0	-	500	3116	2039	coll. 5x5
37/55	0	5	0	-	500	1512	793	coll. 5x5
37/56	1	-	0	-	500	4773	3018	coll. 5x5
37/57	1	5	0	-	500	4213	2519	coll. 5x5
38/59	3	-	0	-	500	4708	2957	coll. 5x5
38/60	3	5	0	-	500	3127	1865	coll. 5x5
38/62	4	-	0	-	500	3475	2098	coll. 5x5
38/61	4	5	0	-	500	1800	1057	coll. 5x5
31/18	2	-	0	-	750	4160	2950	coll. 5x5
30/14	2	-	0	-	1000	5300	3491	
37/52	0	-	0	-	1000	5364	3410	coll. 3x3, reference for measurement of angular response
33/29	0	5	0	-	1000	-	1314	coll. 3x3
33/30	0	-	+5	-	1000	2660	1664	coll. 3x3
34/31	0	-	+10	-	1000	2035	1097	coll. 3x3
34/32	0	-	+15	-	1000	3205	1039	coll. 3x3
34/34	0	-	+20	-	1000	3140	93	coll. 3x3
34/36	0	6	+20	-	1000	1610	641	coll. 3x3
34/35	0	A1	+20	-	1000	965	161	coll. 3x3
34/37	0	-	+25	-	1000	980	0	coll. 3x3
35/38	0	-	+90	-	1000	26400	2	no collimator
35/39	0	6	+90	-	1000	25480	33	no collimator
35/41	0	-	-5	-	1000	2600	520	coll. 3x3
35/42	0	-	-10	-	1000	2640	1489	coll. 3x3
35/43	0	-	-15	-	1000	2840	922	coll. 3x3
36/45,48	0	-	-20	-	1000	4584	137	coll. 3x3
36/47	0	6	-20	-	1000	1360	468	coll. 3x3

Table 3-6 (contd) Calibration runs of the KET - SFS at the DESY 7.9 GeV Synchrotron

Run Identification	Condition HV	FM/A1	ϕ	Δx	Energy [MeV]	Counts Beam	Events PHA	Remark
36/46	0	A1	-20	-	1000	1650	635	coll. 3x3
36/49	0	-	-25	-	1000	1227	0	coll. 3x3
36/50	0	-	-90	-	1000	10888	0	no collimator
36/51	0	6	-90	-	1000	28820	53	no collimator
30/15	2	-	0	-	2000	4300	2676	
39/68	0	-	0	-	2000	3520	1969	coll. 3x3
39/69	0	5	0	-	2000	3070	1630	coll. 3x3
39/63	0	-	0	-	2000	15050	2780	coll. 5x5, Effect of high flux on PM-signals
39/64	0	5	0	-	2000	15460	2680	coll. 5x5, Effect of high flux on PM-signals
39/65	0	5	0	-	2000	74000	2260	Effect of high flux on PM-signals, no collimator
39/66	0	-	0	-	2000	68000	2280	Effect of high flux on PM-signals, E300-counter overflow, no collimator
39/67	0	-	0	-	2000	96000	3640	Effect of high flux on PM-signals, E300-counter overflow, coll. 20x20
31/16	2	-	0	-	3000	2050	1221	
33/27	2	-	180	-	3000	116063	2590	no collimator
31/17	2	-	0	-	5000	2010	1150	
33/28	2	-	180	-	5000	76800	847	no collimator

3.3.2 BONN

Tests at the 2.5 GeV synchrotron at Physikalisches Institut der Universität Bonn lasted from January 21 to January 30, 1985. Figure 3-4 shows a floor plan of the accelerator building, the experiment test location is marked. Energy selection was performed by using one analyzing magnet. Table 3-7 lists the calibration runs made with the SFM, table 3-8 lists the runs made with the SFS.

The beam was collimated for most runs with lead collimators of length 300 mm with square cross sections of 4x4 mm^2, 5x5 mm^2, 10x10 mm^2 and 20x20 mm^2. If a collimator size is not listed in the 'Remark' column, the 10x10 mm^2 was used (nominal condition). In addition to adjusting the beam intensity by choosing the appropriate collimator, the target position in the main beam could be used. For most of the SFM runs, the main beam energy was 1300 MeV, different main beam energies are noted in the 'Remark' column. For the SFS runs, the main beam energy is listed in column 9.

Background in the test area was very high when the synchrotron was operating due to the small distance between the ring and the experiment. The background consisted mostly of gamma-rays and neutrons, which can generate coincidences inside the instrument. With the SFM, the background was tested with 15 cm lead absorbing the test beam (run 44/147). An increase in the number of background particles (γ, n or e^- with unwanted energies) can also be caused by interaction or scattering of high energy electrons at the inner walls of a small collimator (as opposed to a collimator with a large opening).

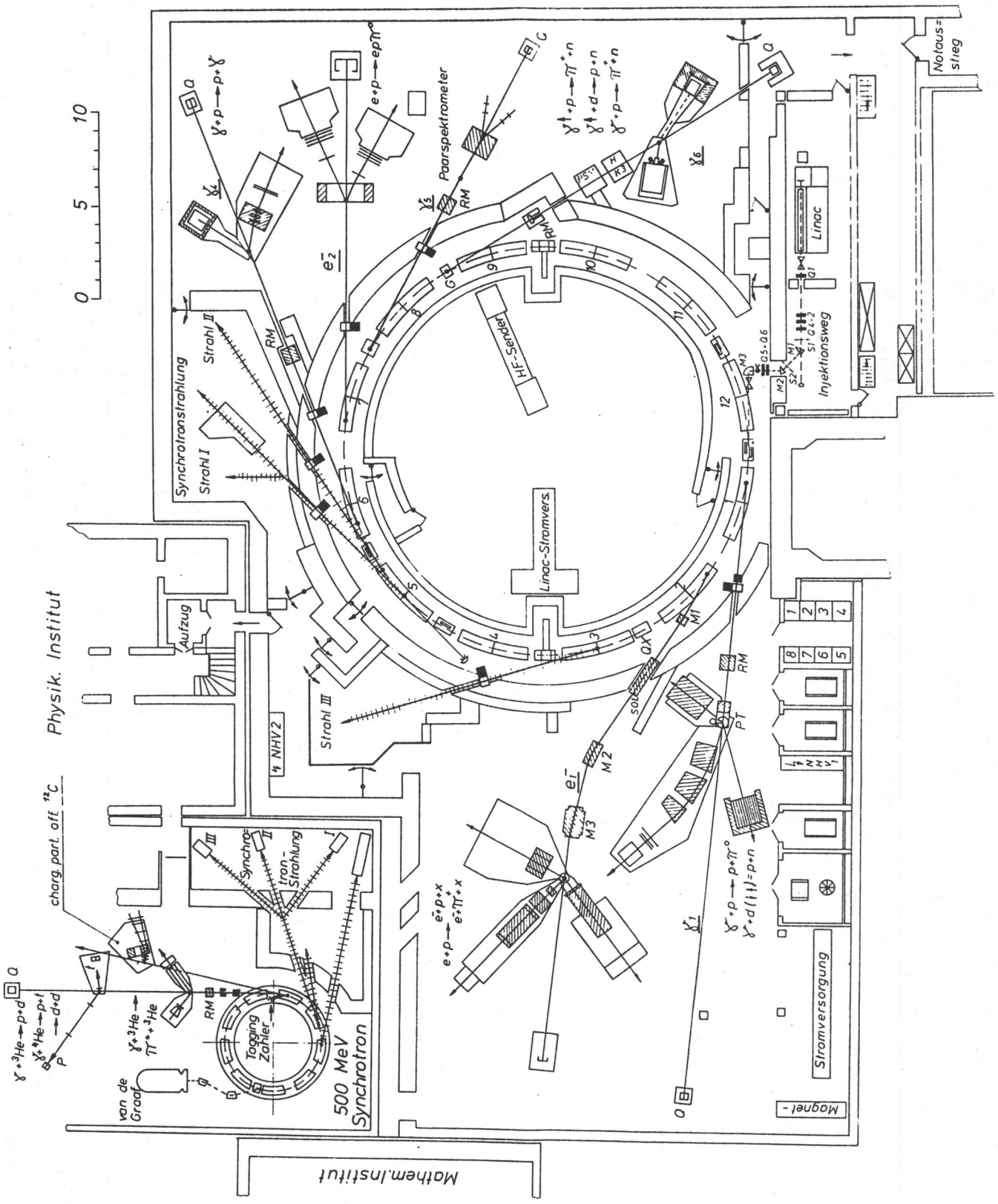

Figure 3-4 Universität Bonn 2.5 GeV Synchrotron experiment area

Table 3-7 Calibration runs of the KET - SFM at the Universität Bonn 2.5 GeV Synchrotron

Run Identification	Condition HV	FM/A1	ϕ	Δx	Energy [MeV]	Counts Beam	Events PHA	Remark
40/110-42/130	2	-	0	-	500	-	-	use the instrument to find center of beam
47/159	2	-	0	-	50	2513	1467	coll. 20x20
47/160	2	6	0	-	50	1840	1058	coll. 20x20
55/204	2	A1	0	-	50	4946	3062	
60/237	0	-	0	-	50	1211	679	
60/238	4	-	0	-	50	1100	782	
47/162	2	-	0	-	100	5400	3525	
55/206	2	6	0	-	100	6102	4427	
55/203	2	A1	0	-	100	5317	2700	
52/187	2	-	+10	-	100	4700	2546	
52/186	2	-	-10	-	100	4401	1794	
63/2	2	-	180	-	100	65500	1251	
63/1	2	6	180	-	100	62046	2036	
53/192	2	-	0	+10	100	915	732	
51/182	2	-	0	-10	100	3020	2249	
47/163,164,50/174	2	-	0	-	150	3684	4678	163,164: coll. 4x4, 174: coll. 10x10
47/165	2	6	0	-	150	3469	3454	coll. 4x4
60/236	0	-	0	-	150	4450	3935	
60/239	4	-	0	-	150	4520	3085	
48/166,49/173	2	-	0	-	200	9209	7783	166: coll. 4x4, 173: coll. 10x10
48/167,49/171,51/180	2	-	0	-	300	17529	13196	167: coll. 4x4, 171: coll. 10x10, 180: coll. 5x5
48/168,49/172	2	6	0	-	300	7546	5536	168: coll. 4x4, 172: coll. 10x10
49/169,170	2	A1	0	-	300	7558	5015	169: coll.4x4, 170: coll. 10x10
60/235	0	-	0	-	300	4601	2648	
60/240	4	-	0	-	300	3916	2251	
52/188	2	-	+10	-	300	-	3668	
52/185	2	-	-10	-	300	5120	3216	
53/191	2	-	0	+10	300	5200	3557	
51/181	2	-	0	-10	300	11300	4094	
50/175	2	-	0	-	400	6201	4542	
43/131	2	-	0	-	500	5888	2060	coll. 4x4
43/132	2	-	+5	-	500	5272	2080	coll. 4x4
43/133	2	-	+10	-	500	5973	2367	coll. 4x4

Table 3-7 (contd) Calibration runs of the KET - SFM at the Universität Bonn 2.5 GeV Synchrotron

Run Identification	Condition HV	FM/A1	ϕ	Δx	Energy [MeV]	Counts Beam	Events PHA	Remark
43/134	2	-	+15	-	500	6573	2020	coll. 4x4
43/135	2	-	+20	-	500	6161	393	coll. 4x4
43/136	2	A1	+20	-	500	4728	1053	coll. 4x4
43/137	2	6	+20	-	500	4686	1280	coll. 4x4
44/138	2	-	+25	-	500	29303	206	coll. 4x4
44/139	2	-	+90	-	500	19410	43	coll. 4x4
44/140	4	-	+90	-	500	14727	26	coll. 4x4
44/141	2	6	+90	-	500	18308	59	coll. 4x4
44/142	2	-	+90	-	500	85015	40	
44/143	2	-	-5	-	500	50710	-	42 counts/sec, E300-overflow
45/147	2	-	-5	-	500	8	6	Test background conditions, 15 cm lead absorber placed in the beam, coll. 10x10
45/146	2	-	-5	-	500	40028	1960	Test effect of large collimator on count rates, coll. 10x10
45/145	2	-	-5	-	500	58757	1776	145: coll. 4x4
45/148	2	-	-10	-	500	4851	1935	coll. 4x4
45/149	2	-	-15	-	500	5001	1822	coll. 4x4
45/150	2	-	-20	-	500	9001	396	coll. 4x4
45/151	2	A1	-20	-	500	6935	1179	coll. 4x4
46/152	2	6	-20	-	500	6603	2614	coll. 4x4
46/153	2	-	-25	-	500	13519	35	coll. 4x4
46/154	2	-	-40	-	500	13001	26	coll. 4x4
46/155	2	-	-90	-	500	9351	3	coll. 4x4
46/156	2	*[4]	180	-	500	8813	326	coll. 4x4
46/157	2	*[4]	180	-	500	102068	2980	coll. 20x20
46/158	2	6	180	-	500	66636	25720	coll. 20x20
62/253	2	-	0	-	500	21031	2760	Beam: 14 c/s, effect of high flux on PM-signals
62/251	2	-	0	-	500	88043	3400	Beam: 40 c/s, effect of high flux on PM-signals
62/252	2	-	0	-	500	146000	4440	Beam: 400 c/s, effect of high flux on PM-signals, E300-counter overflow

[4] The KET status information in the data record shows for run 156 and run 157 the condition FM6:ON. This status seems to be wrong, comparison of the data for the runs 156/157 with the data for run 158 - which is truly in condition FM6:ON - shows that the status for the runs 156/157 is **nominal mode**

Table 3-7 (contd) Calibration runs of the KET - SFM at the Universität Bonn 2.5 GeV Synchrotron

Run Identification	Condition HV	FM/A1	ϕ	Δx	Energy [MeV]	Counts Beam	Events PHA	Remark
50/176	2	-	0	-	600	8899	5381	
50/177	2	6	0	-	600	9791	5734	
50/178	2	A1	0	-	600	6447	960	
59/234	0	-	0	-	600	1802	1364	
60/241	4	-	0	-	600	4035	2040	
61/242	4	5	0	-	600	2855	1787	
52/189	2	-	+10	-	600	7940	4831	
52/184	2	-	-10	-	600	6000	3710	
53/190	2	-	0	+10	600	4300	2502	
51/183	2	-	0	-10	600	3590	1973	
51/179	2	-	0	-	700	4659	4115	
54/197	2	-	0	-	800	6002	3446	Main-beam energy 1500 MeV
54/199	2	6	0	-	800	2010	1220	Main-beam energy 1500 MeV
54/195	2	-	0	-	1000	5202	2635	Main-beam energy 1500 MeV
54/196	2	6	0	-	1000	4306	1660	Main-beam energy 1500 MeV
61/245	0	-	0	-	1000	4345	2419	
61/246	0	5	0	-	1000	3050	2015	
61/243	4	5	0	-	1000	2936	1827	
61/244	4	-	0	-	1000	6122	2142	
63/254	2	-	180	-	1000	34608	1112	
63/255	2	6	180	-	1000	4253	1835	
61/247	2	-	0	-	1000	17937	2480	Beam: 14 c/s, effect of high flux on PM-signals
61/248	2	5	0	-	1000	12750	1740	Beam: 15 c/s, effect of high flux on PM-signals
62/249	2	-	0	-	1000	75017	3620	Beam: 40 c/s, effect of high flux on PM-signals, E300-counter overflow
62/250	2	-	0	-	1000	2500386	4000	Beam: 1260 c/s, effect of high flux on PM-signals, E300- and P4000-counter overflow
53/193	2	-	0	-	1200	6607	1220	Main-beam energy 1500 MeV
54/194	2	6	0	-	1200	1700	1166	Main-beam energy 1500 MeV
55/201	2	-	+10	-	1200	-	3740	Main-beam energy 1500 MeV
55/202	2	-	-10	-	1200	7500	4293	Main-beam energy 1500 MeV
56/207-59/233	Trigger telescope connected to C1 test input for efficiency measurements. Energies from 75 MeV to 1200 MeV, varying instrument conditions. Runs not used in data evaluation (see chapter 4.2.3)							

Table 3-8 Calibration runs of the KET - SFS at the Universität Bonn 2.5 GeV Synchrotron

Run Identification	Condition HV	FM/A1	ϕ	Δx	Energy [MeV]	Counts Beam	Events PHA	Beam [MeV]	Remark
57/180	2	-	0	-	30	2050	1293	750	
57/181	2	6	0	-	30	562	452	750	
57/182	4	-	0	-	30	1600	873	750	
56/176	2	-	0	-	50	3000	1878	750	
59/195	2	-	0	-	50	6401	2220	750	
56/177	2	6	0	-	50	3405	2180	750	
57/179	0	-	0	-	50	2300	1557	750	
57/178	4	-	0	-	50	3801	2366	750	
56/174	2	-	0	-	75	3100	2047	750	
56/175	2	6	0	-	75	3390	2040	750	
56/173	2	-	0	-	100	4002	1958	750	
59/193	2	-	0	-	100	645	601	750	
42/76	2	-	0	-	100	9600	5091	1300	
58/189	2	-	+10	-	100	3701	1923	350	
59/192	2	-	-10	-	100	4600	1904	750	
58/186	2	-	0	+10	100	3100	2564	350	
58/187	2	-	0	-10	100	2250	1950	350	
57/183	2	-	0	-	100	38005	2999	750	Beam: 27 c/s, effect of high flux on PM-signals
57/184	2	-	0	-	100	115106	2360	350	Beam: 94 c/s, effect of high flux on PM-signals
48/120	2	-	0	-	150	3400	2724	750	
59/194	2	-	0	-	150	5208	1580	750	
48/121	2	6	0	-	150	3100	2760	750	
49/122	2	A1	0	-	150	4050	2440	750	
49/123	0	-	0	-	150	6100	2600	750	
49/124	4	-	0	-	150	5600	2798	750	
48/118	2	-	0	-	200	-	1001	750	GSE-PDP/11 hung up during this run
48/119	2	-	0	-	200	3000	2725	750	Repeat of run 48/118
47/112	2	-	0	-	300	3198	2937	1300	
47/113	2	6	0	-	300	2301	2191	1300	
47/114	2	A1	0	-	300	2727	2429	1300	
48/116	0	-	0	-	300	2500	1647	750	
48/115	4	-	0	-	300	4200	3457	1300	
58/190	2	-	+10	-	300	3408	1941	750	
58/191	2	-	-10	-	300	5501	1688	750	

Table 3-8 (contd) Calibration runs of the KET - SFS at the Universität Bonn 2.5 GeV Synchrotron

Run Identification	Condition HV	FM/A1	ϕ	Δx	Energy [MeV]	Counts Beam	Events PHA	Beam [MeV]	Remark
58/185	2	-	0	+10	300	8200	2750	350	
58/188	2	-	0	-10	300	2100	1696	350	
48/117	2	-	0	-	400	2900	2902	750	
47/108	2	-	0	-	500	2800	2640	1300	
47/109	2	6	0	-	500	4601	3336	1300	
47/111	0	-	0	-	500	2800	2355	1300	
47/110	4	-	0	-	500	3000	2028	1300	
49/125	2	-	0	-	500	31500	2340	750	Beam: 35 c/s, effect of high flux on PM-signals
49/126	2	-	0	-	500	3000	2244	750	coll. 4x4
56/172	2	-	0	-	500	4417	2240	750	Repeat of run 49/126 to normalize for run 56/171, coll. 4x4
49/127	2	-	+5	-	500	3400	1849	750	coll. 4x4
49/128	2	-	+10	-	500	4400	3436	750	coll. 4x4
50/129	2	-	+15	-	500	4550	1924	750	coll. 4x4
50/130	2	-	+20	-	500	16700	1136	750	coll. 4x4
50/131	2	6	+20	-	500	13000	2220	750	coll. 4x4
50/132	2	A1	+20	-	500	11000	2098	750	coll. 4x4
50/133	2	-	+25	-	500	15500	95	750	coll. 4x4
50/134	2	-	+40	-	500	260000	84	750	coll. 20x20. Very high intensity during this run, another group has put its target into the beam
50/135	2	-	+90	-	500	130041	35	750	
51/137	2	6	+90	-	500	22025	7	750	
51/136	4	-	+90	-	500	82015	18	750	
56/171	2	-	-5	-	500	4313	1390	750	coll. 4x4
51/139	2	-	-10	-	500	4001	1650	750	coll. 4x4
51/138	2	6	-10	-	500	2007	860	750	coll. 4x4
51/140	2	-	-15	-	500	6750	2310	750	coll. 4x4
51/141	2	-	-20	-	500	7202	506	750	coll. 4x4
52/143	2	6	-20	-	500	5002	1892	750	coll. 4x4
51/142	2	A1	-20	-	500	6208	1718	750	coll. 4x4
52/144	2	-	-25	-	500	4616	-	750	run id is 143 on disc, coll. 4x4
52/145	2	-	-40	-	500	25559	4	750	coll. 15x15
52/146	2	6	-40	-	500	44384	238	750	coll. 15x15
52/147	2	-	-90	-	500	34444	2	750	coll. 15x15
52/148	2	6	-90	-	500	32016	11	750	coll. 15x15

Table 3-8 (contd) Calibration runs of the KET - SFS at the Universität Bonn 2.5 GeV Synchrotron

Run Identification	Condition				Energy	Counts	Events	Beam	Remark
	HV	FM/A1	ϕ	Δx	[MeV]	Beam	PHA	[MeV]	
53/150	2	-	-90	+50	500	102225	13	750	coll. 15x15
52/149	2	6	-90	+50	500	38019	131	750	coll. 15x15
54/160	2	-	180	-	500	21300	896	750	coll. 4x4
54/161	2	6	180	-	500	57000	1327	750	coll. 4x4
53/151	2	-	0	+5	500	3700	2422	750	coll. 4x4
53/152	2	-	0	+10	500	8403	2968	750	coll. 4x4
53/153	2	-	0	+15	500	15001	2682	750	coll. 4x4
53/154	2	-	0	+20	500	16996	1193	750	coll. 4x4
53/155	2	-	0	+25	500	16721	563	750	coll. 4x4
53/156	2	-	0	-5	500	4402	1898	750	coll. 4x4
54/157	2	-	0	-10	500	5001	2024	750	coll. 4x4
54/158	2	-	0	-15	500	6653	1328	750	coll. 4x4
54/159	2	-	0	-20	500	44010	1878	750	coll. 4x4
42/78	2	-	0	-	600	3919	1620	1300	
45/99	2	-	0	-	600	2801	2649	1300	
45/100	2	6	0	-	600	2400	2442	1300	
45/101	2	A1	0	-	600	2158	2039	1300	
46/102	0	-	0	-	600	5824	3019	1300	
46/103	4	-	0	-	600	5185	2865	1300	
46/104	2	-	+10	-	600	4488	2687	1300	
46/105	2	-	-10	-	600	4601	2871	1300	
46/106	2	-	0	+10	600	3500	2053	1300	
46/107	2	-	0	-10	600	-	2003	1300	
42/77	2	-	0	-	700	5150	2612	1300	
44/92	2	-	0	-	800	4000	2804	1300	
44/93	2	6	0	-	800	4400	3190	1300	
44/94	2	A1	0	-	800	4500	3374	1300	
42/82	2	-	0	-	1000	3898	2297	1300	
43/83	2	6	0	-	1000	2900	1899	1300	
43/84	0	-	0	-	1000	3109	2239	1300	
43/85	0	5	0	-	1000	900	639	1300	
43/86	4	-	0	-	1000	3201	2328	1300	
43/87	4	5	0	-	1000	1503	1011	1300	
44/90	2	-	+10	-	1000	4300	2377	1300	
44/91	2	-	-10	-	1000	3950	2506	1300	
43/88	2	-	0	+10	1000	4057	2391	1300	
43/89	2	-	0	-10	1000	3900	2217	1300	
45/96	2	-	180	-	1000	170374	3929	1300	
45/97	2	6	180	-	1000	12830	3775	1300	

Table 3-8 (contd) Calibration runs of the KET - SFS at the Universität Bonn 2.5 GeV Synchrotron

Run Identification	Condition HV	FM/A1	ϕ	Δx	Energy [MeV]	Counts Beam	Events PHA	Beam [MeV]	Remark
44/95	2	-	0	-	1000	620822	3780	1300	Beam: 300 c/s, effect of high flux on PM-signals, E300-counter overflow
45/98	2	-	0	-	1000	11830	1094	1300	Beam: 26 c/s, effect of high flux on PM-signals
42/81	2	-	0	-	1100	3500	1599	1300	
42/79	2	-	0	-	1200	4100	2018	1300	
42/80	2	6	0	-	1200	3650	2398	1300	
54/162-55/170	Trigger telescope connected to C1 test input for efficiency measurements. Energies from 50 MeV to 500 MeV, varying instrument conditions (FM6 ON and OFF). Runs not used in data evaluation (see chapter 4.2.3)								

3.3.3 ORME DES MERISIERS

Calibration at the accelerator AL600 - ORME DES MERISIERS - took place from March 20 to April 2, 1985, the runs performed with the SFM are listed in table 3-9, the SFS runs are listed in table 3-10. The AL600 is a linear accelerator with a maximum energy of 600 MeV. The KET was set up in an experiment test area using a test beam with the main beam energy being dictated by the prime user of the machine. Energy selection was performed using two analyzing magnets, beam intensity was adjusted with the help of three focussing/-defocussing magnets and three momentum and intensity slits (shutters). The number of parasitic particles in the beam (mostly pions and μ-mesons) depends strongly on the energy of the main beam and increases with increasing beam energy. Measurements taken with a main beam energy of 200 MeV are practically free of parasitic particles, measurements taken at 500 MeV are dominated by unwanted particles. Figure 3-5 shows the beam characteristic of the AL600. The monitor telescope was used only part of the time due to the large amount of scatter introduced by this telescope, the trigger telescope was not in the beam for runs marked with a '*' in column 7.

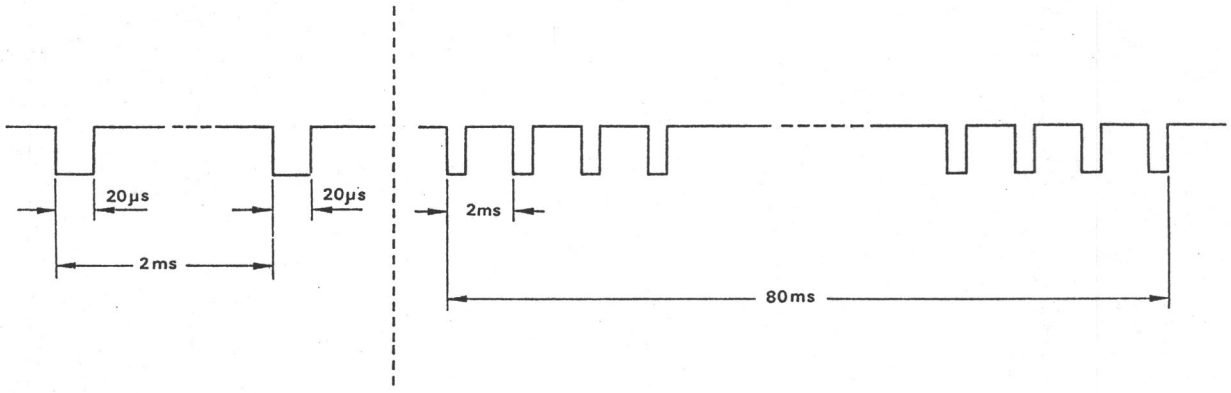

Figure 3-5 AL600 beam characteristic i) machine frequency - 500 Hz, ii) pulse duration - 20 μs, iii) extraction rate - one sequence of 40 pulses in a 80 ms period per second.

Table 3-9 Calibration runs of the KET - SFM at the accelerator ORME DES MERISIERS

Run Identification	Condition HV	FM/A1	ϕ	Δx	Energy [MeV]	Counts Beam	Events PHA	Beam [MeV]	Remark
71/39	2	-	0	-	7.5	3215	2080	200	
71/40	2	6	0	-	7.5	2746	1840	200	
71/41	2	-	0	-	10	4169	2450	200	
72/46	2	-	0	-	15	1689	1879	200	
72/47	2	6	0	-	15	1548	2014	200	
71/42	2	-	0	-	20	3111	1824	200	
71/43	2	6	0	-	20	2764	1741	200	
73/48	2	-	0	-	30	1305	1358	200	
73/49	2	6	0	-	30	1138	1381	200	
73/51	2	-	0	-	30	2068	2050	500	
72/44	2	-	0	-	40	3093	4456	200	
72/45	2	6	0	-	40	2371	3717	200	
69/30,31	2	-	0	-	50	4119	3262	200	
69/32	2	6	0	-	50	3017	1636	200	
69/33	2	5,6	0	-	50	3884	1821	200	
83/89	2	-	0	-	50	1200	1369	500	
84/92	2	-	0	+10	50	1218	1618	500	
84/93	2	-	0	+20	50	1200	1931	500	
84/94	2	-	0	+10	50	1205	1481	500	Repeat of run id 92
84/95	2	-	0	+30	50	1200	851	500	
84/90	2	-	0	-10	50	1216	979	500	
84/91	2	-	0	-20	50	1389	719	500	Run Id is 92 on disc
69/34	2	-	0	-	70	3949	694	200	
75/63	2	3	0	-	80	2642	3239	500	C2 invest.
77/71	2	-	0	-	95	3617	6585	500	C2 invest.
77/72	2	3	0	-	95	3225	6140	500	C2 invest.
70/35	2	-	0	-	98.6	4937	2658	200	
70/36	2	6	0	-	98.6	3600	2996	200	
78/74	2	-	0	-	100	3608	6097	500	C2 invest.
78/73	2	3	0	-	100	3607	7264	500	C2 invest.

Table 3-9 (contd) Calibration runs of the KET - SFM at the accelerator ORME DES MERISIERS

Run Identification	Condition				Energy	Counts	Events	Beam	Remark
	HV	FM/A1	ϕ	Δx	[MeV]	Beam	PHA	[MeV]	
79/75	2	-	0	-	105	3605	4466	500	C2 invest.
79/76	2	3	0	-	105	3600	7200	500	C2 invest.
75/64	2	-	0	-	110	4340	3799	500	C2 invest.
76/65	2	3	0	-	110	1895	1770	500	C2 invest.
80/77	2	3	0	-	110	5400	5810	500	C2 invest.
81/79	2	-	0	-	115	3600	5296	500	C2 invest.
80/78	2	3	0	-	115	3600	5997	500	C2 invest.
76/66	2	-	0	-	120	2289	1693	500	C2 invest.
76/67	2	3	0	-	120	2820	3649	500	C2 invest.
75/61	2	3	0	-	125	1035	1728	500	C2 invest.
76/68	2	-	0	-	130	2597	1427	500	C2 invest.
81/80	2	-	0	-	130	1800	2419	500	C2 invest.
81/81	2	3	0	-	130	3600	6734	500	C2 invest.
83/85	2	-	0	-	140	1980	2165	500	C2 invest.
83/86	2	3	0	-	140	1881	2701	500	C2 invest.
83/87	2	-	0	-	145	1812	2043	500	C2 invest.
83/88	2	3	0	-	145	1883	2273	500	C2 invest.
70/37	2	-	0	-	150	5550	1844	200	
70/38	2	6	0	-	150	3060	1225	200	
73/52	2	-	0	-	150	2447	2703	500	
75/62	2	3	0	-	150	1224	2313	500	C2 invest.
82/83,84	2	-	0	-	150	4075	2767	500	C2 invest.
82/82	2	3	0	-	150	3743	4877	500	C2 invest.
74/54	2	-	0	-	175	6918	6671	500	
74/55	2	6	0	-	175	2573	3706	500	
77/69	2	-	0	-	200	5465	1731	500	C2 invest.

Table 3-10 Calibration runs of the KET - SFS at the accelerator ORME DES MERISIERS

Run Identification	Condition HV	FM/A1	ϕ	Δx	Energy [MeV]	Counts Beam	Events PHA	Beam [MeV]	Remark
81/33,34	2	-	0	-	7.5	*	1903	200	
81/35	2	-	0	-	10	*	304	200	
71/239	2	-	0	-	10	7480	3679	320	
81/36	2	6	0	-	10	*	363	200	
71/240	2	6	0	-	10	8549	4663	320	
71/241	2	-	0	-	15	4031	2944	320	
71/242	2	6	0	-	15	3153	2860	320	
80/31	2	-	0	-	20	*	1943	200	
72/243	2	-	0	-	20	3181	3037	320	
80/32	2	6	0	-	20	*	1312	200	
72/244	2	6	0	-	20	3225	3632	320	
72/245	2	-	0	-	25	2740	3032	320	
72/246	2	6	0	-	25	1850	2750	320	
73/247	2	-	0	-	30	1650	1891	200	
73/248	2	6	0	-	30	2250	3158	200	
73/249	2	-	0	-	40	1640	2467	200	
73/250	2	6	0	-	40	1280	2239	200	
67/228	2	-	0	-	50	2879	4821	320	
74/251	2	-	0	-	50	1420	2492	200	
80/29	2	-	0	-	50	*	3723	200	
79/23	2	-	0	-	50	1187	3238	200	
74/252	2	6	0	-	50	1360	2882	200	
79/27	2	6	0	-	50	2371	2485	200	
80/28	2	5,6	0	-	50	*	2568	200	
75/3	2	-	+5	-	50	1520	2331	200	
75/4,5	2	-	+10	-	50	1470	1429	200	
75/6	2	6	+10	-	50	1441	2015	200	
75/7	2	-	+15	-	50	1011	280	200	Write error on disc during this run
74/255	2	-	-10	-	50	732	185	200	Write error on disc during this run
74/254	2	-	-15	-	50	570	244	200	
74/253	2	-	-20	-	50	590	81	200	
77/15	2	-	0	+5	50	1280	2487	500	
77/16	2	-	0	+10	50	1120	2809	500	

Table 3-10 (contd) Calibration runs of the KET - SFS at the accelerator ORME DES MERISIERS

Run Identification	Condition				Energy	Counts	Events	Beam	Remark
	HV	FM/A1	ϕ	Δx	[MeV]	Beam	PHA	[MeV]	
77/17	2	-	0	+15	50	1120	2687	500	
78/18,19	2	-	0	+20	50	2080	4416	500	
78/20	2	-	0	+30	50	1255	1831	500	
78/21	2	-	0	+40	50	1270	1147	500	
76/14	2	-	0	-5	50	1180	2342	500	
76/13	2	-	0	-10	50	1765	2063	500	
76/11	2	-	0	-15	50	523	385	200	
76/12	2	-	0	-15	50	1217	1062	500	
76/10	2	-	0	-20	50	2420	1505	200	
80/30	2	-	0	-140	50	*	0	200	Instrument below beam to test background
67/229	2	-	0	-	60	1512	3431	320	
67/230	2	-	0	-	70	1352	2623	320	
67/231	2	-	0	-	80	1111	1979	320	
68/232	2	-	0	-	90	1513	2744	320	
81/37	2	-	0	-	100	*	1001	200	
81/38	2	6	0	-	100	*	871	200	
68/233	2	-	0	-	100	1578	2574	320	
82/40	2	-	0	-	105	*	2914	200	C2 invest.
82/41	2	3	0	-	105	*	4617	200	C2 invest.
82/42,43	2	-	0	-	120	*	1919	200	C2 invest.
82/44	2	3	0	-	120	*	-	200	C2 invest.
68/234	2	-	0	-	125	1685	2259	320	
78/22	2	-	0	-	150	445	1166	200	
81/39	2	6	0	-	150	*	853	200	
69/235,236	2	-	0	-	150	2842	4830	320	
69/237,70/238	2	-	0	-	175	9576	18463	320	

3.3.4 CERN

The tests at CERN took place during two time periods in 1985: the SFM was calibrated from April 18 to April 23 and from August 9 to August 23, the SFS was calibrated from August 12 to August 15. The test beam T10 is located in experiment hall 157 in the east experimenters area of the Proton-Synchrotron (PS) in the Meyrin section of CERN near Geneva (see figure 3-6). The PS is operated to serve a number of experiments in the different test areas and also to fill the SPS-ring. The beam extraction to the various users differed considerably during the runs performed with the two KET-instruments. In general the users share the PS-beam during one PS-magnet supercycle lasting 14.4 seconds. The beam for the east area (test beams T7, T9, T10 and T11) is produced by magnetically kicking the proton bunches of the primary beam into the secondary beam. The extracted beam is then split into two branches with each having its own production target (Al, Cu) on which a number of secondary particles is produced. The number of kick-cycles within the supercycle depends on the number of active users of the PS-beam and ranged from 6-12 during the KET calibrations. Each kick-cycle lasted for 2.4 seconds and contained one 600 ms machine burst. The east-area test beam received 1-2 kick-cycles during each supercycle. The primary beam momentum and intensity was P = 24 GeV/c and $I = 2 \cdot 10^{11}$ particles/magnet cycle. The maximum particle momentum in the test beams depends on the production angle ($\phi = 3.53°$ for T10) and is $E_{max} \leq 5$ GeV/c. Six magnets are used to transport, focus and analyze (2 magnets) the beam. To control the beam intensity, two integrated remote controlled beam slits were used, one operating horizontally (momentum slit) and the other operating vertically (intensity), momentum resolution dP/P was less than one percent for all measurements. The beam profile could be monitored using two multi-wire proportional chambers immediately in front of the beam focus. The beam had an elliptical cross section with a width (horizontal) of 15 cm and a height (vertical) of 4 cm.

A gas Cerenkov detector of 5 m length was integrated into the test beam, it was used to discriminate against parasitic particles (e^+, μ^+, and Π^+). The signal of this detector was fed into the detector A test connector of the KET,

generating an anticoincidence cycle in the instrument each time a light particle (i.e. lighter than p) was detected by the Cerenkov detector. The available maximum pressure (3.1 bar) limited the momentum range for which pions could be rejected to from 3 GeV/c to 5 GeV/c.

The calibration runs performed with the SFM are listed in table 3-11 (April 1985) and 3-12 (August 1985), the SFS runs are listed in table 3-13. A '*' in the Δx-column (displacement) indicates a special position of the instrument, which is explained in the 'Remark' column. The angle of incidence listed in column 4 of table 3-11 shows the position of the instrument as defined in figure 3-1 and is consistent with all other listings in this report. The log book record differs from these values and is not correct. The term 'C ON A' in the 'Remark' column indicates, that for this run the external Cerenkov detector was connected to the anticoincidence detector test input of the KET instrument. Separate collimators in the experimenters area were not available.

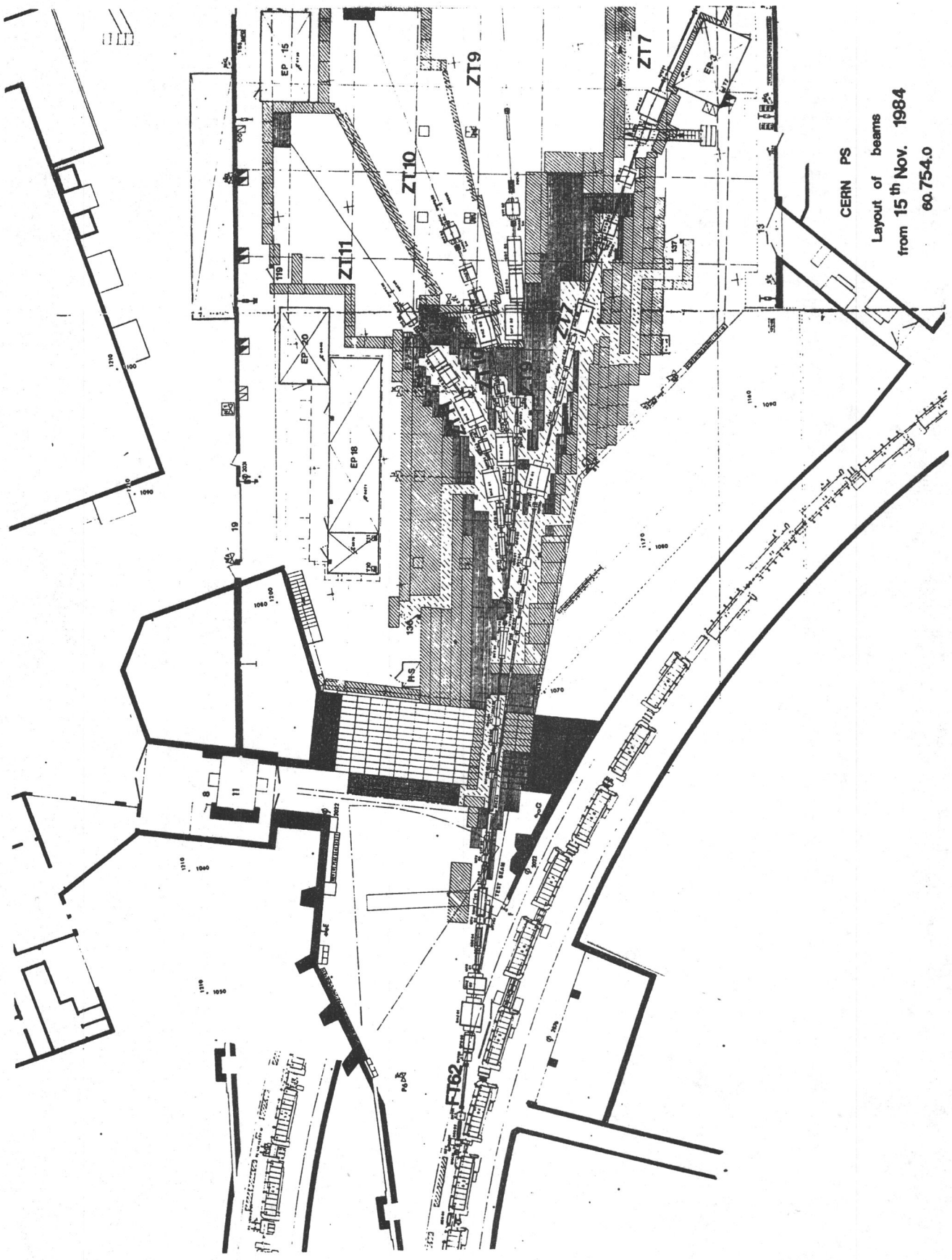

Figure 3-6 CERN/PS East Hall experimental test area

Table 3-11 Calibration runs of the KET - SFM at the CERN/PS Synchrotron (April '85)

Run Identification	Condition HV	FM/A1	ϕ	Δx	Energy [MeV]	Counts Beam	Events PHA	Remark
90/112	2	-	0	-	1270	2095	5906	C ON A
91/113	2	3,5	0	-	1270	1770	5138	C ON A
91/114	2	-	0	-	1270	1590	4782	
92/117	2	-	0	*	1270	701	319	Instrument 30 cm below beam to measure beam halo
91/115	2	-	0	-	1500	5013	4339	C ON A
91/116	2	3,5	0	-	1500	1432	3840	C ON A
89/109	2	-	0	-	1730	5939	5531	C ON A
90/110	2	3,5	0	-	1730	5966	5513	C ON A
90/111	2	-	0	-	1730	5800	6054	
88/106	2	-	0	-	2210	6442	5162	C ON A
89/107	2	3,5	0	-	2210	6504	5087	C ON A
89/108	2	-	0	-	2210	5284	4690	
88/104	2	-	0	-	3170	5486	5730	C ON A
88/105	2	3,5	0	-	3170	4792	4874	C ON A
87/103	2	-	0	-	3170	4590	5162	
87/100	2	-	0	-	4150	4203	4118	C ON A
87/101	2	3,5	0	-	4150	5660	5294	C ON A
87/102	2	-	0	-	4150	4740	4608	
96/128,97/129	2	-	180	-	4150	8822	19923	C ON A
97/130	2	-	180	*	4150	1251	78	C ON A, Instrument 20 cm below beam to test beam halo
97/131	2	-	0	*	4150	1454	97	C ON A, Instrument 30 cm below beam to test beam halo
92/118	2	-	0	*	4150	3201	872	Instrument 30 cm below beam to test beam halo
97/132	2	-	+90	*	4150	5072	5	C ON A, Instrument displaced by 40 mm to allow the beam to pass through C2
97/133	2	-	+140	*	4150	5512	4	C ON A, Instrument displaced by 33.5 mm to allow the beam to pass through C2 and hole of S2
92/119	1	-	0	-	4150	2994	4629	C ON A
93/125	1	3,5	0	-	4150	2471	2773	C ON A
92/120	3	-	0	-	4150	2018	3360	C ON A
93/124	3	3,5	0	-	4150	3170	3476	C ON A
92/121,93/122	4	-	0	-	4150	2043	7710	C ON A
93/123	4	3,5	0	-	4150	1454	2209	C ON A

Table 3-11 (contd) Calibration runs of the KET - SFM at the CERN/PS Synchrotron (April '85)

Run Identification	Condition HV	FM/A1	ϕ	Δx	Energy [MeV]	Counts Beam	Events PHA	Remark
94/126,95/127	2	-	0	-	4150	24136	23146	C ON A, Search for nuclear interactions. Long run with unchanged beam conditions
97/134	2	-	+5	-	4150	2060	2198	C ON A
98/135	2	-	+10	-	4150	2230	1952	C ON A
99/141	2	-	+13	-	4150	2054	1858	C ON A
99/144	2	-	+14	-	4150	568	426	C ON A
98/136	2	-	+15	-	4150	2691	1725	C ON A
99/142	2	-	+17	-	4150	2030	1342	C ON A
99/140	2	-	+18	-	4150	3342	1686	C ON A
99/143	2	-	+19	-	4150	1900	842	C ON A
98/137	2	-	+20	-	4150	5172	1182	C ON A
98/138	2	-	-15	-	4150	942	434	C ON A
98/139	2	-	-20	-	4150	4309	855	C ON A

Table 3-12 Calibration runs of the KET - SFM at the CERN/PS Synchrotron (August '85)

Run Identification	Condition HV	FM/A1	ϕ	Δx	Energy [MeV]	Counts Beam	Events PHA	Remark
109/47,48	2	-	0	-	4150	-	3289	C ON A
109/49	2	5	0	-	4150	-	1556	C ON A
110/51	3	-	0	-	4150	-	2400	C ON A
109/50	3	5	0	-	4150	-	1680	C ON A
111/55	2	-	0	-	4150	652	1711	C ON A
111/56	2	-	+5	-	4150	881	2244	C ON A
111/57	2	-	+10	-	4150	986	1983	C ON A
111/58	2	-	+15	-	4150	820	1024	C ON A
111/59	2	5	+15	-	4150	567	688	C ON A
110/52	2	-	+16	-	4150	-	1610	C ON A
112/60	2	-	+17	-	4150	671	696	C ON A
110/53	2	-	+18	-	4150	-	1490	C ON A
112/61	2	-	+20	-	4150	749	328	C ON A
112/65	2	1,5	+45	*	4150	4484	176	C ON A, Instrument displaced by 33 mm to allow beam to go through C2 and hole of S2
110/54	2	1,5,6	+45	*	4150	-	459	C ON A, Instrument displaced by 33 mm to allow beam to go through C2 and hole of S2
112/62	2	-	-15	-	4150	605	862	C ON A
112/63	2	5	-15	-	4150	427	557	C ON A
112/64	2	-	-163	-	4150	609	624	C ON A

Table 3-13 Calibration runs of the KET - SFS at the CERN/PS Synchrotron (August '85)

Run Identification	Condition HV	FM/Al	ϕ	Δx	Energy [MeV]	Counts Beam	Events PHA	Remark
106/94	2	-	0	-	1270	932	1967	
106/95	2	3,5	0	-	1270	1222	2501	
106/92	2	-	0	-	1500	178	566	
106/93	2	3,5	0	-	1500	411	1445	
106/90	2	-	0	-	1730	255	507	
106/91	2	3,5	0	-	1730	195	391	
105/88	2	3,5	0	-	1970	307	540	
106/89	2	-	0	-	1970	361	673	
105/86	2	-	0	-	2210	462	963	
105/87	2	3,5	0	-	2210	337	566	
105/84	2	-	0	-	3170	604	1282	
105/85	2	3,5	0	-	3170	581	1175	
105/82	2	-	0	-	4150	2559	5114	
105/83	2	3,5	0	-	4150	725	1568	
107/96	2	3,5	0	-	4150	1759	2272	
107/97	1	-	0	-	4150	3130	4037	
107/98	1	3,5	0	-	4150	2085	2579	
107/100	3	-	0	-	4150	2364	2880	
107/99	3	3,5	0	-	4150	2702	3475	
108/102,103	4	-	0	-	4150	2428	3111	
107/101	4	3,5	0	-	4150	2647	2573	
110/118	2	-	0	-	4150	192	216	Beam shutter closed, background in test area (mostly γ and n)
109/113	2	-	+5	-	4150	2292	2420	
109/112	2	-	+10	-	4150	1701	2201	
108/108	2	-	+15	-	4150	929	1148	
109/109	2	5	+15	-	4150	677	737	
109/110	2	-	+17	-	4150	1046	921	
108/104	2	-	+20	-	4150	736	316	
108/107	2	-	+22	-	4150	834	81	
110/122	2	1,5	+45	-	4150	17284	465	Beam hits S1, D2, C2 and S2
110/119	2	-	180	-	4150	1812	2357	
109/114	2	-	-5	-	4150	2439	2774	
109/115	2	-	-10	-	4150	1779	2052	

Table 3-13 (contd) Calibration runs of the KET - SFS at the CERN/PS Synchrotron (August '85)

Run Identification	Condition HV	FM/A1	ϕ	Δx	Energy [MeV]	Counts Beam	Events PHA	Remark
110/116	2	-	-15	-	4150	1926	1844	
110/117	2	5	-15	-	4150	1697	1552	
108/105	2	-	-20	-	4150	837	409	
108/106	2	-	-22	-	4150	676	122	
110/121	2	-	-90	40	4150	3027	4	Instrument shifted by 40 mm to allow the beam to pass through C2
110/120	2	-	-163	-	4150	13102	1413	Beam passes through hole in S2
111/123	2	-	0	-	4150	626	1629	Reference for run 111/124-126
111/124	2	-	8	-	4150	749	1728	Latitude
111/125	2	-	15	-	4150	1490	1702	Latitude
111/126	2	5	15	-	4150	1003	1031	Latitude

3.3.5 MOUND

An RTG compatibility test was performed for both instruments during the period March 11 to March 15 1985 at Mound Laboratories, Monsanto Corp., Miamisburg, Ohio. Tests were carried out in a radiation safe cell No. 112 (no floor plan available) with the actual GALILEO flight RTG (F3). Walls, floor and ceiling were of approx. 50 cm reinforced concrete, the RTG was mounted in its transport cart approx. 100 cm above the floor with the long axis horizontal and the S/C mounting bracket facing the KET. The KET instrument(s) were placed on a table with the sensor axis orientation and distance equal to the position in the spacecraft (see fig. 2-3) with an accuracy of approx. 1.5 inch. Due to the limited space available in this cell, both the RTG and the KET had to be placed close to one wall (distance approx. 100 cm). A large pressure tank was located also in the cell at a distance of approx. 200 cm from the RTG and 300 cm from the KET.

Table 3-14 KET - SFM RTG compatibility test at Mound Laboratories

Run Id	Condition HV	Condition FM/A1	Time [sec]	Events PHA	Remark
65/13	2	-	49252	572	Strong noise increase during this overnight run
66/22	2	-	52683	528	Overnight run
65/10	0	-	1372	7	
65/11	2	-	4607	33	
67/24	3	-	4269	41	
65/12	4	-	3528	44	
65/14	2	-	10738	116	
65/15	2	-	883	7	3 mm aluminum shield between RTG and KET
65/17	2	1	3433	668	D2 single detector spectrum in P32
66/20	2	2	1628	1476	D1 single detector spectrum (above D11) in P32
66/21	2	3	1619	17	
66/23	2	4	2650	22	
66/19	2	5	1766	14	
66/18	2	6	3237	57	
67/25	2	2,3	1267	2580	D1 single detector spectrum (below D11) in E4
67/26	2	1,3	1519	3100	D2 single detector spectrum (below D21) in E4
67/27	2	1,2,3	5912	12040	C2 single detector spectrum in E12 S2 single detector spectrum in P116
68/28	2	1,2,5	1208	2460	C1 single detector spectrum (below C11) in E4

Table 3-15 KET - SFS RTG compatibility test at Mound Laboratories

Run Id	Condition HV	Condition FM/A1	Time [sec]	Events PHA	Remark
63/213	2	-	54464	502	Overnight run
65/225	2	-	56982	526	Overnight run with a 10 cm lead-brick wall between RTG and KET
63/211	0	-	2796	24	
63/212	3	-	3533	33	
65/224	4	-	3534	39	
63/214	2	1	5889	784	D2 single detector spectrum in P32
63/215	2	2	1746	1452	D1 single detector spectrum (above D11) in P32
63/216	2	3	1914	26	
64/218	2	4	-	-	Read error on disc
64/219	2	5	1767	22	
64/217	2	6	6331	107	
64/221	2	1,3	1463	2980	D2 single detector spectrum (below D21) in E4
64/220	2	2,3	1522	3100	D1 single detector spectrum (below D11) in E4
64/223	2	1,2,3	1636	3340	C2 single detector spectrum in E12 S2 single detector spectrum in P116
64/222	2	1,2,5	1470	3000	C1 single detector spectrum (below C11) in E4
63/210	0	-	589	5	Read error on disc

4 Results of the Calibrations

4.1 Response of the Individual Detectors

4.1.1 Semiconductor Detectors

4.1.1.1 Selection Criteria

The essential part of the performance testing for these detectors has been done prior to their integration into the sensors in the high vacuum detector test facility. Important criteria for the selection were

- Detector does not show any degradation of the energy resolution during several long-term exposures in vacuum of $P \leq 10^{-9}$ Torr.
- Detector electric parameters (reverse current, depletion voltage) do not change during its life time in the test laboratory in or out of vacuum.
- Energy resolution for α-particles from an uncollimated source is better than 50 KeV for the D1-type detector and 25 KeV for a D2-type detector.
- Detector surface is not damaged, gold or aluminum electrode are not porous or contaminated.

Each detector has been extensively tested in vacuum using α-particle and β-particle sources prior to integration into the sensor. The following detectors are integrated into the respective sensors:

SFM	D1:	ORTEC 24-106B	Bias-Voltage: 423 Volt
	D2:	ORTEC 23-609A	Bias-Voltage: 418 Volt
SFS	D1:	ORTEC 24-106D	Bias-Voltage: 423 Volt
	D2:	ORTEC 23-609E	Bias-Voltage: 418 Volt

4.1.1.2 Reverse Current

The reverse current of the detectors is not monitored individually in the KET-instrument. To save telemetry channel capacity, the reverse currents for both

detectors are summed and transmitted as one value after digitization. The expected values of the reverse current as a function of temperature - based on laboratory tests, can be derived from the following equations

$$\text{SFM} \qquad I_D\,[\mu A] = 0.6529 \cdot e^{(0.07337 \cdot T\,[^\circ C])}$$

$$\text{SFS} \qquad I_D\,[\mu A] = 0.2656 \cdot e^{(0.09850 \cdot T\,[^\circ C])}$$

4.1.1.3 Detector response as a Function of Energy

Figure 4-1 (a) and (b) show peak location and width (at the 1σ-level) of the energy loss spectrum as a function of energy for electron energies between E_e = 7.5 MeV and E_e = 5000 MeV (open circles) and for one proton energy of E_p = 4150 MeV (open diamond) for the SFM detectors. The error in determining the peak value is less than 1%, the error bars would lie completely inside the graph symbols. A least square fit using a polinomial has been added to the figures to aid the eye. At very low energies, the energy loss distribution in D2 is broadened and shifted to higher values due to the intense scattering of the particles in the entrance telescope. D1 shows the same effect too but to a lesser degree. At high energies the energy loss increases with the particle energy. Figure 4-2 (a)-(d) show pulse height distributions of D1 and D2 for (a) 7.5 MeV electrons, (b) 100 MeV electrons, (c) 3000 MeV electrons and (d) 4150 MeV protons. The proton distribution is essentially dominated by the familiar shape of the Landau distribution, deviation from this distribution at the high energy end are probably due to δ-rays. The 7.5 MeV energy loss distribution in D2 (a) shows clearly the effect of electron scattering, additional energy loss is superimposed on the distribution of a minimum ionizing particle. The observed increase in average energy loss for high energy electrons corresponds to the predicted increase for relativistic particles. Figure 4-3 (a) and (b) and figure 4-4 (a)-(d) show the same data for the SFS.

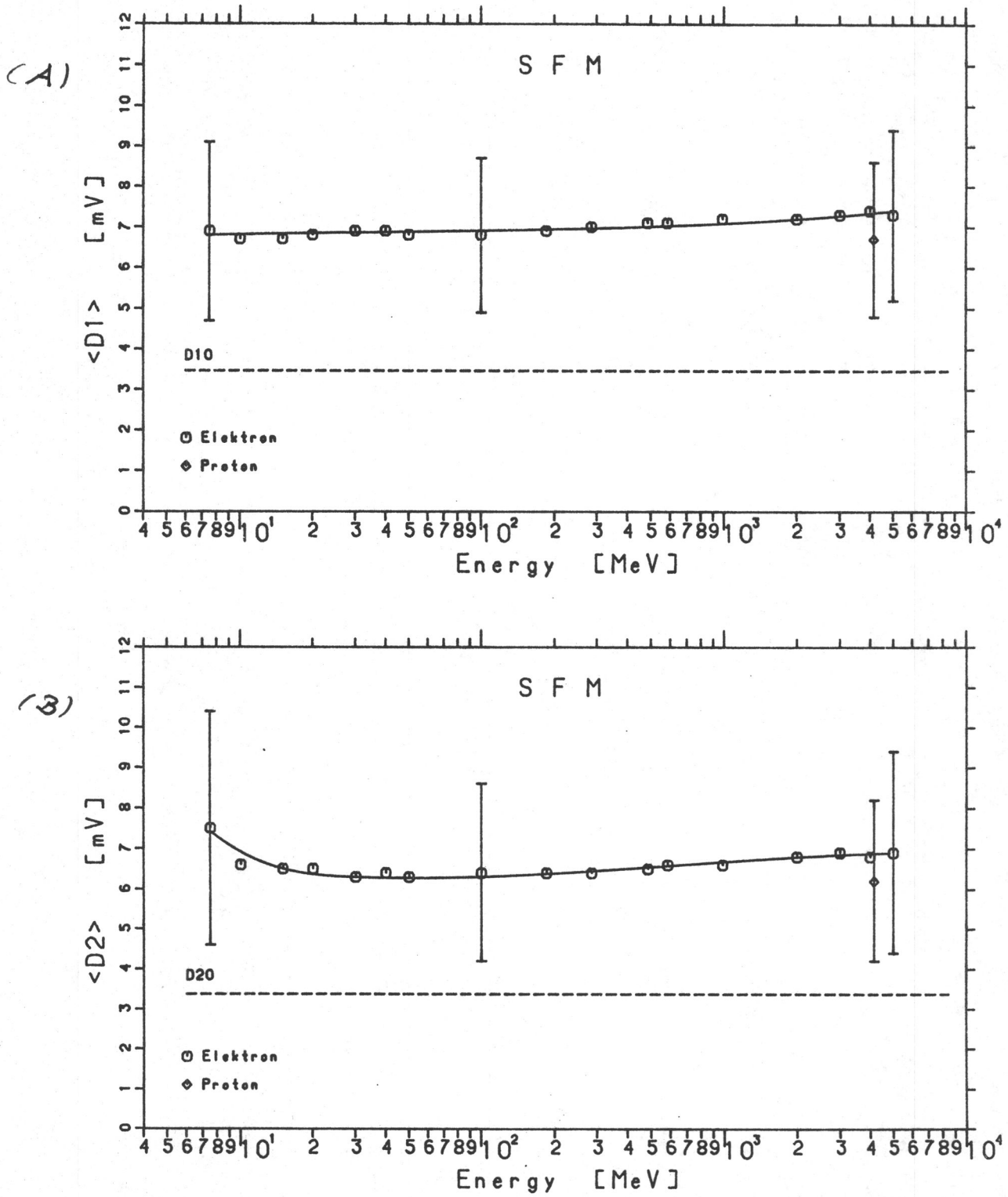

Figure 4-1 Peak location and width of the energy loss distribution for the semiconductor detectors D1 (a) and D2 (b) in the Selected Flight Model (SFM) as a function of electron energy

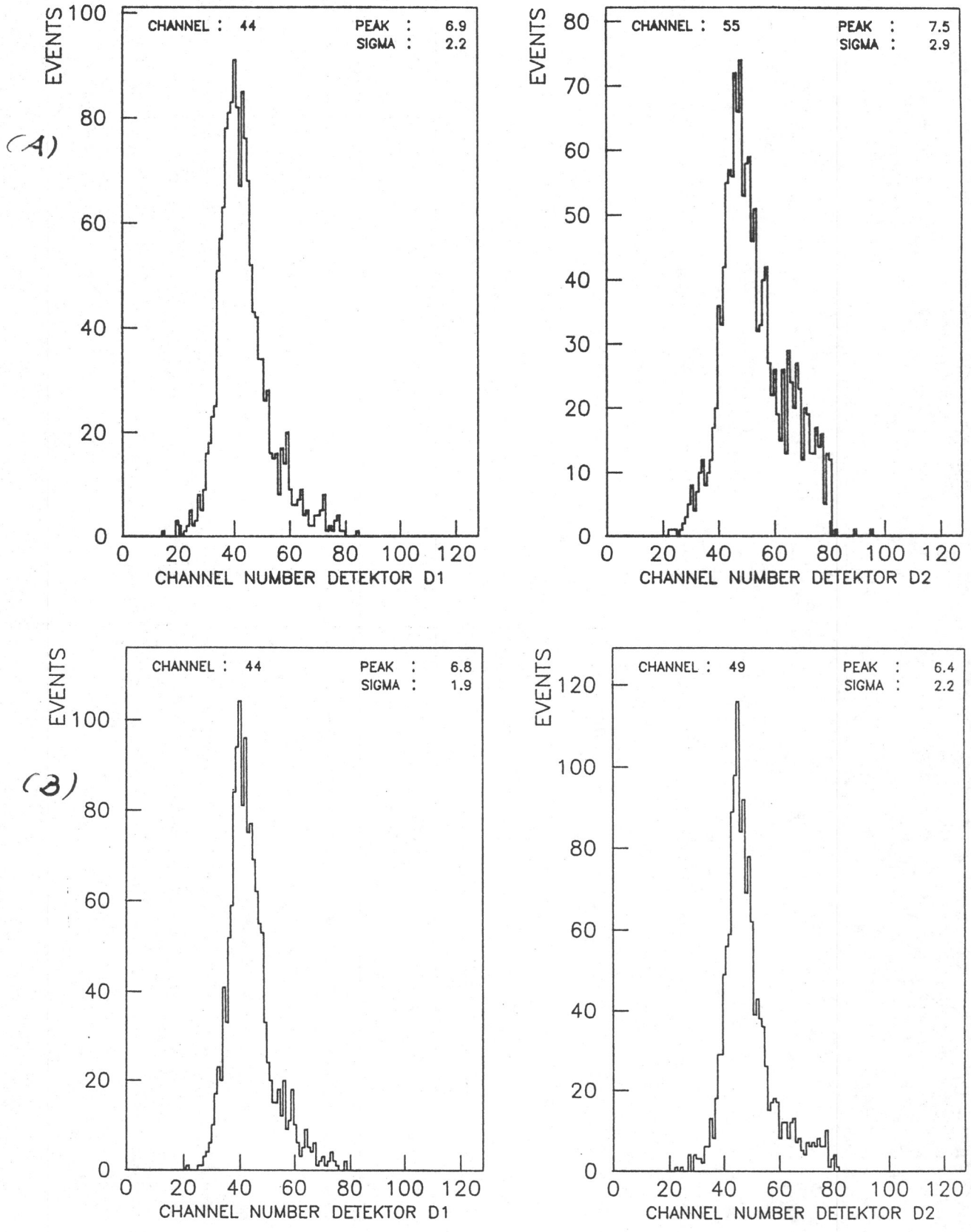

Figure 4-2 Pulse height distribution of the SFM detectors D1 and D2 for (a) 7.5 MeV electrons and (b) 100 MeV electrons

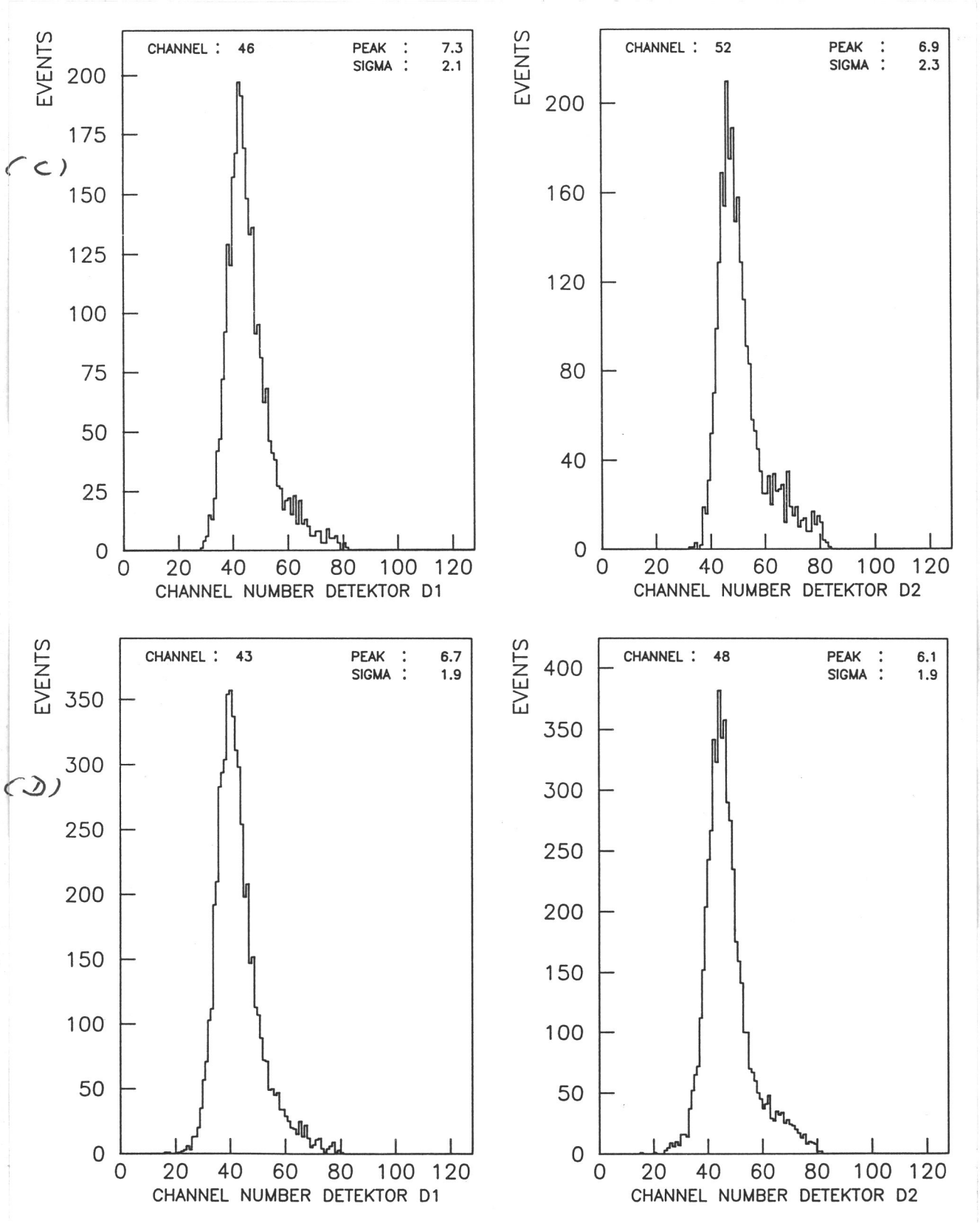

Figure 4-2 (continued) Pulse height distribution of the SFM detectors D1 and D2 for (c) 3000 MeV electrons and (d) 4150 MeV protons

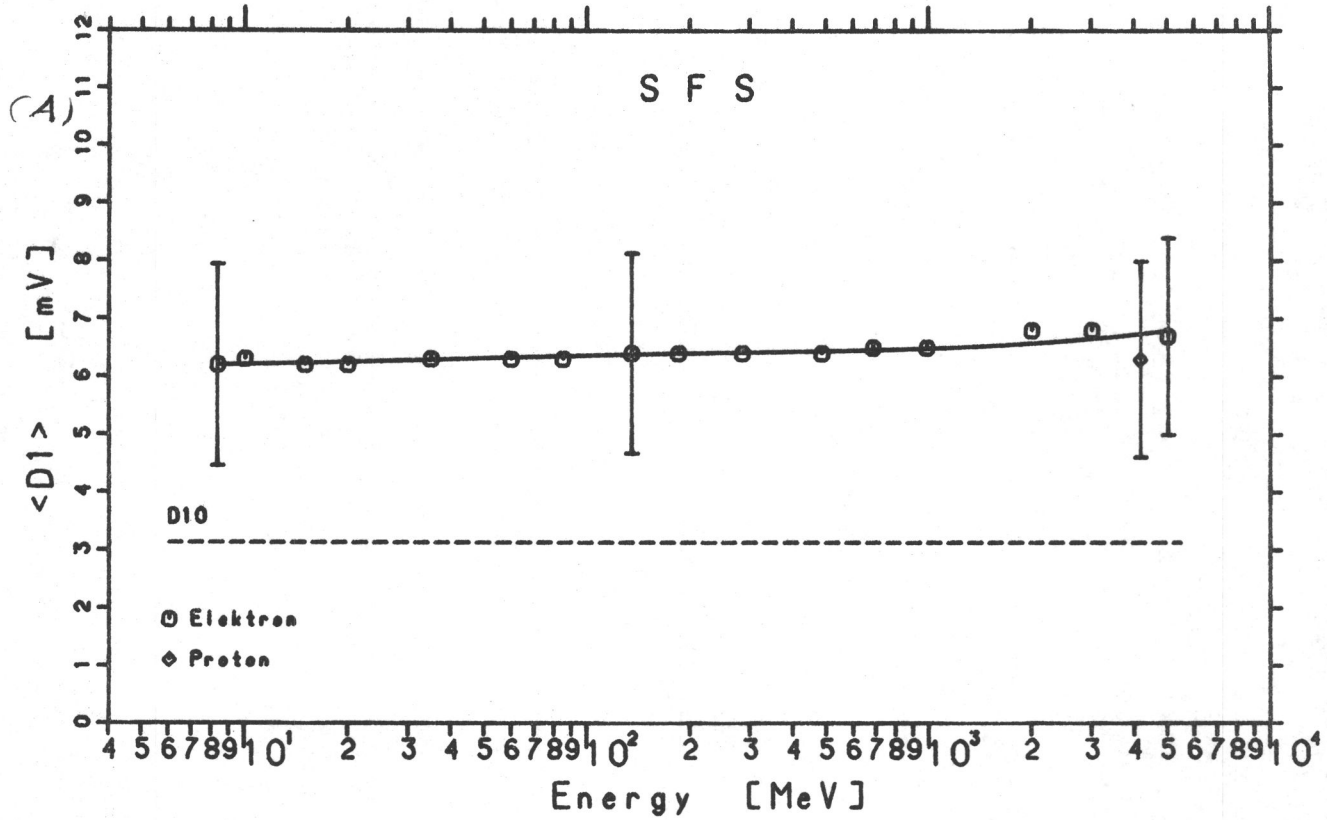

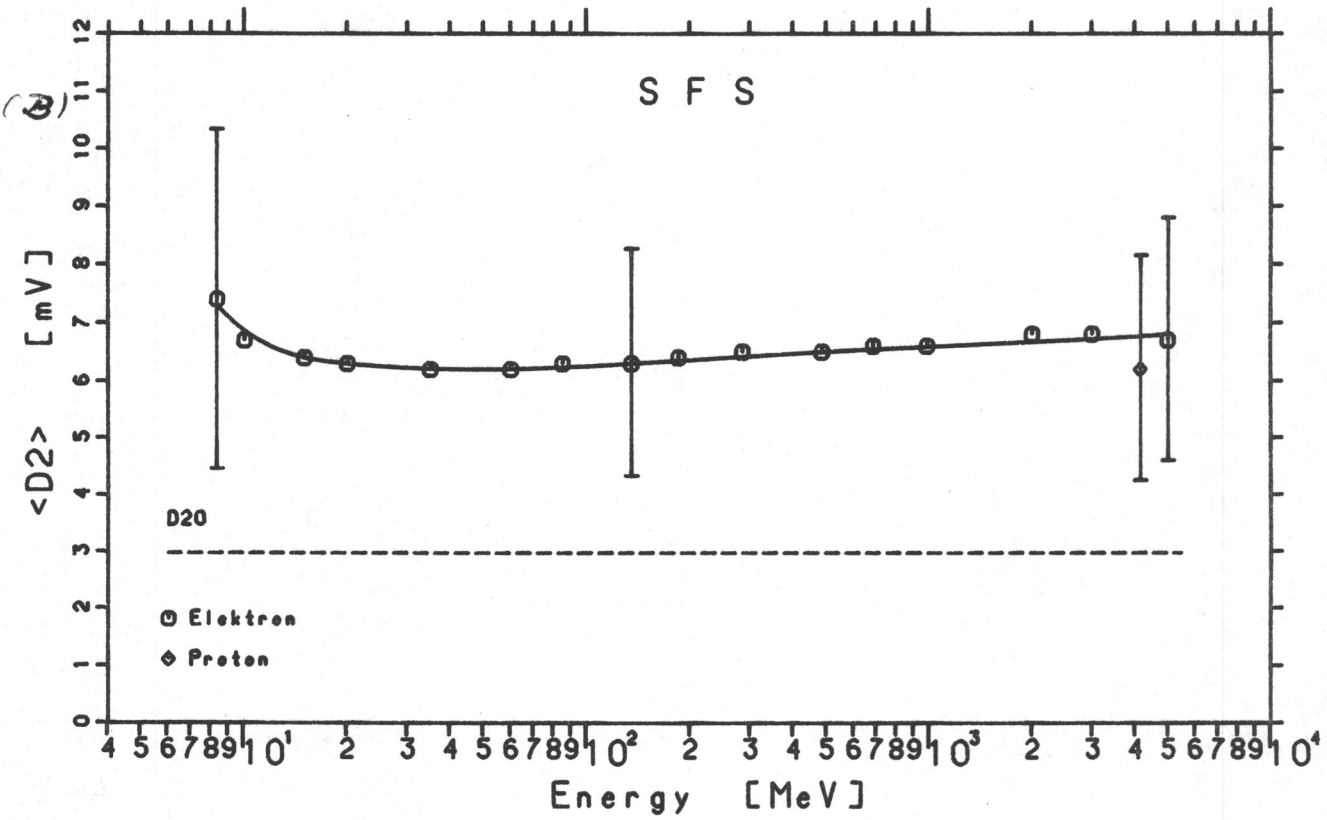

Figure 4-3 Peak location and width of the energy loss distribution for the semiconductor detectors D1 (a) and D2 (b) in the Selected Flight Spare (SFS) as a function of electron energy

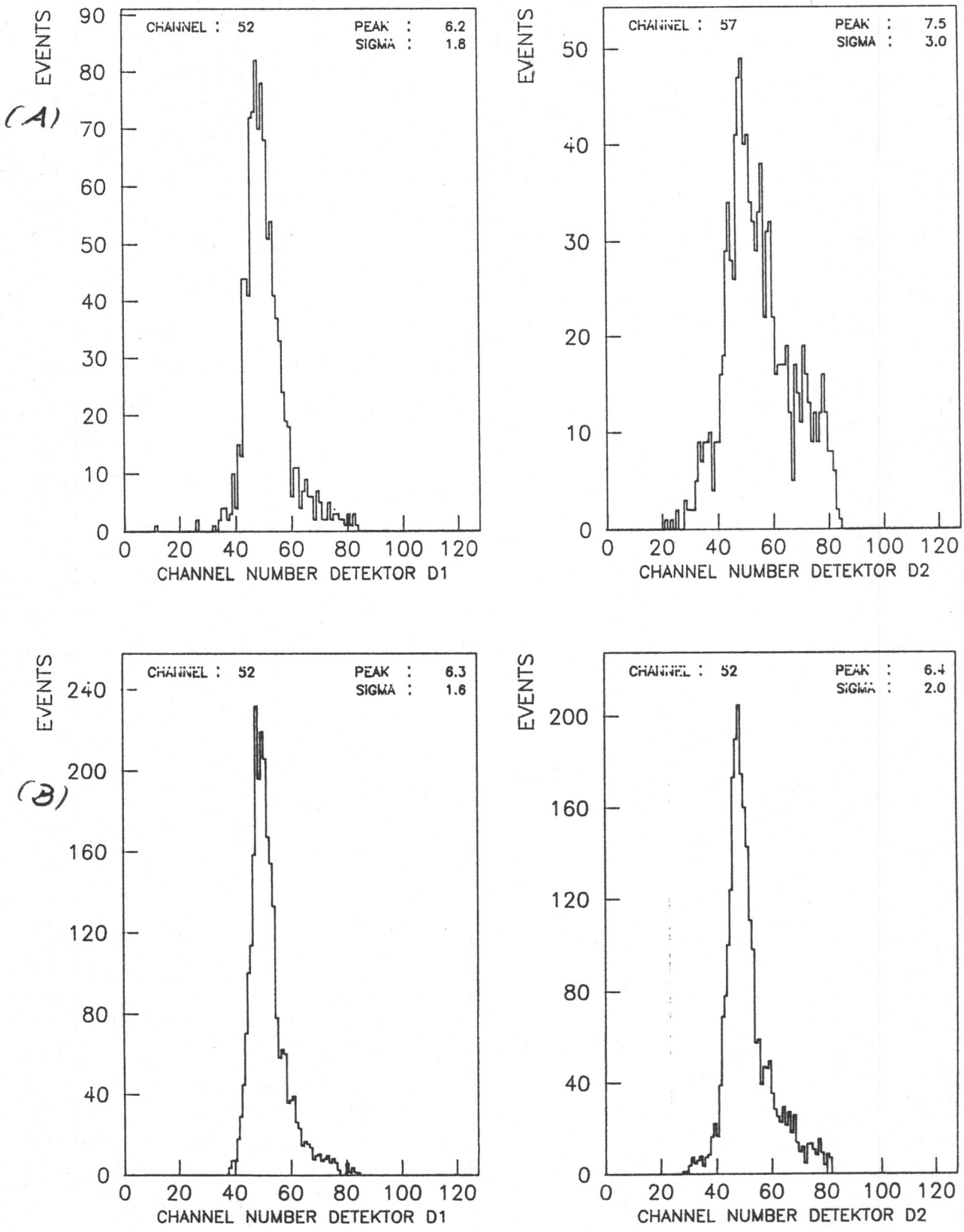

Figure 4-4 Pulse height distribution of the SFS detectors D1 and D2 for (a) 7.5 MeV electrons and (b) 185 MeV electrons

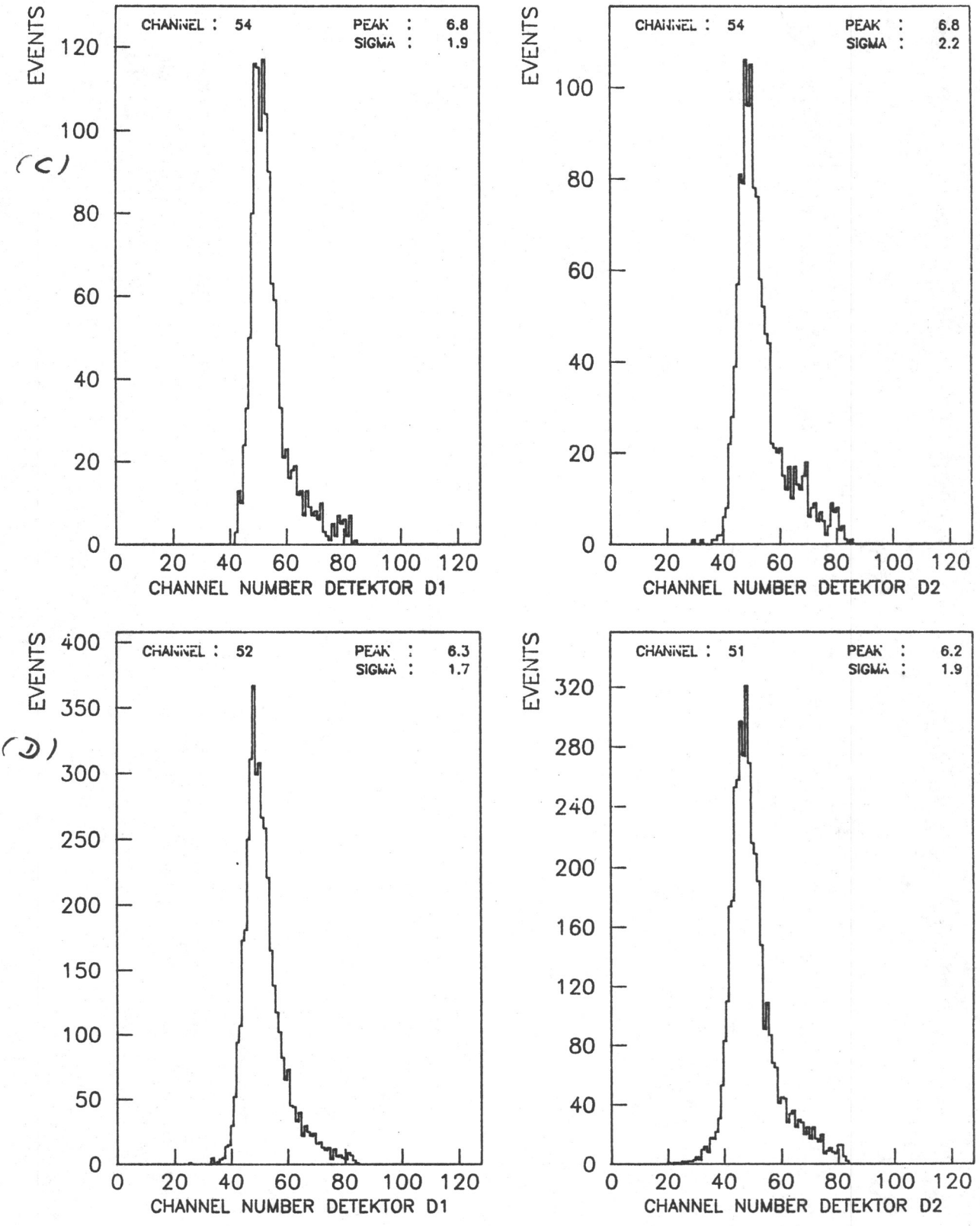

Figure 4-4 (continued) Pulse height distribution of the SFS detectors D1 and D2 for (c) 3000 MeV electrons and (d) 4150 MeV protons

4.1.2 Cerenkov Trigger Detector C1

4.1.2.1 Detector Response as a Function of Energy

Figure 4-5 (a) and (b) show peak location and width (at the 1σ-level) of the C1 pulse height distributions as a function of energy for electron energies between E_e = 7.5 MeV and E_e = 1000 MeV (open circles) and for one proton energy E_p = 4150 MeV (open diamond) for (a) the SFM detector and (b) the SFS detector. Electrons in this energy range effectively yield a saturation signal since the Cerenkov threshold for electrons in aerogel is approx. at E_e = 1 MeV (see below). Thus the average signal is basically constant with energy. The solid lines represent the computed Cerenkov signals as a function of energy for electrons and protons after an 'eye-ball' fit to the data points. The dashed line represents the electronic thresholds for the detection of light, the intersection of this line with the Cerenkov response for protons yields the lower detection threshold for the P4000-channel.

If one uses the measured gain of the photomultiplier tubes and the amplifiers, and assumes a quantum efficiency for the photocathode of Q_{eff} = 20%, then one can determine the average number of photoelectrons created at the photocathode by the passage of a high energy electron through the C1 to be $N_{Ph} \simeq 6$. The width of the pulse height distributions ($\sigma \simeq 60\%$) is larger than corresponding to the statistic of the photoelectrons. The silica aerogel material shows a significant amount of self-absorption for the light produced in the detector. Since the detector is viewed by only one multiplier from the side, one has to expect a broadening of the distribution due to geometrical effects, the light collected at the photocathode depends on the location where the particle traverses the material.

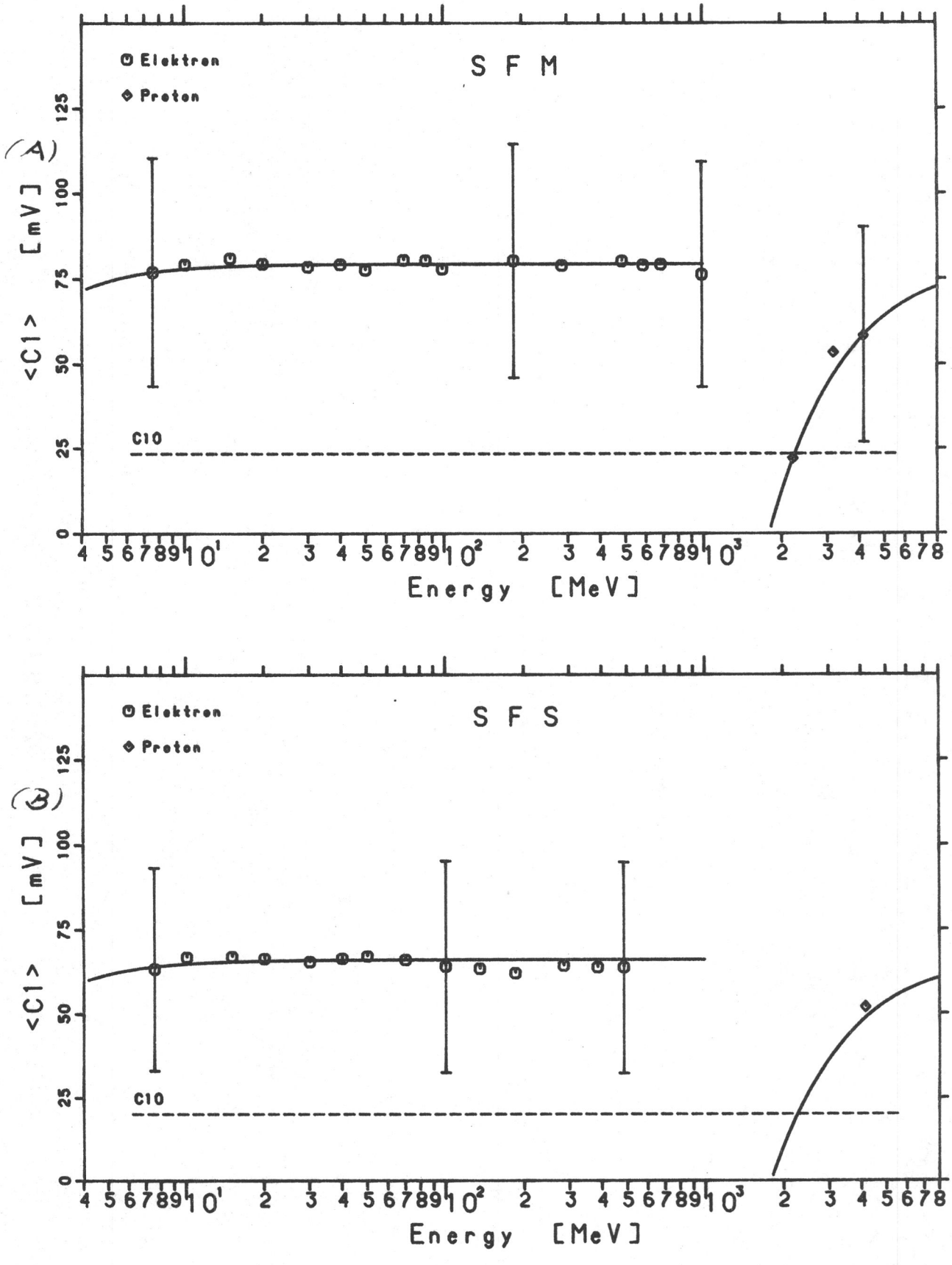

Figure 4-5 Peak location and width of the C1 - Cerenkov signal for (a) the SFM and (b) the SFS detector as a function of electron energy

4.1.2.2 Cerenkov Threshold for Protons

Figure 4-6 (a) and (b) show C1 pulse height distributions for (a) the SFM detector and (b) the SFS detector. The C1 detector

- serves as a discriminator between electrons and low energy protons and alpha-particles and
- determines the detection threshold for the highest (integral) proton and alpha-particle count rate channels - P4000 and A4000.

Protons, which trigger the C10 threshold, will be counted in the same channel as those electrons for which the C2-signal is too small to trigger the C21-threshold.

The density of the silica aerogel material can be chosen during manufacturing by varying the process temperature and pressure. Density ρ and refractive index n are related by the empirical formula $\rho \simeq 4(n-1)$. By choosing the process parameters accordingly, aerogel can be made with refractive indexes ranging from n = 1.01 to n = 1.10. At the very low densities, however, the aerogel material becomes too brittle and is therefore very difficult to handle. The detector material would not be able to withstand the vibration and shock levels during the launch of the instrument. As a compromise a material with a refractive index of $n \simeq 1.055$ was chosen for the KET, giving a Cerenkov threshold at $\beta \geq 0.948$ corresponding o a proton energy of $E_p \geq 2000$ MeV. The actual refractive index of the detector chosen was after manufacture determined by measuring the density of the material (this is however a difficult task and not very precise). It was therefore necessary to establish the detection threshold for protons with the detector integrated into the diffusive box using high energy particles.

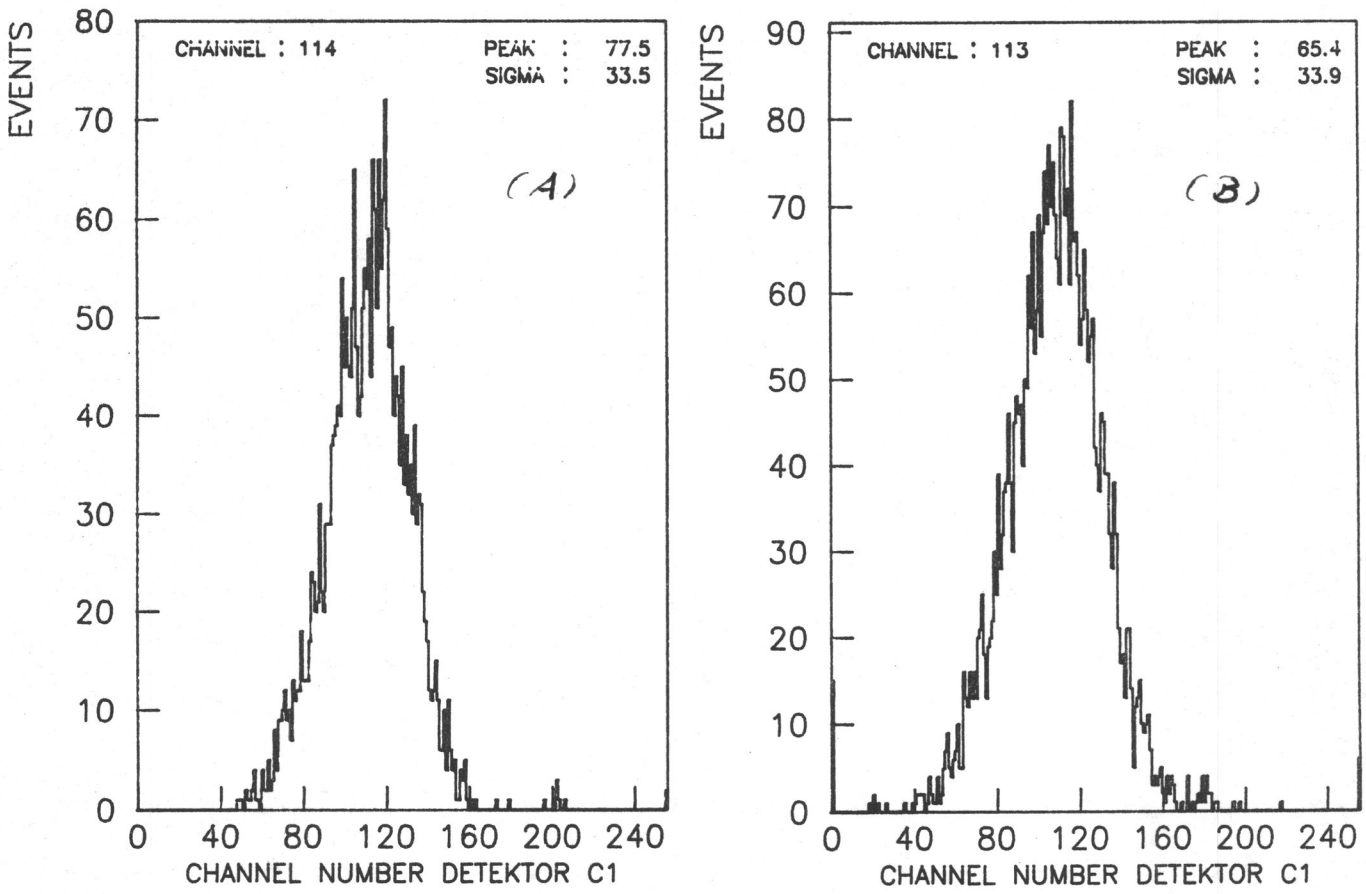

Figure 4-6 Pulse height distributions at an electron energy of 50 MeV measured at the AL600 for (a) the SFM and (b) the SFS sensor

Figure 4-7 (a)-(d) show C1 pulse height spectra for various proton energies measured at the CERN/PS at

(a) E_p = 4150 MeV (5 GeV/c),
(b) E_p = 3170 MeV (4 GeV/c),
(c) E_p = 2210 MeV (3 GeV/c and
(d) E_p = 1500 MeV (2.25 GeV/c).

Failure Mode 3 and 5 were set in all runs to enable registration of all particles entering the telescope. FM 5 results in all events being registered as E12-events allowing the analysis of the C1-spectrum. Setting of failure-

mode 3 will assure that those the particles, which do not create a signal in C1, will be analyzed too. They will registered in channel number '0' of the C1-spectrum.

The proton beam at CERN is contaminated with parasitic particles, namely Π^+, μ^+ and e^+. To discriminate against these unwanted particles, a separate CO_2-gas Cerenkov detector assembly integrated into the beam was used. The output signal of this detector was connected to the test input of the A-detector, creating an anticoincidence signal trigger in the KET instrument for each particle having a higher velocity than a proton. The maximum pressure attainable was P = 3.1 bar, effectively limiting the discrimination to beam momenta $M \geq 3$ GeV/c. The refractive index of CO_2 at P = 3.1 bar is n = 1.00143 giving a $\beta = 0.9986$: a Π^+ with $M \leq 2.59$ GeV/c will not be detected anymore. If one considers light losses in the Cerenkov detector due to self-absorption, and small collection efficiency due to the geometry of the detector, then the detection threshold will more likely be near M = 3 GeV/c.

The C1-spectra for E_p = 4150 MeV and E_p = 3170 MeV in figure 4-7 show undisturbed proton spectra with the peak decreasing with energy. Graph (c) shows the spectrum obtained at E_p = 2210 MeV. When compared to the undisturbed spectrum of graph (a), it is clearly visible that two different particle groups are represented in this spectrum. The proton distribution has shifted to the left and the parasitic pions can be found at higher channel numbers. At even lower energies (E_p = 1500 MeV) the protons are not fast enough anymore to reach the Cerenkov threshold, they have disappeared from the spectrum and only Π^+ are left. H. Sierks (1988) has attempted to subtract the pion distribution from graph (c) and to determine the peak location of the remaining proton distribution. He found a peak around channels 60-70 corresponding to U [mV] $\simeq$ 20-26.

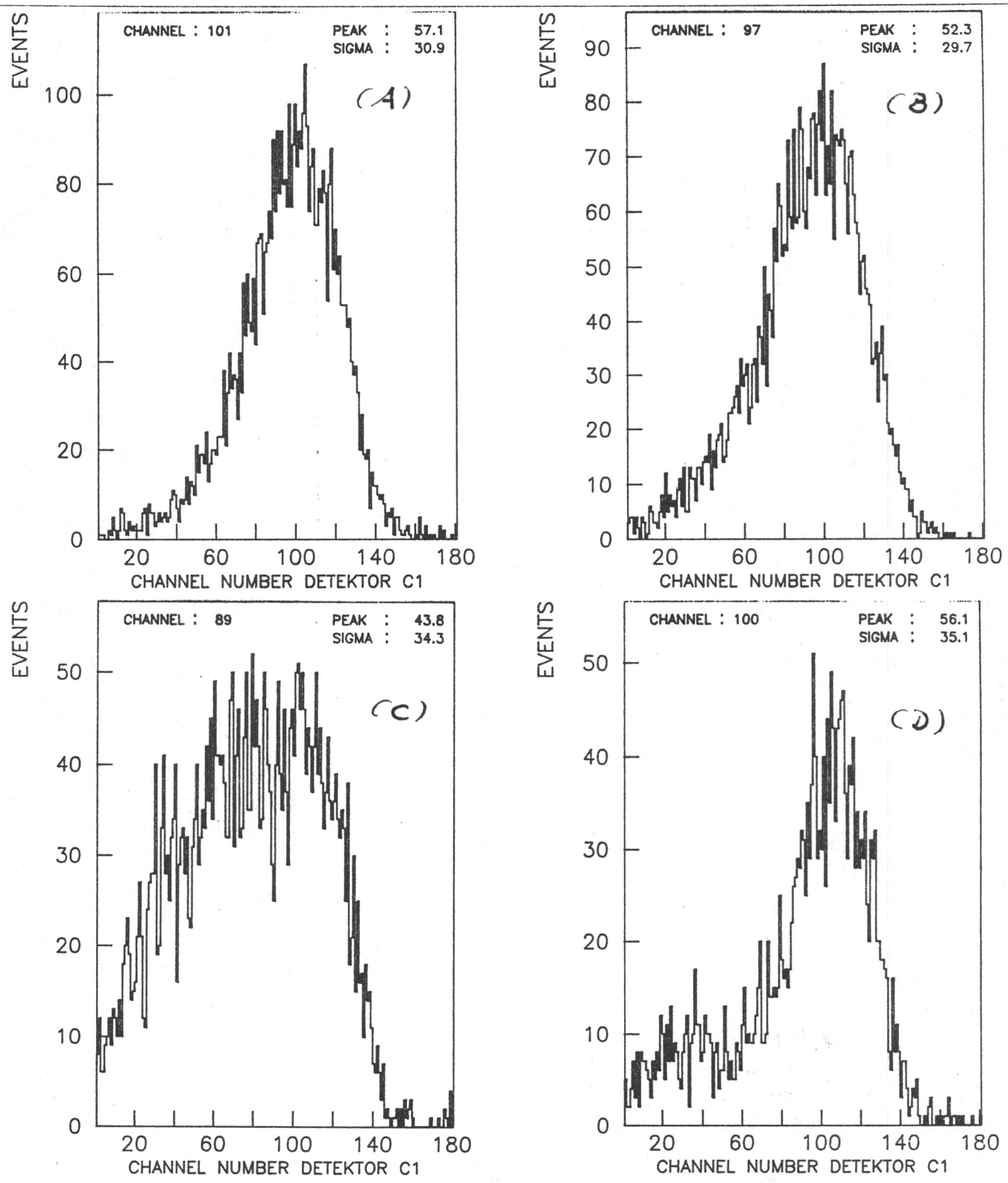

Figure 4-7 C1 pulse height spectra of the SFM sensor for different proton energies measured at CERN/PS: (a) E_p = 4150 MeV, (b) E_p = 3170 MeV, (c) E_p = 2210 MeV and (d) E_p = 1500 MeV

Figure 4-8 shows the peak locations (SFM) for protons and electrons as a function of $1/\beta^2$ (Sierks, 1988). The error bars for the two high energy data points are of the same size as the symbols. For the data point at E_p = 1500 MeV the error bar indicates the uncertainty with which the peak could be determined. The electron data is represented by the Cerenkov plateau (at β = 1, see figure 4-5) and by the peak for E_e = 7.5 MeV. All points fall reasonably well on or close to a straight line (solid), which intersects the abszissa at

$$1/\beta^2 = 1.136 \pm 0.007$$

The dashed lines represent the errors and the uncertainties and result in an error for $1/\beta^2$ of 0.007.

$$n = 1.066 \pm 0.003$$
$$\beta = 0.983 \pm 0.003$$

The resulting Cerenkov threshold for nuclei is

$$E_n = 1770 \pm 70 \text{ MeV/nuc}$$

and for electrons

$$E_e = 960 \pm 40 \text{ KeV}$$

Using the electronic threshold C10 (dashed horizontal line in figure 4-8), the energy thresholds for the integral countrate channels P4000 and A4000 can be determined:

$$1/\beta^2 = 1.096 \pm 0.006$$
$$\beta = 0.955 \pm 0.002$$
$$E_n = 2230 \pm 80 \text{ MeV/nuc}$$

The numbers are valid for the SFM only. The SFS-C1 spectra measured for different proton energies could not be evaluated. The spectra obtained with failure mode conditions 3 and 5 contain noise and background contributions of unknown source and magnitude.

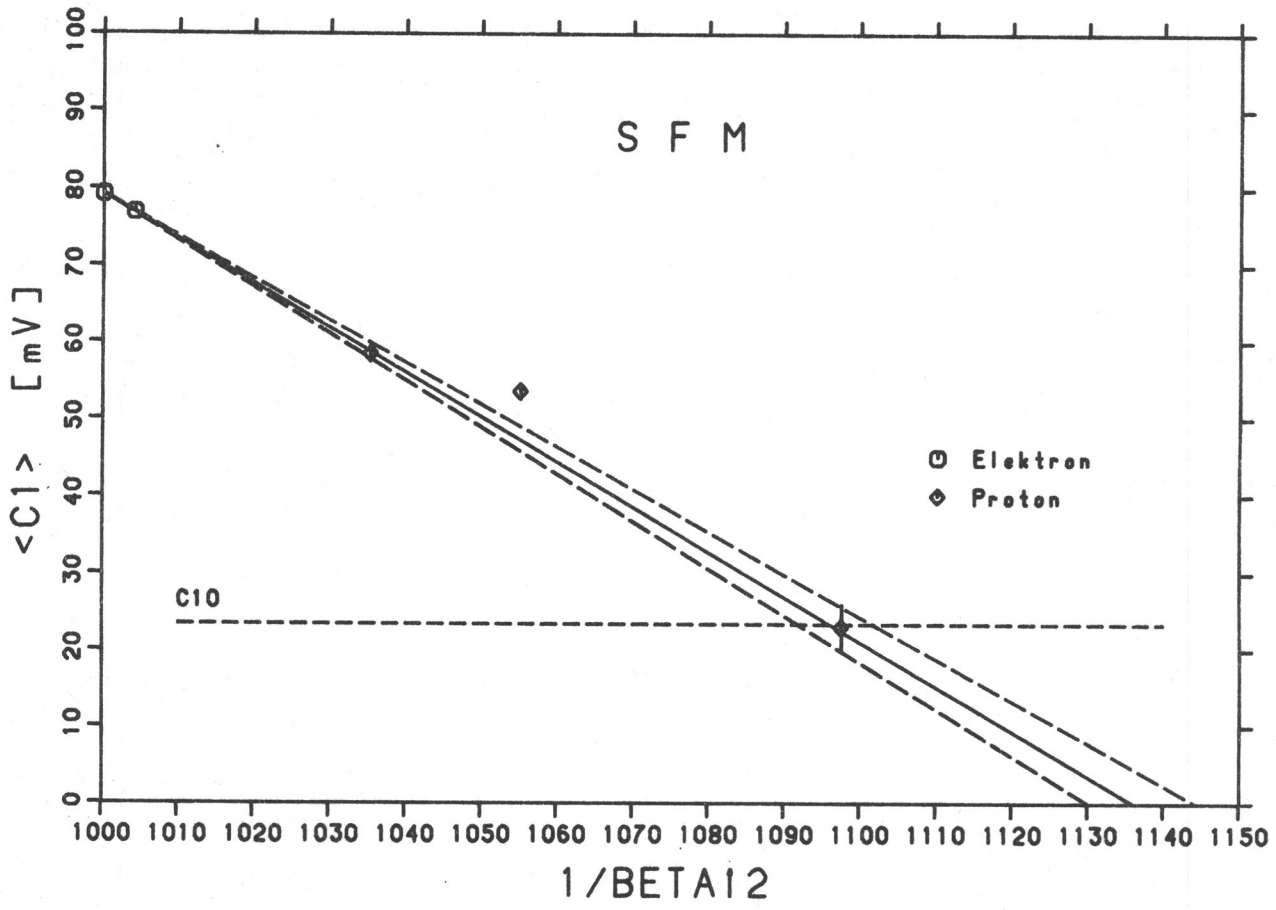

Figure 4-8 The average C1 signal of electrons and protons of different energies as a function of $1/\beta^2$. The electron value at $\beta = 1$ represents the plateau of figure 4-5 (Sierks, 1988)

Using the KET count rates to establish the Cerenkov threshold, one gets a similar result. In case a penetrating particle does not trigger the C10-threshold, it will not be counted as a P4000 or a E300. Instead, it will be registered in the P190 channel. The ratio

$$C1_{th}\ [\%] = \frac{P4000 + E300}{P190 + P4000 + E300} \cdot 100$$

should rise from '0' at the Cerenkov threshold and increase with increasing proton energy. Figure 4-9 shows a plot of $C1_{th}$ versus proton energy. $C1_{th}$ decreases initially with decreasing energy, as expected. Below an energy of approx. 2000 MeV, however, it is evident, that the instrument starts registering a particle species other than protons. We have attempted to establish the beam composition as a function of energy by varying the Cerenkov detector gas pressure. Table 4-1 summarizes the beam composition and indicates which particles are being analyzed by KET.

Table 4-1 CERN/PS beam composition as a function of energy

Momentum [GeV/c]	Beam Characteristic			
5	*p : 43%			$(e^+ + \mu^+ + \Pi^+)$: 57%
4	*p : 35%	(*)Π^+ : 41%		$(e^+ + \mu^+)$: 24%
3	*p : 30%	*Π^+ : 45%	e^+ : 5%	μ^+ : 20%
2		(*p + *Π^+) : 65%	e^+ : 12%	μ^+ : 23%
1		(*p + *Π^+ + μ^+) : 28%	e^+ : 72%	

* : This particle type is registered by KET
(*) : Only a fraction of this particle type is registered at this energy

From this table one can estimate the proton content of the beam at 2.5 GeV/c (E_p = 1730 MeV) to be between 20% and 25%. The data point at E_p = 1730 MeV can then be corrected to yield a Cerenkov threshold of $E_c \simeq$ 1670 MeV. The error bars in figure 4-9 are the statistical errors of the data points, the uncertainty in determining the proton content of the beam is much larger and is not known.

Figure 4-10 shows the same plot for the SFS, the Cerenkov threshold for protons is here $E_c \simeq$ 1700 MeV. Table 4-2 shows the same data also for electrons.

The gain setting of the photomultiplier strongly influences the detection efficiency. Included in the table are also the values for two proton energies, and for μ-mesons registered during test runs in Kiel.

From the data in figure 4-9 and 4-10 and from table 4-2 it is evident, that the response of the two instruments is not identical. Although we had tried to build the two sensors as identical as possible, the original Spare Model (now designated Selected Flight Model) shows a much better light collection efficiency than the SFS. This result was one factor in choosing this model as the preferred flight model.

Table 4-2 Detection efficiency of the C1-Cerenkov detector

Energy	Step 0		Step 2		Step 4	
	SFM	SFS	SFM	SFS	SFM	SFS
50	-	-	97.3	92.3	-	-
100	-	-	98.6	92.4	-	-
135	91.2	86.0	97.9	94.4	99.5	97.7
285	91.5	85.6	98.5	96.7	99.8	98.6
485	-	87.3	99.0	97.4	-	99.3
585	91.6	88.5	99.1	98.0	99.9	99.5
985	93.7	91.5	99.4	98.7	99.9	99.8
1185	-	-	99.6	98.9	-	-
3170	-	-	86.6	76.8	-	-
4150	-	-	89.7	83.5	95.3	89.1
μ-meson	70.2	-	86.1	81.6	-	-

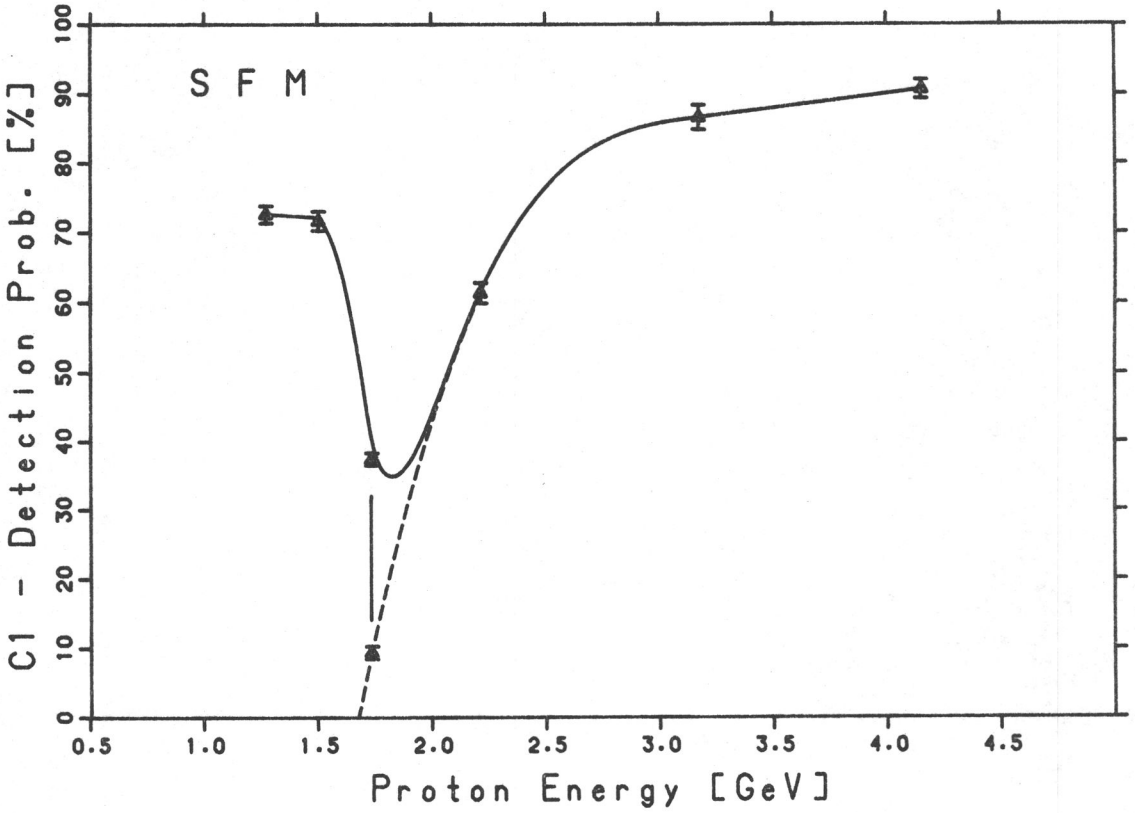

Figure 4-9 C1 detection probability as a function of energy for the SFM. The C1-threshold can be estimated to be at $E_p \approx 1670$ MeV

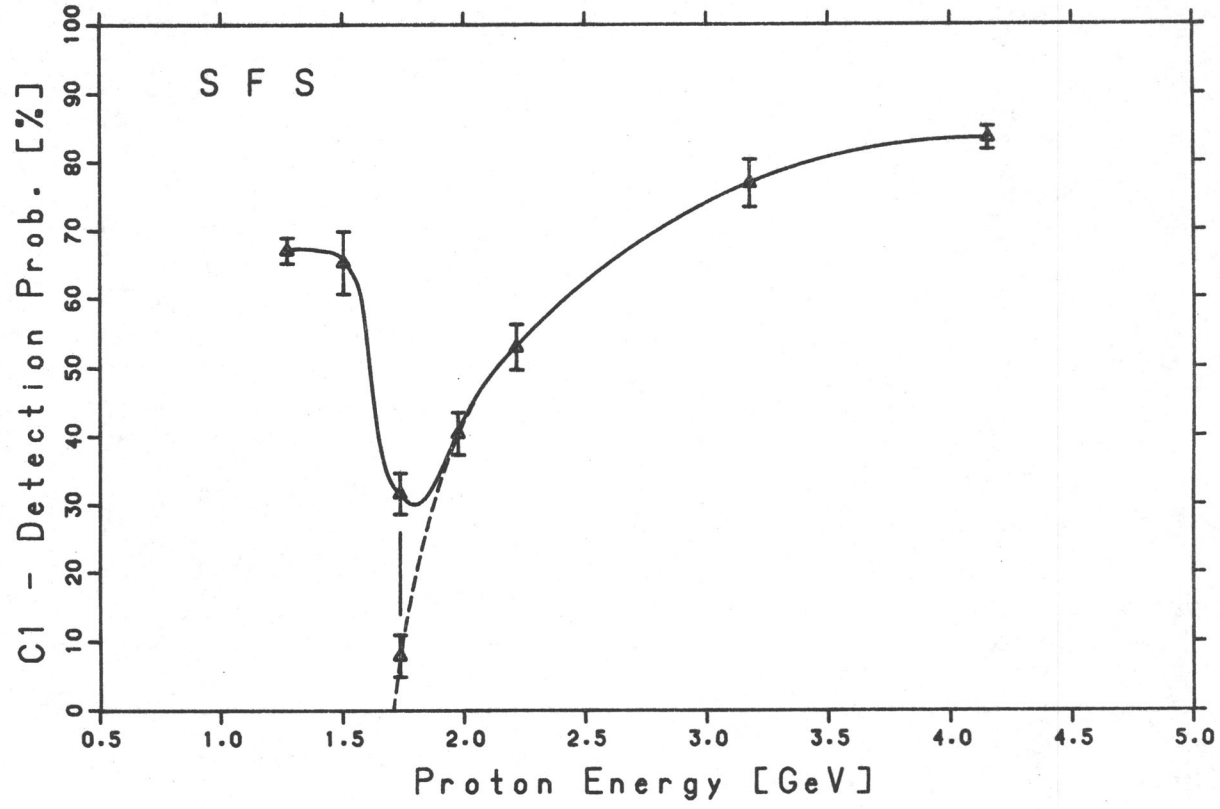

Figure 4-10 C1 detection probability as a function of energy for the SFS. The C1-threshold can be estimated to be at $E_p \approx 1700$ MeV

4.1.3 Lead Fluoride Cerenkov Calorimeter C2

Figure 4-11 (a) and (b) show the peak location of the C2-spectra as a function of energy combining data from four different accelerators. The DESY data points were taken in November 1984, a preliminary evaluation of the detector responses led to the decision to lower the photomultiplier gains and the amplification factors of the C2 and S2 channels for both instruments. The energetic electrons caused saturation effects and the peak location for protons was estimated to be too close to the C21-threshold (which separates high energy electrons from the high energy protons). These data points have been scaled at low energies to fit to the data obtained with the other accelerators. Errors in the graph indicate the width of the distributions at the 1σ-level, not the error of the mean for each peak location. For most spectra, the number of recorded events was so large that the error of the mean of the distribution is quite small.

Results of Monte-Carlo shower simulations (Julliot, 1980) have been added to the graphs after normalization at E_e = 200 MeV. The instrument responses follow very closely the predicted theoretical values. The abscissa is scaled in units of [mV] and is equal to the test signal which generates a charge equivalent to the charge signal of the photomultiplier. For any given photomultiplier high voltage is the signal height equivalent to a specific number of photoelectrons created at the photocathode by the light produced by an energetic charged particle passing through the detector.

High energy protons give the same detector response as electrons with E_e = 40 MeV, this signal corresponds (see table 2-3) to $N_{ph} \simeq 19$ photoelectrons for the SFM and to $N_{ph} \simeq 12$ photoelectrons for the SFS. The responses calculated using the Monte Carlo shower simulation do not fit in absolute values to the experimental data points since the calculation does not consider the effects of light losses in the detector, in the diffusive box, and in the photocathode. Figures 4-12 (a)-(d) and 4-13 (a)-(d) show C2 pulse height spectra of the SFM and the SFS respectively for the following particles and energies

(a) E_e = 50 MeV electrons (coincidence channel E12)
(b) E_e = 500 MeV electrons (coincidence channel E300+P400)

(c) E_e = 1200 MeV electrons (coincidence channel E300+P4000)
(d) E_p = 4150 MeV protons (coincidence channel E300+P4000)

If one compares the width of the proton peak distribution to the electron distributions one can clearly see the effect the shower statistics have on the shape of the electron spectra - they are dominated by this statistic. The distribution for protons is basically governed by the small number of photons hitting the photomultiplier faceplate. The width of the pulse height distribution for high energy protons is at the 1σ-level $\sigma(C2)/\langle C2\rangle$ = 36.6% for the SFM and $\sigma(C2)/\langle C2\rangle$ = 48.4% for the SFS. Figure 4-14 (a) and (b) shows the width of the pulse height distributions of absorption mode particles as a function of energy for the SFM and the SFS for (the particle energy is completely absorbed in the calorimeter, this does not include the fraction of the energy escaping the instrument in the way of γ-particles), and figure 4-15 (a) and (b) the same for penetration mode particles (only a fraction of the total energy is absorbed in the calorimeter and at least one shower particle has triggered the S2-detector). Also included are the results of the model calculation (Julliot, 1980), an 'eye-ball' fit has been drawn through these values. The calibration data points scatter strongly, but agree basically with the model predictions. The variance is constant at a value of $\sigma(C2)/\langle C2\rangle \simeq 40\%$ for particle energies up to E_e = 100 MeV, for energies larger than that it increases slowly due to a smaller fraction of the particle energy being absorbed in the detector.

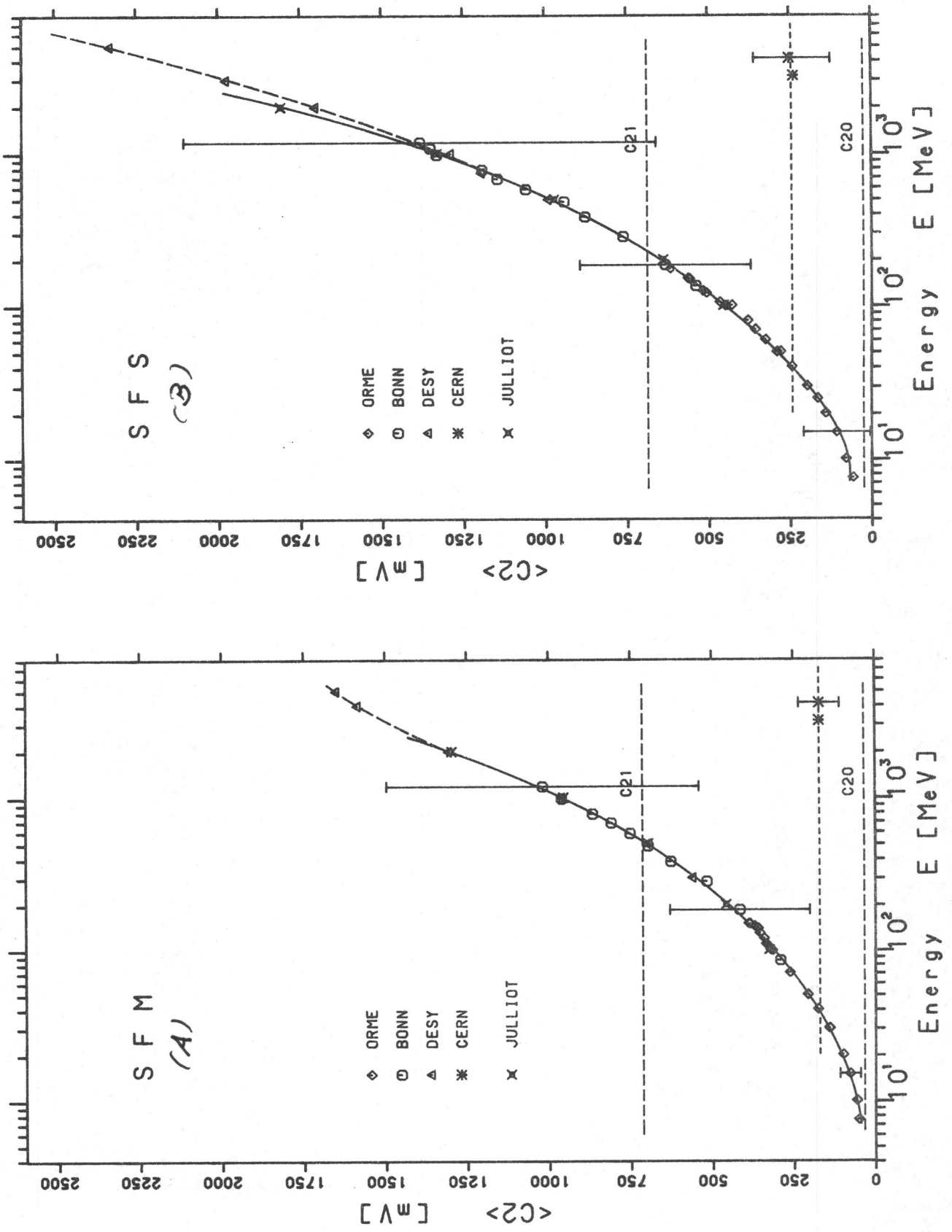

Figure 4-11 Peak location (mean) and variance of the C2 pulse height distributions as a function of energy for the SFM (a) and the SFS (b). The error bars do not denote the error of the mean, but represent the width of the distribution

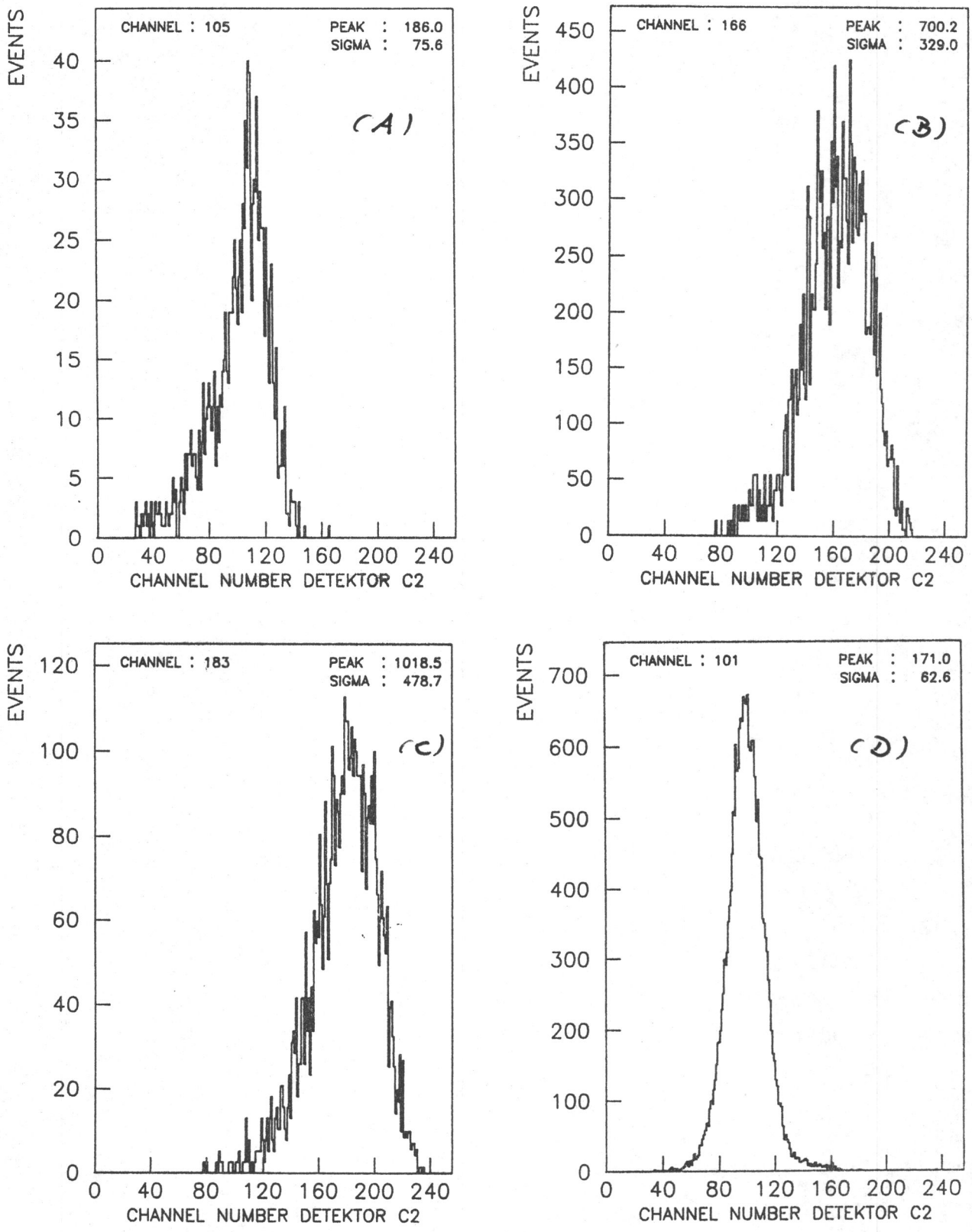

Figure 4-12 SFM C2 pulse height spectra of (a) E_e = 50 MeV electrons, (b) E_e = 500 MeV electrons, (c) E_e = 1200 MeV electrons and (d) E_p = 4150 MeV protons

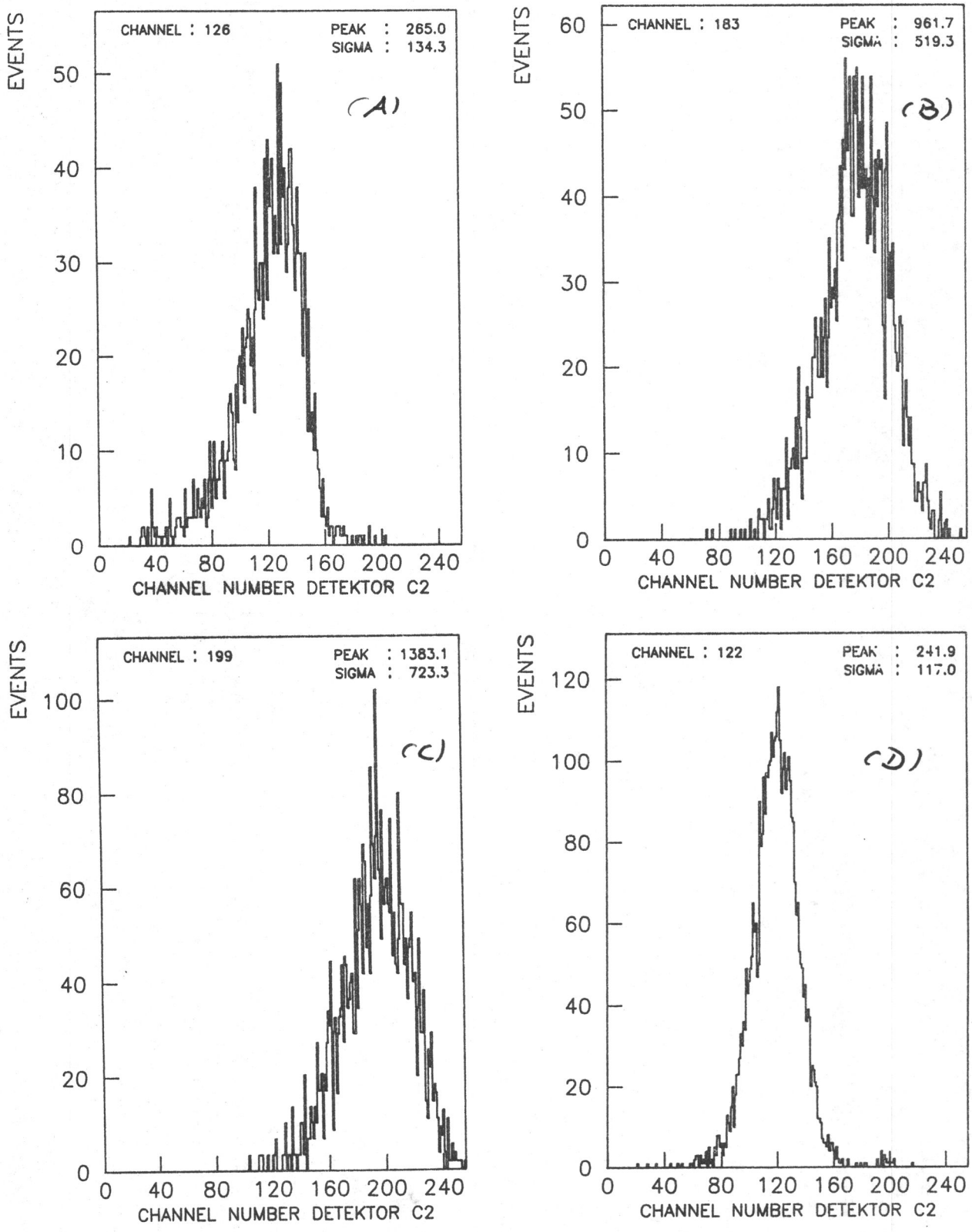

Figure 4-13 SFS C2 pulse height spectra of (a) E_e = 50 MeV electrons, (b) E_e = 500 MeV electrons, (c) E_e = 1200 MeV electrons and (d) E_p = 4150 MeV protons

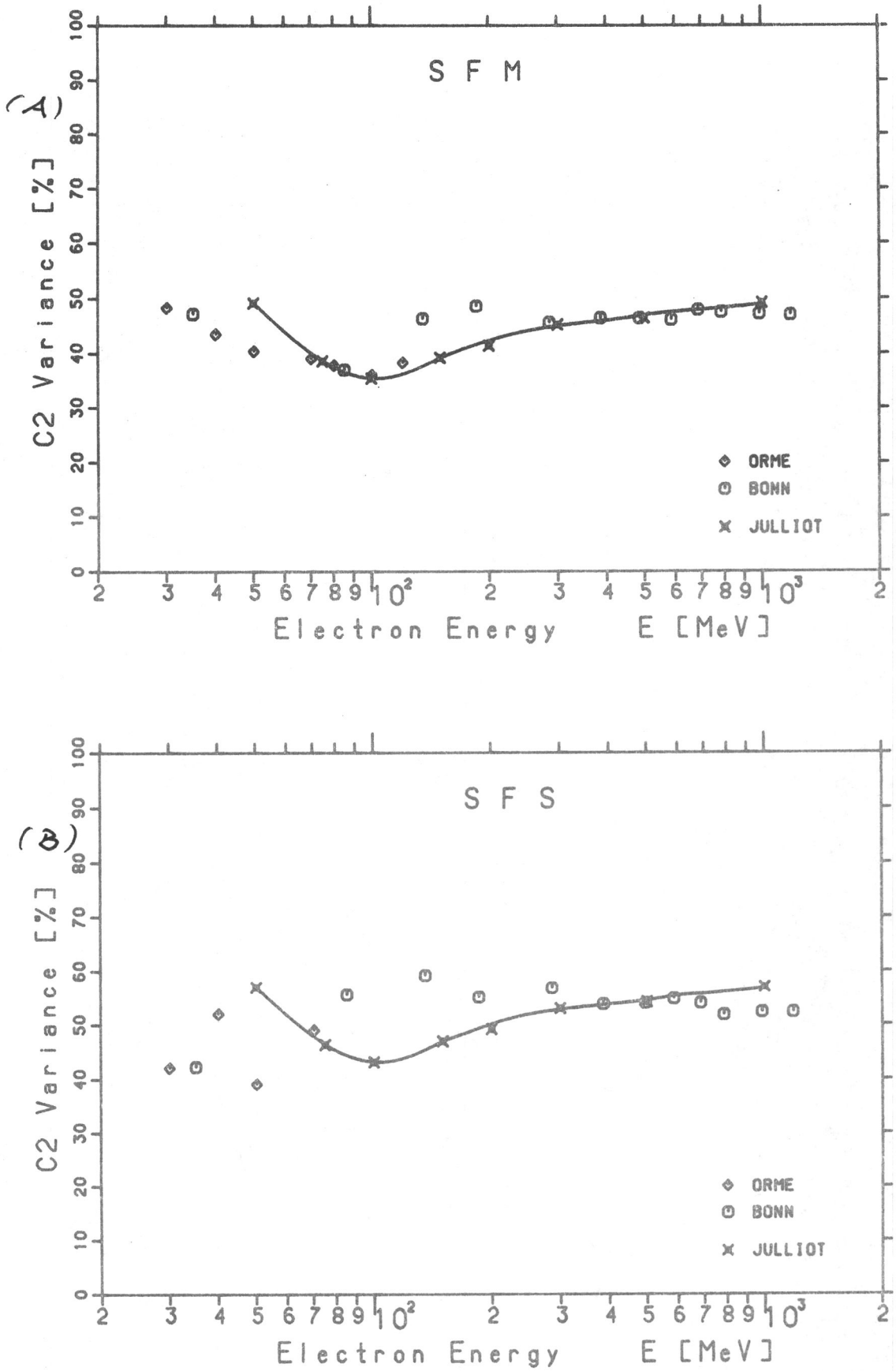

Figure 4-15 Variance of the pulse height distributions in C2 for penetration mode electrons as a function of energy for the SFM (a) and the SFS (b)

4.1.4 Scintillation Detector S2

The plastic scintillation detector S2 (material NE104) is used mainly to discriminate between events where a particle or a shower is completely absorbed in C2 (absorption mode) and those events where either the particle penetrates C2 or at least one shower particle leaves C2 and reaches S2 (penetration mode). Together with the A detector it forms a complete enclosure of the central calorimeter, assuring that no particle can leave (or enter) the calorimeter undetected, except through the front aperture. The shape of the S2 is dictated by the fact, that it has to enclose the C2 diffusive box completely, and that light produced at locations far away from the photomultiplier is collected as efficiently as possible at the photocathode.

Figure 4-16 (a) and (b) shows the peak location of the S2-spectra as a function of energy for the SFM and the SFS respectively. The symbols used for the data points are the same as in figure 4-11. High energy protons give the same detector response as electrons having E_e = 125 MeV for the SFM and E_e = 90 MeV for the SFS. Since the signal produced by these protons is that of a single minimum ionizing particle, the corresponding electron energies are those for which the average number of shower electrons escaping from C2 is $\langle nes \rangle = 1$. The corresponding number of photoelectrons is $N_{ph} \simeq 350$ for the SFM and $N_{ph} \simeq 340$ for the SFS (see table 2-3). Figure 4-17 (SFM) and 4-18 (SFS) show S2 pulse height distributions for

(a) E_e = 100 MeV electrons (coincidence channels E300+P4000)
(b) E_e = 500 MeV electrons (coincidence channels E300+P4000)
(c) E_e = 1200 MeV electrons (coincidence channels E300+P4000)
(d) E_p = 4150 MeV protons (coincidence channels E300+P4000)

The double peak structure visible in the proton spectrum is an unwanted side effect of the efforts to optimize light transmission in the detector. Since the proton beam diameter at CERN was larger than the instrument aperture, the individual protons penetrated the detector at different locations with different material thicknesses.

During the design and development phase of the sensor, a number of S2-detectors with different shapes and surface treatments were tested to find the most efficient form. The largest negative impact on the uniformity of light transmission is caused by the necessity for the C2 photomultiplier to view the diffusive box through a hole in the side wall of the S2. This required an extension to the S2-base so as not to allow penetrating particles to escape through this hole undetected. As one can see from figure 2-1, material thickness varies strongly for particles with angles of incidence between $\phi = -3°$ and $\phi = +20°$ (the + sign denotes angles of incidence towards the C2-photomultiplier). Machining of this detector was very difficult, it proved to be impossible to manufacture a more uniform single detector. The consequences of the nonuniform S2-response are

- large width of the pulse height distribution,
- number of particles in a shower cannot be determined for a single event.

Figure 4-19 (a) and (b) show the variance of the S2-distributions as a function of energy for the electron calibrations, data points from shower calculations are not available for this detector.

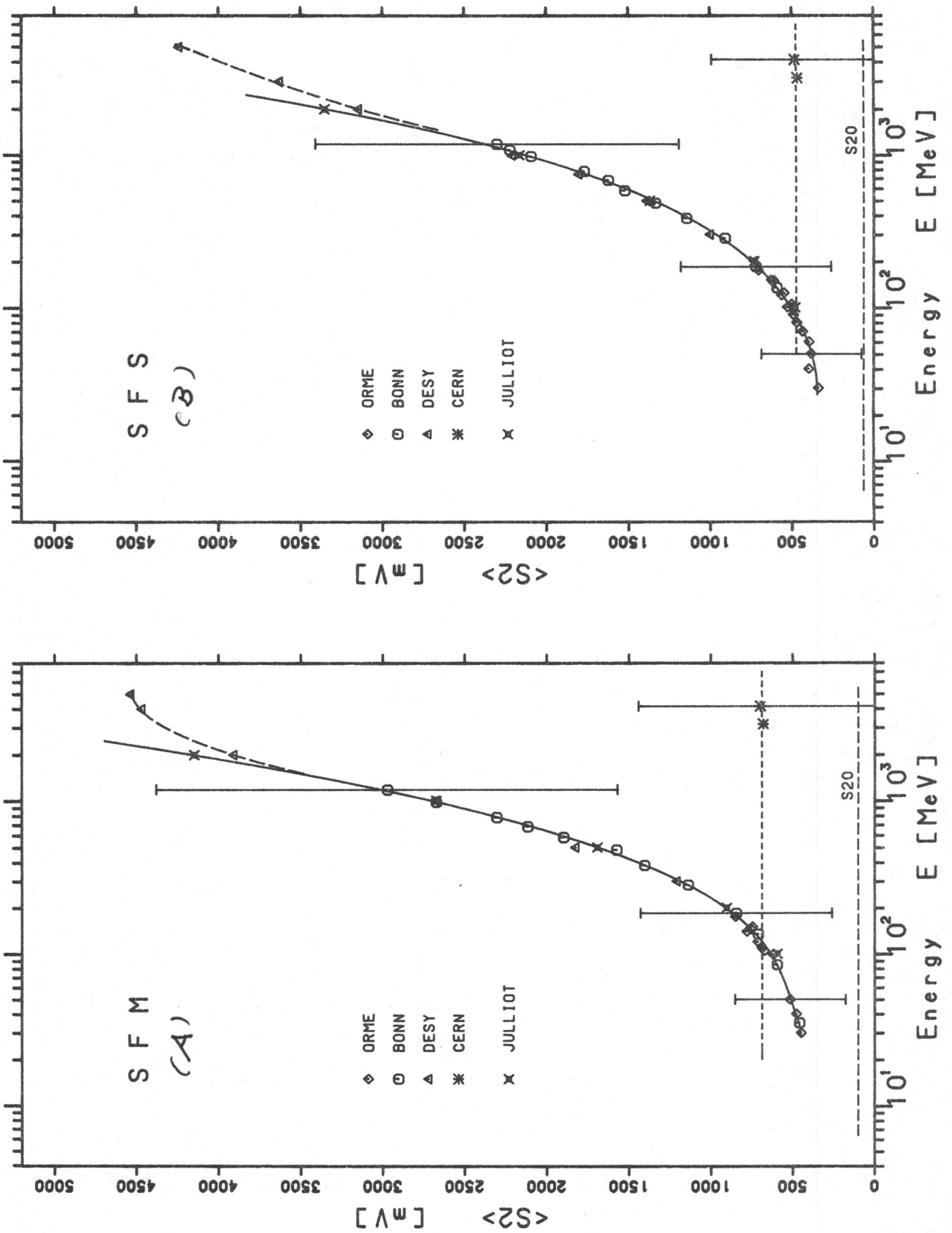

Figure 4-16 Peak location (mean) and variance of the S2 pulse height distributions as a function of energy for the SFM (a) and the SFS (b).

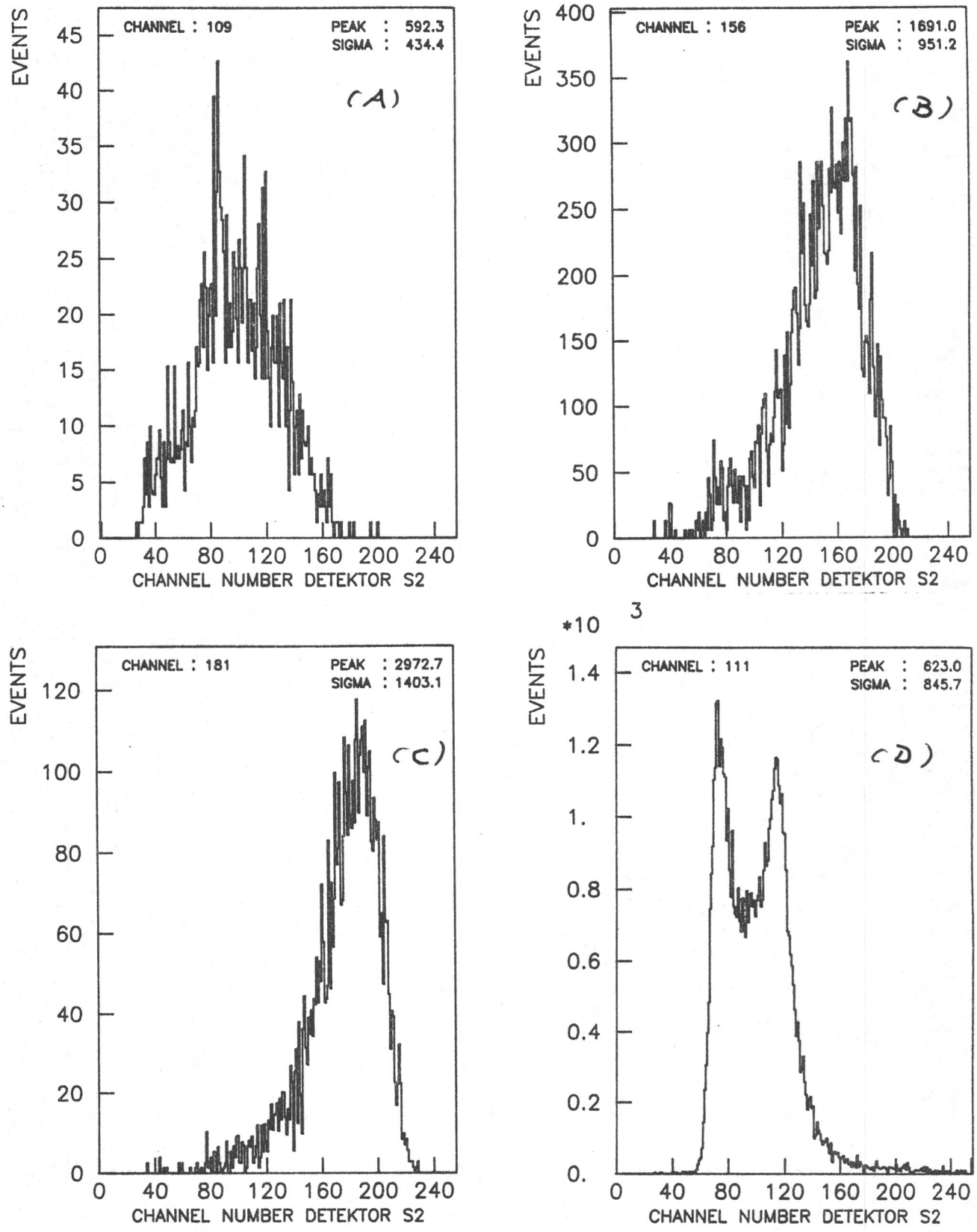

Figure 4-17 SFM S2 pulse height spectra of (a) E_e = 100 MeV electrons, (b) E_e = 500 MeV electrons, (c) E_e = 1200 MeV electrons and (d) E_p = 4150 MeV protons

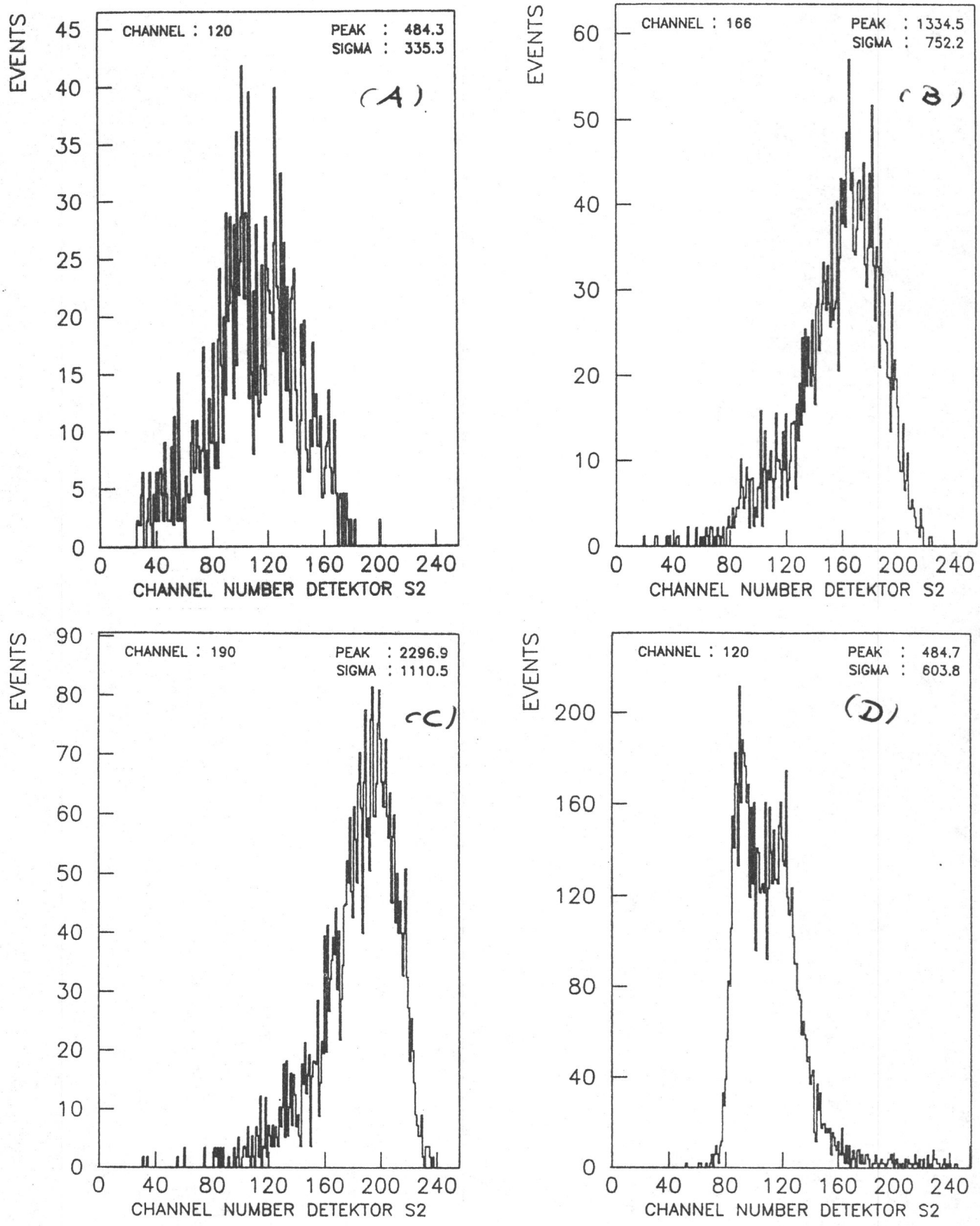

Figure 4-18 SFS S2 pulse height spectra of (a) E_e = 100 MeV electrons, (b) E_e = 500 MeV electrons, (c) E_e = 1200 MeV electrons and (d) E_p = 4150 MeV protons

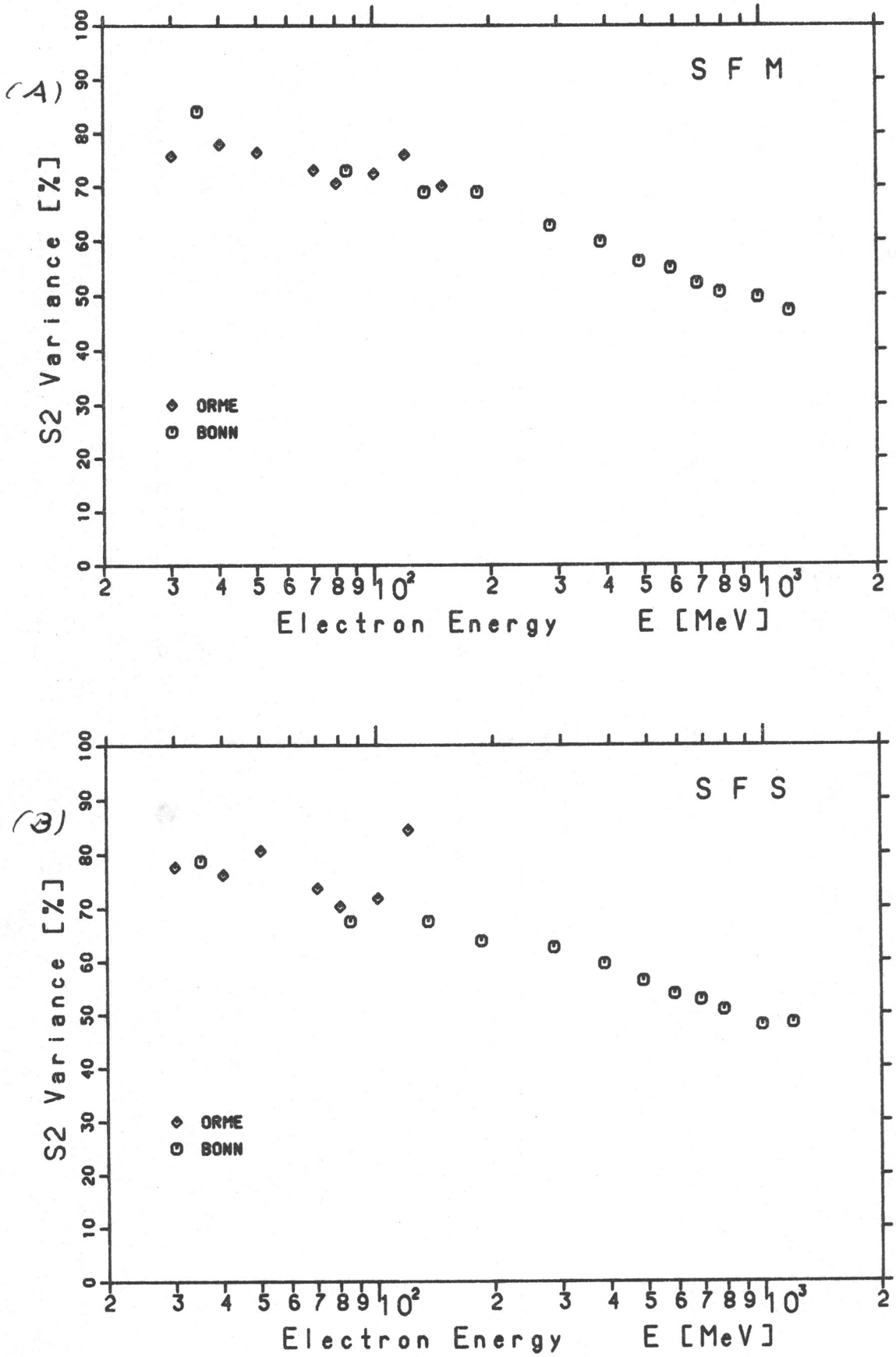

Figure 4-19 Variance of the pulse height distributions in S2 for penetration mode electrons as a function of energy for the SFM (a) and the SFS (b)

4.2 Response of the Telescope

4.2.1 Absorption

The KET registers incident particles in one of two categories: (a) as an event with the energy totally absorbed in the calorimeter detector, i.e. S2 is not triggered and (b) as a penetrating event, i.e. S2 has been triggered - a part of the total energy has escaped detection. Figure 4-20 shows the computed absorption probability (Julliot, 1980)

$$F_{abs} = \frac{N_{(abs=1)}}{N_{tot}}$$

with

$$N_{(abs=1)} = E4+E12 \quad , \quad N_{tot} = E4+E12+E300+P4000$$

and the measured absorption factor as a function of energy. SFM data points are denoted by an open square, the SFS points by an open circle and the computed probability by a star. The values for the calculated absorption factor have been connected by straight lines. Except for the data points at very high energies, the measured data fits the model calculations very well.

4.2.2 Angular Response

During flight, particles will enter the aperture from all directions isotropically. Figure 4-21 shows the gathering power (differential geometrical factor)

$$dF = 2\,\pi\,\cos\theta\,\sin\theta\,d\theta\,A(\theta)$$

as a function of the angle of incidence θ. The directional response function $A(\theta)$ (Sullivan, 1971) describes the gathering power of a telescope consisting of two circular parallel detectors with the respective radii R_1 and R_2 and distance ℓ and is given by

$$A(\omega) = A(\theta,\phi) = \pi R_s^2 \cos\theta \qquad ,\theta_c \geq \theta \geq 0$$

$$= \cos\theta \, [0.5 R_1^2 (2\Psi_1 - \sin 2\Psi_1) + 0.5 R_2^2 (2\Psi_2 - \sin 2\Psi_2)] \qquad ,\theta_m \geq \theta \geq \theta_c$$

$$= 0 \qquad ,\theta \geq \theta_m$$

with $R_s = \min (R_1, R_2)$

$$\theta_c = \tan^{-1}\left[\frac{\text{abs}(R_1 - R_2)}{\ell} \right]$$

$$\theta_m = \tan^{-1}\left[\frac{R_1 + R_2}{\ell} \right]$$

$$\Psi_1 = \cos^{-1}\left[\frac{R_1^2 + \ell^2 \tan^2\theta - R_2^2}{2\ell R_1 \tan\theta} \right]$$

$$\Psi_2 = \cos^{-1}\left[\frac{R_2^2 + \ell^2 \tan^2\theta - R_1^2}{2\ell R_2 \tan\theta} \right]$$

In the case of the KET, the geometry is defined by two surfaces (see figure 2-1) :

(1) the aperture of the anticoincidence detector A, and
(2) the active area of the D2 detector.

The actual response of a telescope may differ from the geometrically expected response for a number of reasons, one of them being the fact that a detector usually does not respond completely uniformly to particles hitting it at different points. To verify the angular response and to determine the 'effective geometry' - i.e. to find the actual values for R_1, R_2 and ℓ - is an important task to be performed with the help of a particle accelerator. Measurements of this response were therefore performed at all accelerators for a few selected energies. The angle of incidence - in the horizontal plane as referred to the instrument axis (see figure 3-1) - varied between $\theta = -22°$ to $\theta = +22°$. The energies used were at

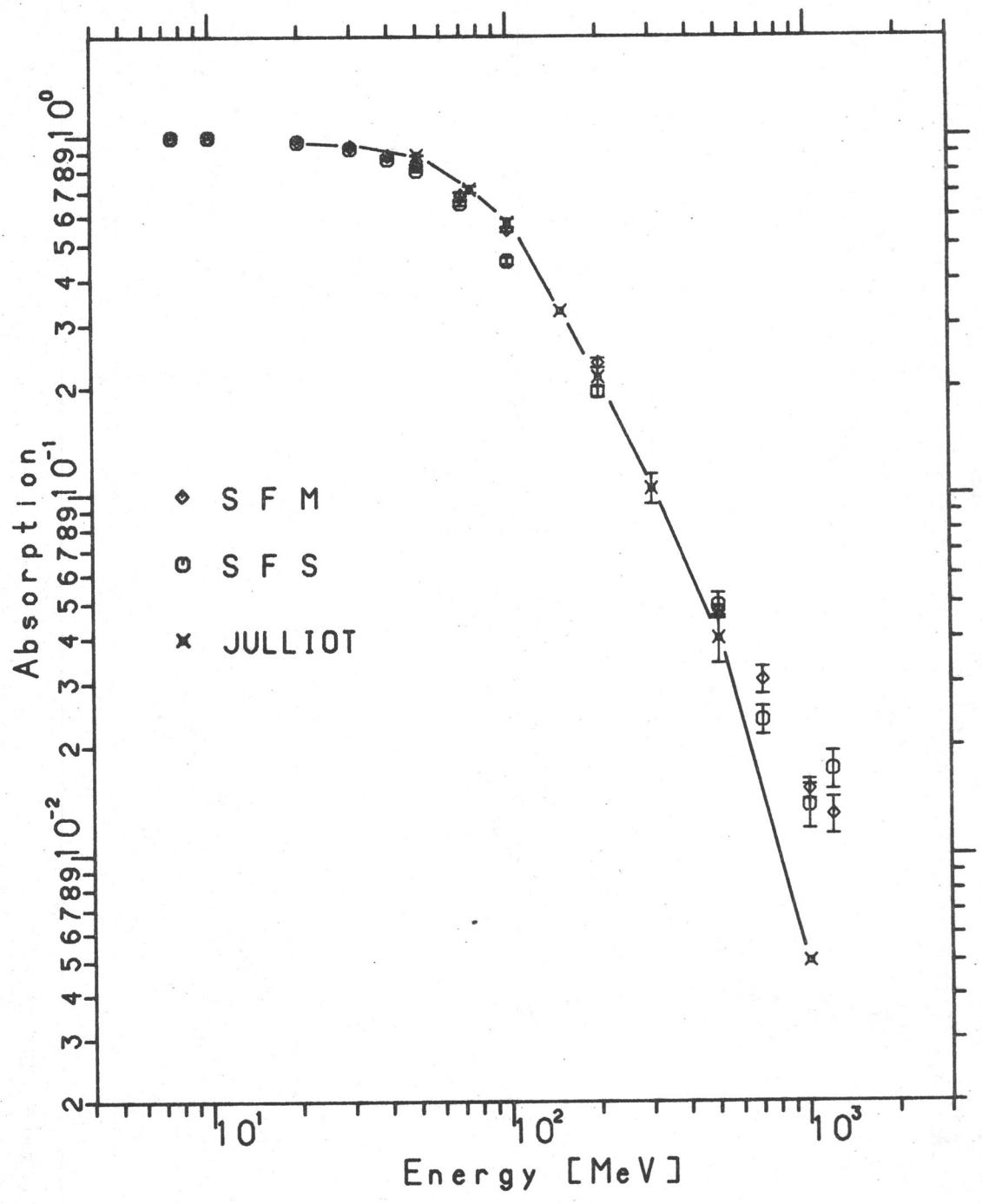

Figure 4-20 KET measured absorption mode probability for SFM (open square), SFS (open circle) and computed absorption mode probability (star) as a function of electron energy

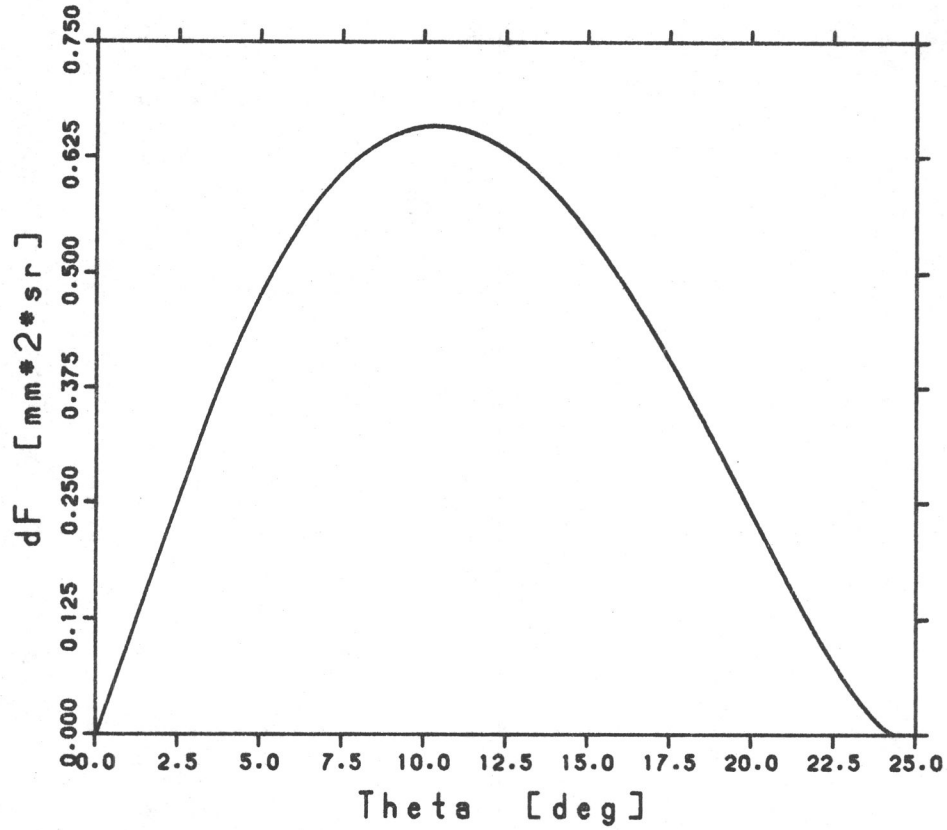

Figure 4-21 KET differential geometrical factor $dF = 2\pi \cos\theta \sin\theta \, d\theta \, A(\theta)$ as a function of the angle of incidence θ ($A(\theta)$: directional response function (Sullivan, 1971))

- CERN : E_p = 4150 MeV
- ORME : E_e = 50 MeV
- BONN : E_e = 485 MeV

To test the response to backward incident particles, measurements were taken for $\theta = 180°$ at

- CERN : E_p = 4150 MeV
- BONN : E_e = 85, 485 and 985 MeV

4.2.2.1 Geometrical Factor

Considering the shape of the A-detector, one can see that only a small fraction of the scintillation light, which has been produced by a particle hitting the inner edge of the A-detector aperture, will be registered by the PM4-photocathode. In order to reach the photomultiplier, the light has to undergo a large number of reflections, each of which causes a loss of light. If the amount of light is too small, the A0-threshold will not be triggered. Thus, the 'effective aperture' might be somewhat larger than the geometrical opening. Likewise, the D2 active area may be larger than the surfaces covered by the electrodes, it may even extend to the full wafer diameter.

The CERN/PS beam could not be collimated, so we did not have a well defined beam to probe the geometry of the detector arrangement. Instead, the beam diameter was so large, that it could be considered to approximately represent isotropically incident particles. Figure 4-22 shows the result of the CERN/PS angular measurements for the SFM (August '85). Different symbols show the relative contributions of the energy channels to the overall detection of protons. The curve labeled 'SUM' represents the sum of the three penetration mode channels P190, P4000 and E300. The number of events recorded by the KET were normalized for each individual run to the number of events recorded by the T1T2-scintillation telescope (see figure 3-2). As one can see from figure 4-22, the data points are arranged symmetrically around an angle of incidence $\theta = 0°$, thus, the instrument was aligned well with the beam axis. The solid line superimposed on each set of points represents the instrument response function with the parameters chosen to best match the data points. The corresponding values of the instrument parameters are

- aperture diameter $R_1 = 34$ mm
- D2 diameter $R_2 = 26$ mm (wafer diameter is d = 27 mm)
- distance A-D2 $\ell = 66.2$ mm

The best fit was chosen by comparing the measured response to a set of curves describing the instrument response function obtained by varying the parameters R_1 and R_2, the same values fit both instruments. The value chosen for the aperture R_1 is larger than the 'real' diameter of the opening (Ø = 31 mm) by 3

mm, defining an 'effective aperture'. This need to use a larger opening could well be explained by assuming that high energy particles do not deposit enough energy in an area close to the edge of the aperture opening for the particle to be detected. The light has to travel a long way in the A-detector before it reaches the photomultiplier, however, an asymmetric response could not be found. The geometrical factor and the full opening angle derived from these values are therefore

$$\underline{G = 1.03 \text{ cm}^2 \text{ sr} \quad \text{and} \quad \gamma = 48.8^\circ}$$

The number of high energy protons recorded in the P190 coincidence channel differ significantly for both instruments. The SFM registers 88% of all particles as P4000-type events and 10% as P190, whereas the SFS registers only 82% P4000 and 16.5% as P190. Although the C1-threshold is lower for the SFS than for the SFM, more protons pass the SFS-C1 undetected. One has to conclude therefore, that the SFM-C1 light collection efficiency is better due to less self-absorption of photons in the C1 material. The remaining approx 1.5% of the particles are recorded as P116 and E12, which have been omitted from the graph.

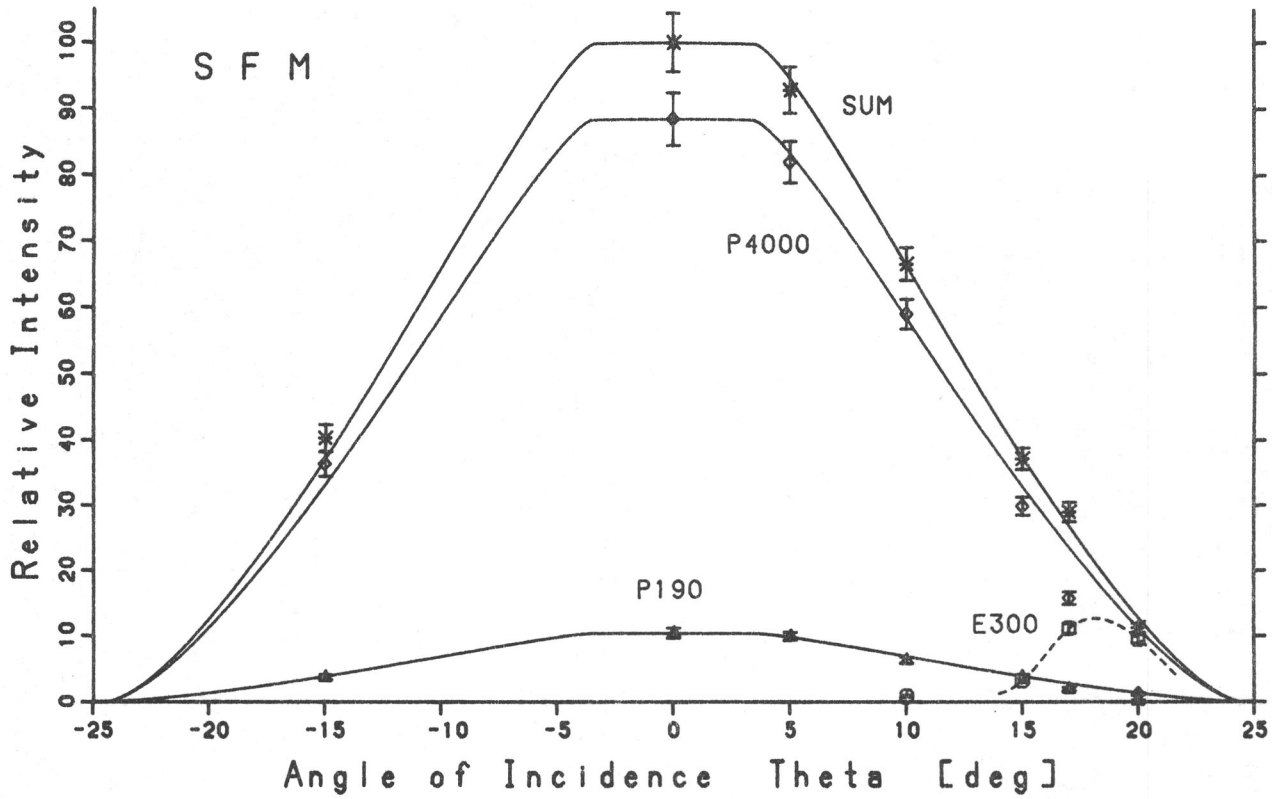

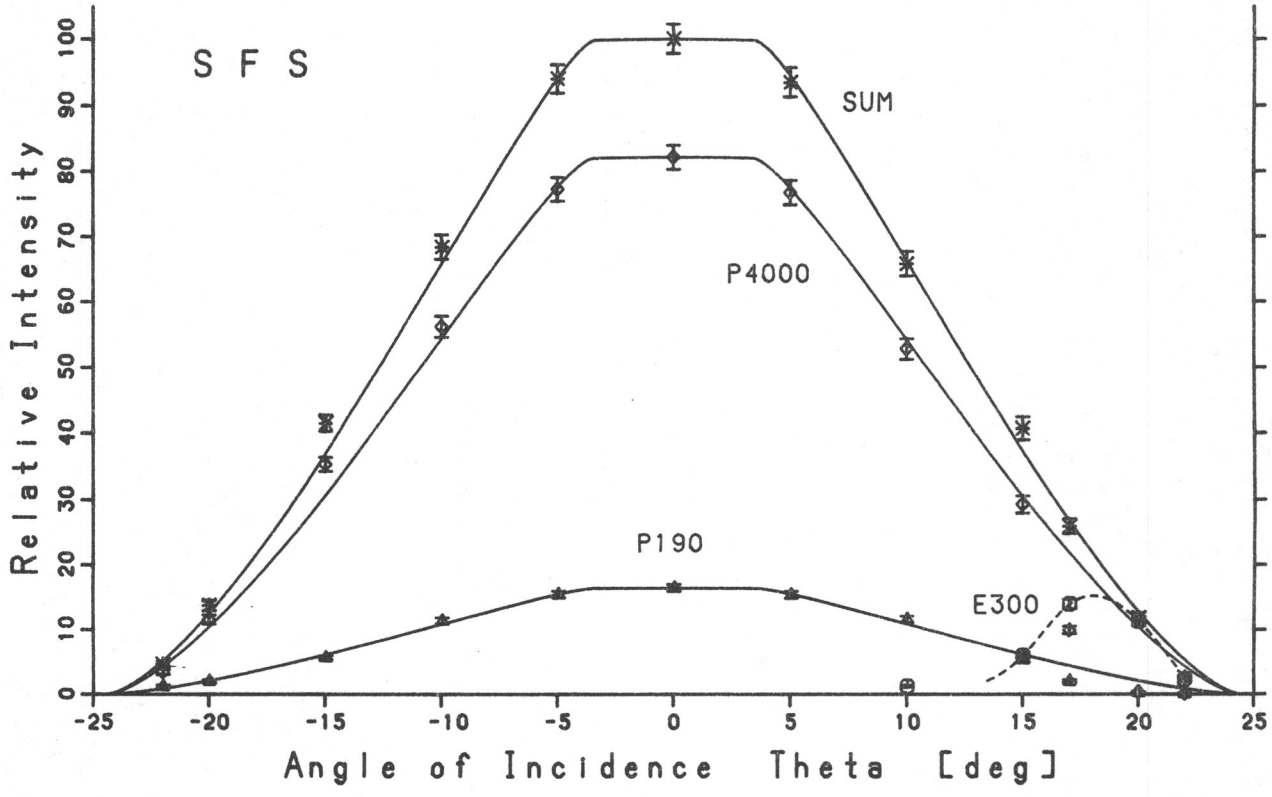

Figure 4-22 KET response to protons with E_p = 4150 MeV as a function of the angle of incidence θ. The solid lines represent the directional response function for parameters given in the text

4.2.2.2 Proton Induced E300 Events

An unexpected behaviour showed for both instruments for angles $\theta > +15°$, the count rates showed a significant increase in E300-type events. This phenomenon did not occur at 'negative' angles of incidence, thus it is a geometrical problem based on a certain asymmetry of the instrument response. Inspecting figure 2-1 one can see, that some particles entering the telescope with $\theta \geq +15°$ penetrate the photomultiplier PM2 with the effect, that additional Cerenkov - and scintillation light is produced in the photomultiplier quartz faceplate and glass envelope.

Figure 4-23 shows C2-spectra for different angles of incidence for E_p = 4150 MeV. Figure 4-23(a) shows the spectrum obtained for $\theta = 0°$, beginning with $\theta = +15°$ (figure 4-23(b)) a second peak at higher channel numbers starts showing, all of these additional events are registered in coincidence channel E300. At $\theta = +17°$ (graph (c)) the second peak contains as many events as the original C2-distribution and at $\theta = +20°$ (graph (d)) only the peak at high channel numbers remains. To understand this effect one can try to estimate the contributions to the total amount of light produced by the different absorber materials traversed by an energetic proton (a more detailed description of this effect can be found by Sierks, 1988). Using the analog to digital conversion lines (correlation between the charge signal at the input of the charge sensitive amplifier and the resulting digital pulse height information) and the gain of PM2, one can estimate the respective number of photoelectrons which give rise to the two peaks in the C2-spectrum. For the 'normal' C2-peak one gets

$$N_{ph}\ (\theta=0°) = 17 \pm 3 \text{ photoelectrons}$$

and for the second peak

$$N_{ph}\ (\theta=+17°) = 78 \pm 13 \text{ photoelectrons}$$

Figure 4-24 (Sierks, 1988) illustrates the path lengths a proton will traverse in the photomultiplier quartz faceplate and glass envelope. The path length in the respective materials are

$$L_q = 5.5 \pm 0.3 \text{ mm} \quad \text{and} \quad L_g = 1.1 \pm 0.1 \text{ mm}$$

The number of Cerenkov photons produced per cm in the wavelength interval λ_1 to λ_2 by a particle of velocity $v = \beta c$ in a material with refractive index n is given by

$$I = \frac{2\pi}{137} \left(1 - \frac{1}{\beta^2 n^2}\right) \left(\frac{1}{\lambda_2} - \frac{1}{\lambda_1}\right)$$

The wavelength interval is determined by the sensitivity range of the photocathode material. One can estimate the number of additional photoelectrons produced by the photomultiplier envelope using the following parameters:

β	= 0.9829	- velocity of a proton with an enenrgy E_p = 4150 MeV
n_q	= 1.47	- index of refraction for fused quartz at λ = 400 nm
n_g	= 1.54	- index of refraction for envelope glass
Q_E	= 22%	- quantum efficiency of the photocathode
λ_2	= 300 nm	
λ_1	= 500 nm	

and the additional assumptions, that:

(1) all of the light produced in the faceplate is seen by the photocathode,and that

(2) approx. 50% of the Cerenkov light produced in the glass envelope reaches the photocathode.

Then by using the above values, one can estimate the number of additional photoelectrons produced in the quartz faceplate and in the glass envelope to be $N_{ph} = 43 \pm 5$. The observed extra signal on the other hand is

$$\Delta N = N(\theta=+17°) - N(\theta=0°) = 61.$$

The estimated number of photcelectrons depends strongly on the sensitivity range of the photocathode of the individual photomultiplier. Since the sensitivities of the multiplier actually used in the instruments are not known, we have used a conservative estimate. A bialkali type photocathode with a quartz window has a typical sensitivity (quantum efficiency) $Q_E \simeq 20\text{-}30\%$ over the wavelength range from $\lambda_2 = 200$ nm to $\lambda_1 = 400$ nm with a steep drop towards longer wavelength, so by extending the sensitivity to smaller wavelength in the above formula (e.g. $\lambda_2 = 250$ nm), N_{Ph} would result in a 50% higher value. In addition, two more effects could contribute to the smaller height:

- Scintillation light being emitted by the glass envelope, to estimate the contribution is very difficult and requires additional information about the scintillation characteristics of the envelope material.
- Secondary electrons emitted from the surfaces by the passage of the particles through the material

Approximately 4% of all isotropically incident protons will hit the photomultiplier faceplate, thus the contamination of the electron channel will be of the order of $\kappa = 15\text{-}20\%$ assuming near-unmodulated galactic spectra (Fulk, 1975). Since these protons will produce a signal in C2 close to the C21-threshold and since the accompanying S2 signal is also small, reduction techniques applied to the C2-S2 matrix should further allow to reduce this proton contamination.

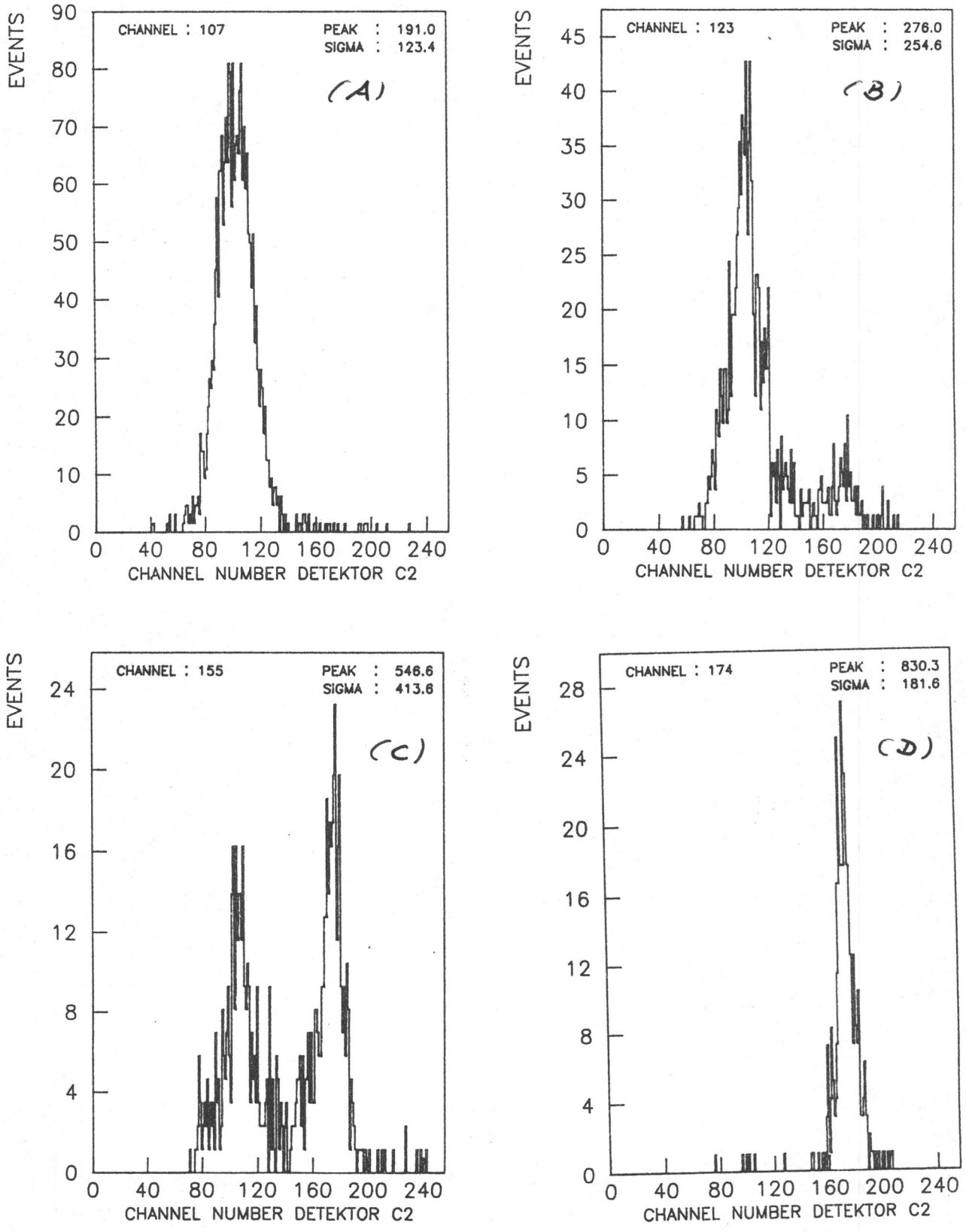

Figure 4-23 C2-spectra for E_p = 4150 MeV for different angles of incidence: (a) $\theta = 0°$, (b) $\theta = +15°$, (c) $\theta = +17°$, and (d) $\theta = +20°$

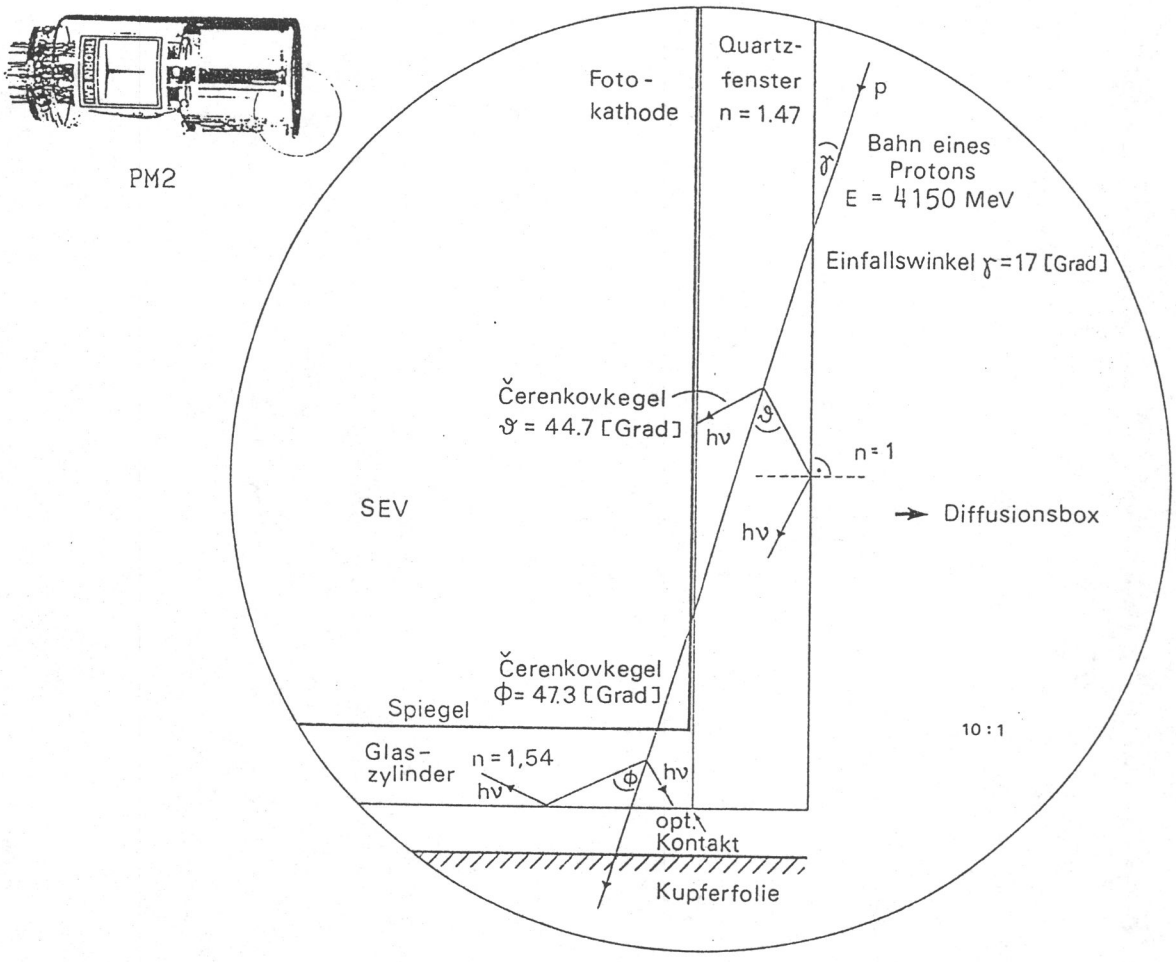

Figure 4-24 Trajectory through photomultiplier PM2 for a particle incident under $\theta = +17°$. The path length of the particle in the quartz faceplate is $L_q = 5.5 \pm 0.3$ mm and in the glass envelope $L_g = 1.1 \pm 0.1$ mm (Sierks, 1988)

4.2.2.3 S2 - Response

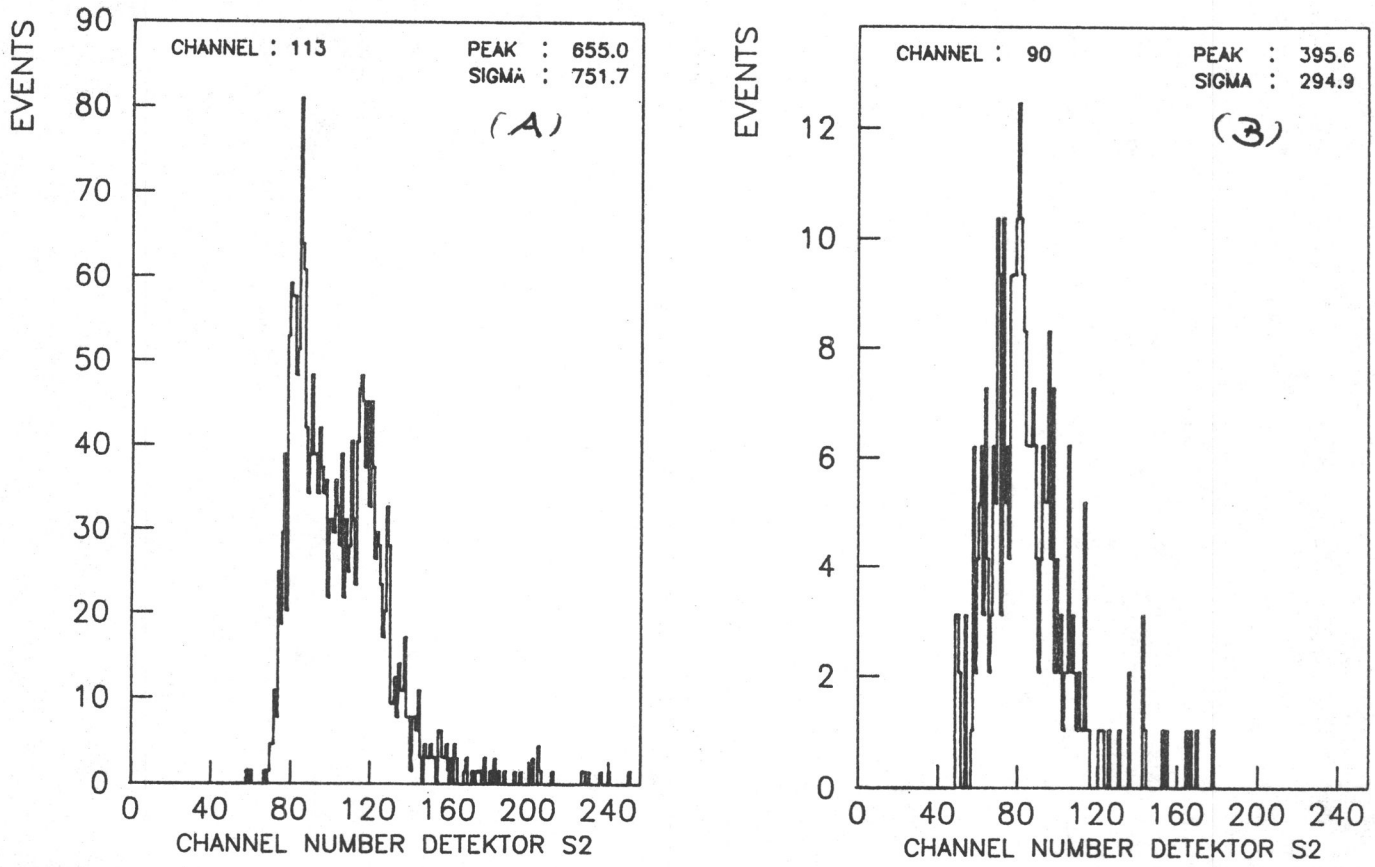

Figure 4-25 S2-spectra for E_p = 4150 MeV for (a) $\theta = 0°$ and (b) $\theta = +15°$

Figure 4-25 shows the S2-spectra for two different angles of incidence - (a) $\theta = 0°$ and (b) $\theta = +15°$. The spectrum for $\theta = 0°$ shows a distinct double peak feature. Since the proton beam was not collimated, particles are registered within the whole acceptance area of the instrument. The different material thickness of the S2 give rise to different light signals, this unavoidable effect prevents the determination of shower size for electrons. This double peak exists only for a range of angles of incidence between $\theta = -5°$ and $\theta = +10°$. Graph (b) does not show this effect anymore.

Measurements with backward incident protons ($\theta = 180°$) have shown, that the instrument response is symmetric with respect to the direction of incidence. For penetrating protons the total geometric factor is therefore

$$G_p = 2 \cdot G_o = 2.06 \text{ cm}^2 \text{ sr}$$

The angular measurements performed with electrons at BONN and at ORME essentially confirm the results obtained with protons, the response curves reflect the fact that collimators had been used to limit the beam size. More detailed information can be found by Sierks (1988).

4.2.2.4 Backward Incident Electrons

The KET response to backward incident penetrating electrons differs considerably from the one for electrons incident under $\theta = 0°$. The sensor was designed to collect the maximum possible amount of light from the C2-calorimeter. Therefore no effort was made to reject backward incident particles. Figure 4-26 shows pulse height spectra of the D1 (a) and the D2 detector (b) with the beam energy set to $E_e = 985$ MeV and the instrument oriented backwards ($\theta = 180°$). To produce this graph, all pulse height analyzed events of the coincidence types P4000, E300 and A4000 have been summed together.

In this instrument orientation, the electromagnetic shower is seen by the semiconductor detectors and causes very extended pulse height distributions. One can see peaks corresponding to the passage of one and two (minimum) ionizing particles, scattering of the particles smears over the other peaks. Since the signals in D1 and D2 are so high, the coincidence requirements (see table 2-2) for registration as a A400-type event are satisfied. Thus backward incident electrons can simulate high energy alpha particles. Fortunately only a small number of backward incident electrons are registered as a valid event. Graph (c) and (d) show the pulse height spectra of D1 and D2 with the instrument in the failure mode configuration FM6:ON, i.e. the anticoincidence detector A cannot veto an event anymore. Comparison of graph (a) with graph (c) (and (b) with (d)) shows however, that only a very small number of electrons is registered.

(1) If the lateral extension of the shower is large enough so that at least one particle hits the A-detector, then a veto signal is generated and the event is rejected.

(2) If the signal exceeds the D21 threshold and the signal in D1 is too small to trigger the D11 threshold, then the event will not be registered either.

The net effect of this situation is that, depending on the energy of the particle, the efficiency for detecting backward incident electrons is considerably lower than for forward incident electrons (see chapter 4.2.3 for a discussion of the electron detection efficiency). In addition, the events fall into quite different countrate channels. In table 4-3 and table 4-5 the respective responses are compared for the two instruments. In the column 'Total' the number of events registered is compared to the beam counter and the ratio set to 100 for forward incident electrons. For the backward incident particles the number of registered events is then referenced to the above number; so a value of 3.6% means that 96.4%of all backward incident electrons are rejected at an energy of E_e = 985 MeV. For the individual countrate channels the response differs quite considerably between $\theta = 0°$ and $\theta = 180°$ (column 4-8). For energies above E_e = 100 MeV a substantial number of electrons are registered as A4000 events. Sierks (1988) has tried to estimate the amount of contamination in the A4000 channel caused by backward incident electrons.

(1) The ratio of the integrated particles fluxes is

$$I_\alpha / I_e \simeq 2.5$$

for energies $E_\alpha > 2$ GeV/nuc and $E_e > 500$ MeV.

(2) The efficiency is $\varepsilon_\alpha = 1$ for alpha particles and $\varepsilon_e = 0.03$ for electrons.

(3) About 15% of the registered backward incident electrons are counted as A4000.

(4) Reduction techniques (e.g. consistency checks for the energy losses in D1 and D2) can further reduce the number of falsely registered events by 70%.

The resulting contamination can therefore be estimated to be < 0.1% and will not disturb the α-particle measurements.

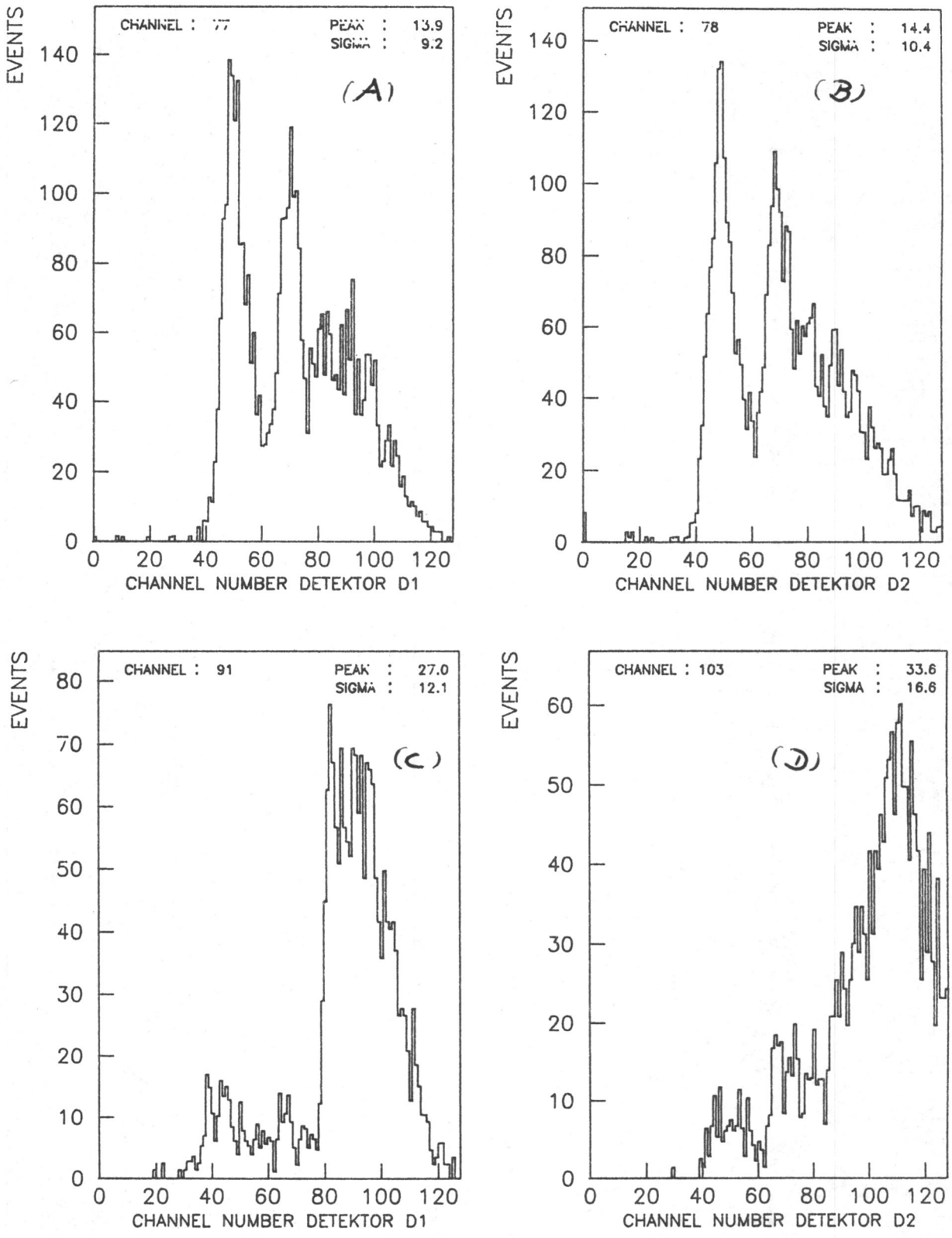

Figure 4-26 D1 and D2 spectra obtained at the Universität Bonn 2.5 GeV Synchrotron for E_e = 985 MeV with KET in nominal mode in graph (a) and (b); and with detector A logically switched off (FM6 : ON) in graph (c) and (d).

Table 4-3 Effect of backward incident electrons of different energies on the SFM countrate channels

Instrument Orientation	Particle Energy	Total	Registered events Countrate Channels				
θ [°]	E [MeV]	[%]	[%]				
			E12	E300	P190	P4000	A4000
0	985	100.0	1.7	27.6	6.3	64.4	-
180	985	3.6	17.6	13.9	1.2	46.3	21.0
0	485	100.0	6.1	51.1	0.7	42.1	-
180	485	7.7	16.9	16.0	1.4	59.2	6.6
0	85	100.0	54.1	1.0	0.9	43.9	-
180	85	10.6	28.2	0.4	2.8	52.5	-

Table 4-4 Effect of backward incident electrons on the SFS countrate channels

Instrument Orientation	Particle Energy	Total	Registered events Countrate Channels				
θ [°]	E [MeV]	[%]	[%]				
			E12	E300	P190	P4000	A4000
0	985	100.0	1.3	83.7	1.3	13.6	0.1
180	985	3.2	19.2	33.2	2.2	21.2	24.2
0	485	100.0	6.1	82.8	2.5	7.4	-
180	485	6.6	19.0	42.0	1.9	29.8	7.4

4.2.3 Electron Detection Efficiency

One of the key parameters, which has to be determined for an electron detector during the calibrations, is the detection efficiency as a function of energy. An accelerator is a 'calibrator' with some advantages and some disadvantages. The biggest advantage is that it delivers particles of a very well known energy. If the beam contains only a few 'parasitic' particles, or if the experimenter can discriminate against these unwanted particles, then the energy response for each detector can be determined very precisely. One of the biggest disadvantages is usually the fact that the number of particles in the beam is (a) not very well known , and (b) varies very strongly during the course of a data gathering run. It is therefore difficult to establish a reference for the determination of absolute values like the efficiency, where the number of particles having entered the telescope must be known precisely.

4.2.3.1 Beam Reference

We had planned to operate the KET in coincidence with an external telescope consisting of a crossed pair of plastic scintillators T1 and T2 (thickness d = 1 mm) positioned at a distance of between 20 an 50 cm in front of the KET aperture (see figure 3-2). The coincidence signal of this reference telescope was fed to the test input of the C1-detector, while the connector of the C1-photomultiplier was removed from the signal input. The results obtained in this configuration for electrons with energies $E_e > 500$ MeV were quite consistent with theoretical expectations. At lower energies however, the measured detection efficiency was so low as not to be realistic. We had to conclude , therefore, that the amount of scatter introduced by the small amount of scintillator material of $d \simeq 0.2$ g/cm^2 was so large, that it was not possible to use these runs to determine the efficiency correctly (these runs have for this reason been omitted from the tables in chapter 3.3).

We therefore had to use one of the KET detectors as a reference. For low energies, only the D1-detector can be used, since a substantial number of particles are scattered out of the acceptance cone after passing D1 and C1. This

can be seen very clearly from figure 4-27 (a) and (b). Here the ratio of the countrates of D1 and D2 has been plotted as a function of energy for the measurements made at the AL600 accelerator at ORME. Both rates have been corrected for background, which was low for these measurements. For energies above E_e = 40 MeV the scattering of particles does not influence the countrates anymore and the ratio is virtually constant at

$$C_{sfm} = 1.30$$
$$C_{sfs} = 1.35$$

This value represents the 'effective' surface ratio of the two detectors. A fairly large collimator had been used for these measurements, the beam spot was larger than the diameter of detector D2, but smaller than the geometric surface ratio of C = 1.5 . For energies below E_e = 40 MeV the ratio increases considerably reflecting the effect of the strong scattering caused by D1 and C1. At the lowest measured energy of E_e = 7.5 MeV only approximately 30% of all incident particles reach the D2. The graphs do not contain all data points gathered, only the runs with a primary beam energy of 200 MeV could be used. Background and beam conditions (amount of parasitic particles) were different for higher machine energies. It is not clear, whether the apparent minimum of the data points between 20 and 40 MeV is real or is being caused by a decrease of background counts in the D1-detector.

The measurements at the BONN accelerator were performed at considerably higher energies for which the scattering of the electrons in the entrance telescope is very small and can be neglected. The background count of the D1-detector was higher by a factor of 10 than at the AL600. Inspecting the D1/D2-ratios for the BONN measurements revealed an effective surface ratio of C ≈ 1 for both instruments consistent with the fact, that smaller collimators had been used.

4.2.3.2 Efficiency

The electron detection efficiency ε_i for the individual countrate channels (E4, E12, E300, P190 and P4000) is therefore given by the ratio of the respective countrate and the D1 countrate corrected for background and with the effective surface ratio of D1 and D2

$$\varepsilon_i = \frac{R_i}{D1/C} \qquad \text{(ORME)}$$

The overall detection efficiency is the sum of the individual efficiencies

$$\varepsilon = \sum \varepsilon_i$$

As mentioned above, the background registered by D1 at BONN was so high that this rate could not be used as a reference. Since scattering in the entrance telescope does not effect the efficiency anymore at the energies at which we calibrated the KET in BONN, the D2 rate was used, i.e.

$$\varepsilon_i = \frac{R_i}{D2} \qquad \text{(BONN)}$$

Figure 4-28 shows the data for the SFM and figure 4-29 the data for the SFS. The data for each instrument is presented in two graphs with graph (a) containing the contribution of the proton channels and the sum (ε) of all channels and graph (b) showing the contribution of the electron channels. No separate symbols have been used to distinguish between data points from ORME and BONN, the data points overlap in the energy range between 100 - 150 MeV. Each graph contains the data of the respective other graph as a dashed line.

The overall efficiency is remarkably similar for both instruments, although noticeable differences exist for the individual channels. The efficiency rises steadily from low energies due to a decrease in scattering until it reaches a maximum of ε = 80% at E_p = 140 MeV for the SFM and also ε = 80% at E_p = 150 MeV for the SFS. For higher energies the efficiency decreases slowly due to an increased probability for a shower particle to hit the A-detector, consistent with model calculations (Julliot, 1980). The SFS registers about a factor of 4 more P190-type events than the SFM, the detection efficiency of the SFS C1-detector obviously is lower.

The lowest energy which could be measured was E_e = 7.5 MeV at ORME, so we could not probe the detection threshold of the E4-channel. It is assumed to be close to E_{min} = 4 MeV at an efficiency $\varepsilon \simeq 5\%$. At this energy scattering in the entrance telescope is so large, that approx. 95% of the electrons hitting the D1-detector do not reach the D2-detector. We define the energy thresholds for a channel as the point on the energy scale, where the efficiency values of the lower and the next higher countrate channel are equal (cross over point).

Electrons are not only registered in the dedicated electron countrate channels but also in the proton channel P4000. The C21-threshold is needed to discriminate high energy protons from electrons. The threshold level has to be set to a fairly high level to assure a good separation of the two particle types considering that

(a) the galactic e/p-ratio is approx. 0.1 (see chapter 4.2.4) and
(b) that KET has only a low energy resolution ($\sigma_p \simeq 60\%$, $\sigma_e \simeq 100\%$).

Thus when the shower grows large enough so that it finally starts triggering the S2-detector, it is not yet large enough to trigger the C21-threshold, and in an intermediate energy range the electrons are registered in the proton channel P4000. As can be seen from table 2-2 and table 2-3, the C21 threshold differs considerably for the two instruments - the SFS threshold is lower. The energy range over which electrons are registered as protons is smaller for this instrument as is the share this channel has at a fixed energy. The energy ranges of the countrate channels are summarized in table 4-5 for the two instruments.

Table 4-5 Energy ranges for the electron countrate channels

	SFM	SFS
E4	4 - 9	4 - 9
E12	9 - 230	9 - 150
E300	230 - ∞	150 - ∞
P4000	110 - 525	100 - 220

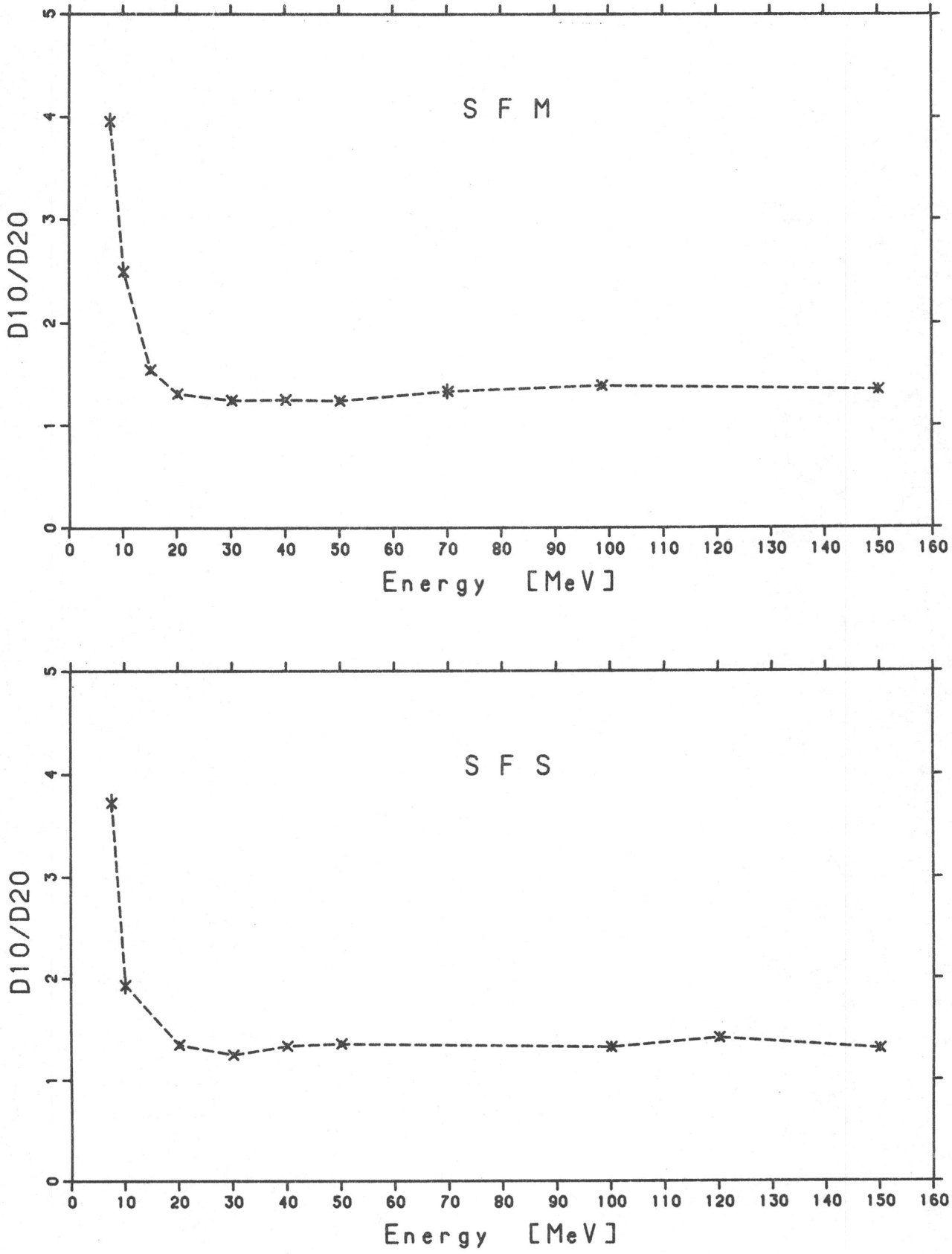

Figure 4-27 Ratio of the D1 and D2 single detector count rates (corrected for background) as a function of energy for some AL600 runs.

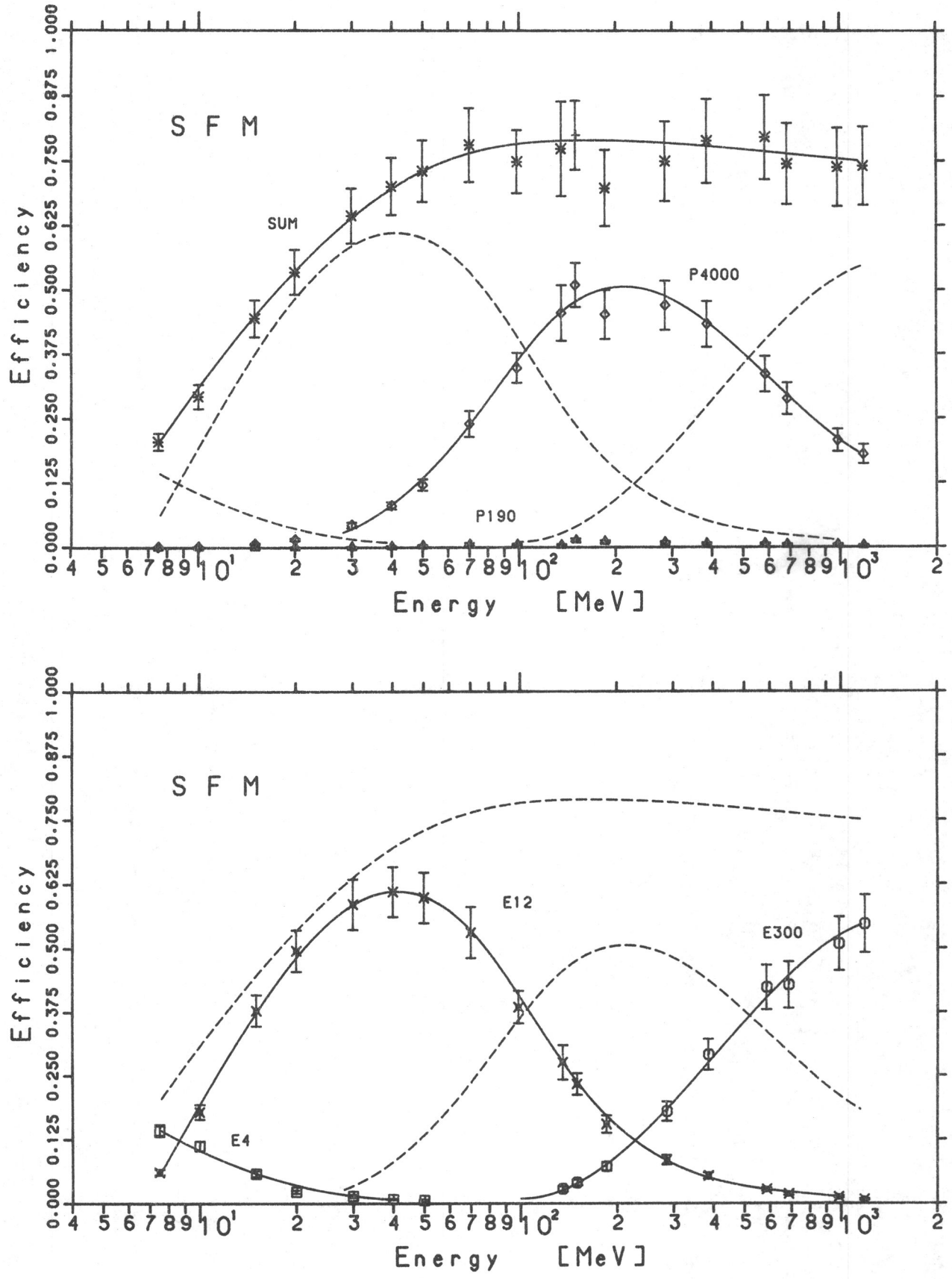

Figure 4-28 SFM efficiency as a function of energy (Sierks, 1988).

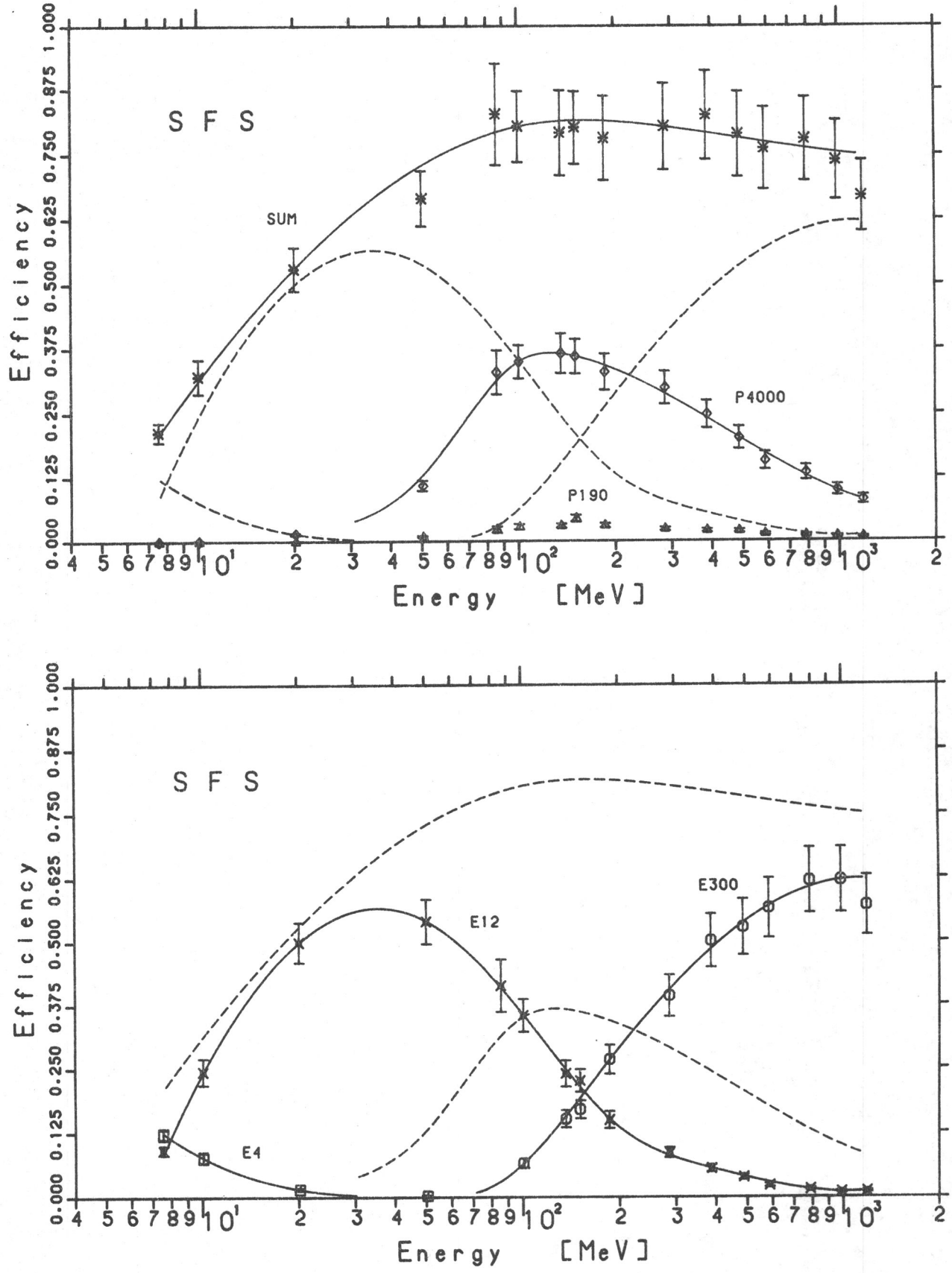

Figure 4-29 SFS efficiency as a function of energy (Sierks, 1988)

4.2.4 Proton - Rejection

The integral electron channel E300 has to be as free as possible of background caused by high energy protons. This background can consist of events of two different origins

1. protons which undergo nuclear interactions in the sensor, and
2. protons which, due to an instrumental effect, can be registered as an electron (see chapter 4.2.2.2 for a discussion of this effect).

Several runs performed at CERN with high energy protons can be used to determine the amount of contamination in the E300 channel, see table 4-6. No runs with energies below E_p = 3170 MeV (4 GeV/c) are listed because at these energies the beam was already contaminated with pions. The orientation of the instrument is given as the angle of incidence in column 3 (θ = 180° means backward incident particles), the energy of the beam in column 4 and the collection time for each run in seconds in column 5. Column 6 and 7 contain the number of events recorded in the E300 channel and in the proton channels P190 and P4000 respectively.

The response of the instruments differs slightly, the number of falsely registered protons is ≈ 0.8% for the SFM and ≈ 1.0% for the SFS. The nuclear interaction length for PbF_2 is λ_0 ≈ 24 cm, this is about ten times the material thickness of the C2-detector. We would expect therefore a nuclear interaction rate of ≈ 10%. For an interaction event to be registered as an electron it is necessary to create approx. 6 times the amount of Cerenkov light of a single high energy particle. This requires that a large number of singly charged particles of sufficient energy is created in the interaction. Another ≈ 2% of the incident protons interact in a way that they do not cause a large signal in C2 but instead have a large energy deposit in S2. These hadronic cascades consist of a number of low energy particles with a high atomic charge, which loose a large amount of energy in the S2-detector due to ionization. These particles can be identified easily in a C2-S2-matrix and they do not contaminate the E300-channel.

Table 4-6 Nuclear interaction rate for the SFM and the SFS, number of protons registered as E300 for some runs at CERN.

Run	Sensor	Angle [θ]	E [MeV]	T [sec]	E300 [counts]	∑P [counts]	E300/(∑P+E300) [%]
47/8	SFM	0	4150	2978	128	14240	0.89±.07
126/7	SFM	0	4150	11892	473	69865	0.67±.03
128/9	SFM	180	4150	14975	14	34852	0.04±.01
104	SFM	0	3170	3054	72	9775	0.73±.09
82	SFS	0	4150	4186	114	10421	1.08±.10
84	SFS	0	3170	1209	21	2208	0.94±.21

Sierks (1988) has used the modulated interstellar spectra at 1 AU for protons and electrons published by Fulks (1975) to estimate the p/e-ratio. Assuming a power law dependency for the spectra and integrating he obtained

$$S_e \simeq 200\ [m^{-2}\ s^{-1}\ sr^{-1}] \quad \text{for } E_e > 500\ \text{MeV}$$

$$S_p \simeq 1600\ [m^{-2}\ s^{-1}\ sr^{-1}] \quad \text{for } E_p > 2000\ \text{MeV}$$

yielding a proton to electron ratio p/e ≃ 8. Thus for every 100 electrons registered 6 protons will be counted as well, giving a background level of

$$\varepsilon_{had} \simeq 6\%$$

This amount is small compared to the number of protons being counted in the E300 channel due to geometrical reasons (see chapter 4.2.2.2)

$$\varepsilon_{geo} \simeq 24\%$$

Figure 4-30 shows in a schematic form the distribution of the pulse heights in the C2-S2-matrix for high energy protons and electrons (penetration mode P4000 and E300). The dotted areas represent the response of the instrument to high energy protons. These protons will be registered in three distinct areas

1. Bounded dotted area at the bottom of the graph: 95% of all isotropically incident protons with energies above E_p = 2200 MeV, geometrical factor $G_p = 2 \cdot G_o$.

2. Bounded dotted area to the upper left of the graph: 4% of all isotropically incident protons with energies above E_p = 2200 MeV will enter the sensor aperture with such an angle, that they hit the PM2-faceplate and are registered as electrons. Provided that the signal is large enough to trigger the C21-threshold. If it is not, the contamination of the E300-channel is lower than 24%, the geometrical factor for these protons is $G_p = 2 \cdot G_o$.

3. The dotted area to the upper right of the graph represents the effect of the hadronic cascades. Approximately 0.8% of all normally incident protons (SFM) are registered in the E300-channel with a geometrical factor of $G_p = 2 \cdot G_o$.

The pulse height distribution of electrons registered as E300 are represented by the bounded hatched area. Electron events with energies from E_e = 100 MeV to E_e = 1200 MeV have been summed up to produce this graph. The boundary represents the 1%-level of the resulting distribution. One can see from figure 4-28, that the energy at which electrons are registered with the same efficiency in the E12-channel and in the P4000-channel is E_e = 100 MeV. The electrons with this energy constitute, however, a contamination of the P4000-channel, to use pulse height data to retrieve more detailed spectral information for electrons in the energy range 100 - 200 MeV will be very difficult. For this range the clean data from the E12-type events should be used.

Reduction techniques based on the pulse height information can be used to identify the protons in area (2) of figure 4-30. A correction of the nuclear interaction events requires the application of model calculations to the data

reduction, the signals in these detectors do not differ from the ones produced by electrons. A precise model representation is being developed to enable the experimenters to simulate the KET response to high energy isotropically incident protons, the results of this model calculations can be varyfied using the data obtained at the accelerator.

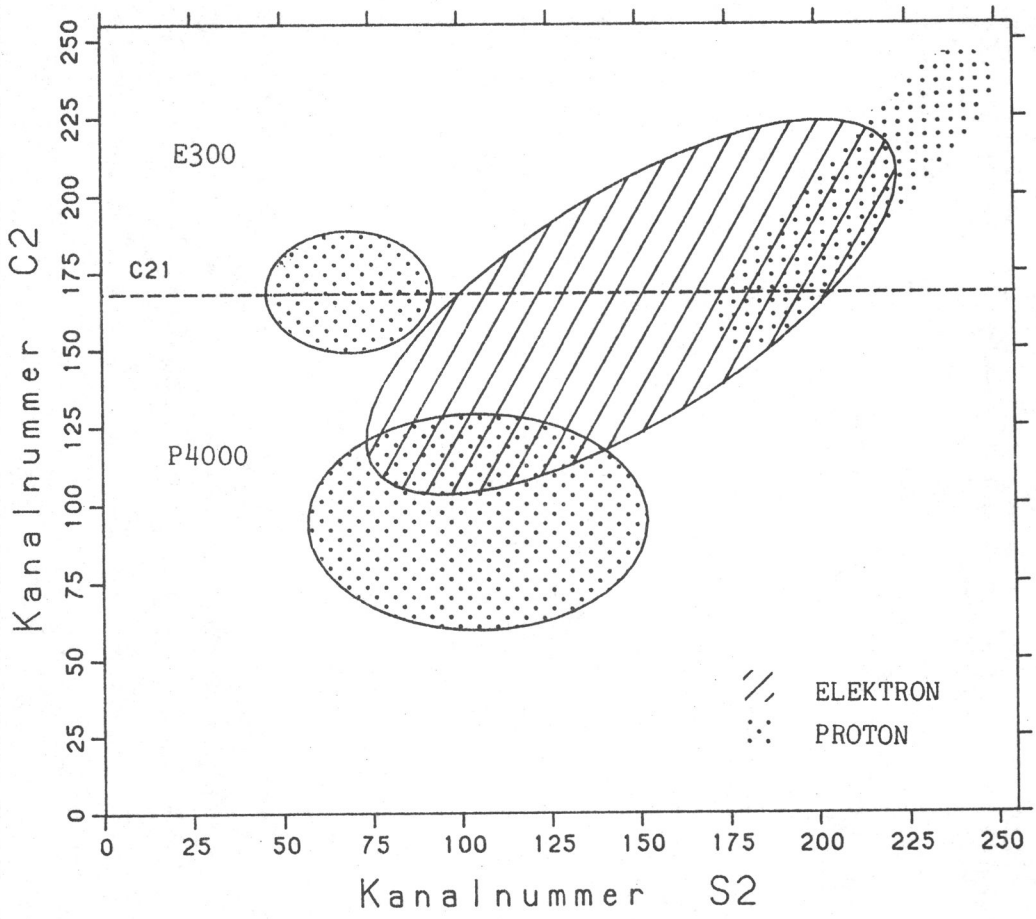

Figure 4-30 Schematic representation of the loci of penetration mode electrons and protons in the C2-S2-matrix. Events of coincidence types P4000 and E300 have been added together to produce this graph (Sierks, 1988).

4.2.5 RTG

4.2.5.1 Description of RTG

To provide power to the spacecraft and the experiments, ULYSSES uses a standard 4500W-(th) General Purpose Heat Source (GPHS) built at Mound Laboratories of Monsanto Research Corporation for the U.S. Department of Energy. Such a source contains about 9.9 kg of plutonium in the form of plutonium dioxide pellets (Anderson, 1985), similar sources have been used for the VIKING, PIONEER and VOYAGER missions. Figure 4-31 is a cutaway drawing of the RTG (Anderson, 1985) showing some of the 18 heat source modules stacked along the longitudinal axis with each heat source containing eight PuO_2-pellets. The isotopic composition of the fuel is given in table 4-7.

Table 4-7 Isotopic composition of the RTG fuel

Plutonium Isotope	Weight (Percent)	Half-Life (Years)	Radioactivity Curies/gram of PuO_2
236	0.00012	2.85	476
238	83.6	86	15.4
239	14.0	24400	0.054
240	2.0	6580	0.195
241	0.4	13.2	100.4
242	0.1	379000	0.0034

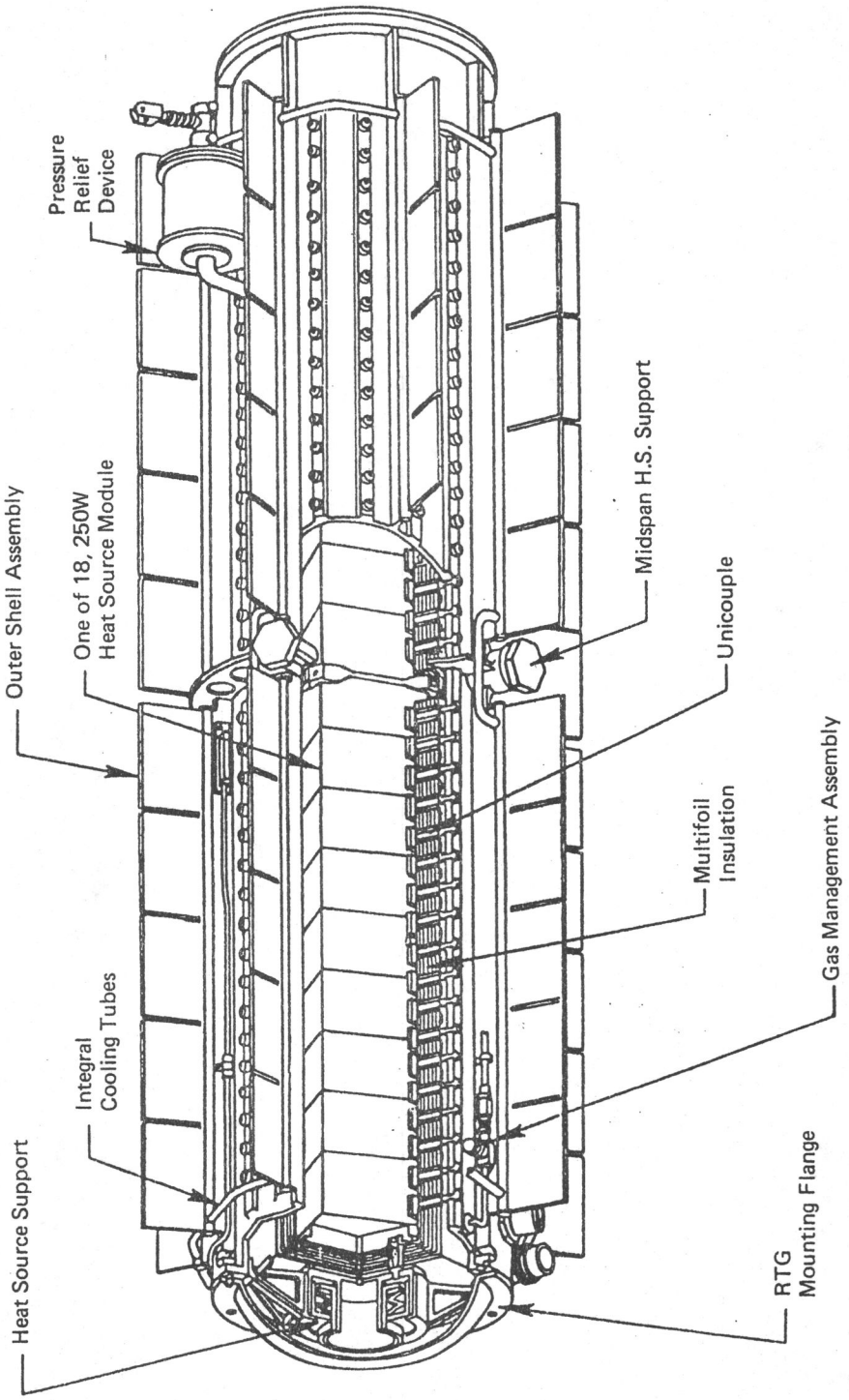

Figure 4-31 Cutaway drawing of the RTG (Anderson, 1985)

4.2.5.2 Response of KET to the RTG-produced background

Radioactive thermal generator compatibility tests with both instruments were performed in March 1985 at Mound Laboratories using the RTG-F3 (Galileo source). The tests were made in RTG cell 112, the instrument was placed on a table with the horizontal distance and axis orientation equal to the orientation of the instrument in the S/C. The cell is a cubicle of approximate dimensions 6×6×2.5 m^3 with concrete walls of 0.5 m thickness (refer to tables 3-14 and 3-15 for a list of the tests made). Of particular interest was

(1) to establish the level of the RTG induced background counts for the coincidence countrate channels with the instrument in nominal condition, and
(2) the investigation of the instrument response to the various failure mode conditions.

Table 4-8 and 4-9 summarize the countrates obtained with the different experiment conditions for the SFM and the SFS respectively. Stringent radiation safety and security requirements limited the data gathering time available to the experimenters. The runs to test the response to different high voltage and failure mode conditions lasted between one and two hours. Overnight runs with a duration of approx. 15 hours were performed to establish the background levels for the individual countrate channels.

Another test run was performed with the SFM during the final spacecraft Integrated System Test (IST) at KSC on 2/12/1986. Table 4-10 shows all the data collected with the different instruments at the various locations, instrument condition is nominal for all these runs. The test with the Simulated RTG performed at JPL on 10/13/1982 was done with the original KET-FM prior to detector refurbishment, so the data cannot be compared with the later measurements. It is noteworthy, however, that the rates differ considerably from the later runs even for the semiconductor detectors, for which the refurbishment had only little effect - thresholds and gain were not changed.

Table 4-8 SFM countrate summary of RTG induced events

Run	HV	FM	P1	P4	P32	P116	P190	P4000	E4	E12	E300
66/22	**2**	**0**	32341	142	6	0	0	2	540	37	0
			0.6122	**0.0027**	**0.0001**	0.0000	0.0000	0.0000	**0.0102**	**0.0007**	0.0000
67/24	3	0	2530	15	1	0	0	0	33	9	1
			0.5729	0.0034	0.0002	0.0000	0.0000	0.0000	0.0075	0.0020	0.0002
65/12	4	0	1900	15	0	0	0	0	39	8	0
			0.5240	0.0041	0.0000	0.0000	0.0000	0.0000	0.0108	0.0022	0.0000
66/17	2	1	0	0	53	48	3	2	595	32	0
			0.0000	0.0000	0.0152	0.0138	0.0009	0.0006	0.1709	0.0092	0.0000
66/20	2	2	0	0	1056	22	0	1	565	1	0
			0.0000	0.0000	0.6407	0.0133	0.0000	0.0006	0.3428	0.0006	0.0000
66/21	2	3	1168	3	1	0	0	0	19	1	0
			0.6614	0.0017	0.0006	0.0000	0.0000	0.0000	0.0108	0.0006	0.0000
66/23	2	4	1707	12	0	0	0	0	0	21	0
			0.6103	0.0043	0.0000	0.0000	0.0000	0.0000	0.0000	0.0075	0.0000
66/19	2	5	1163	13	0	0	0	0	15	1	0
			0.6080	0.0068	0.0000	0.0000	0.0000	0.0000	0.0078	0.0005	0.0000
66/18	2	6	2732	24	0	0	1	0	68	4	0
			0.8073	0.0071	0.0000	0.0000	0.0003	0.0000	0.0201	0.0012	0.0000

Table 4-9 SFS countrate summary of RTG induced events

Run	HV	FM	P1	P4	P32	P116	P190	P4000	E4	E12	E300
63/213	**2**	**0**	32390	60	10	0	1	5	451	83	0
			0.5931	**0.0011**	**0.0002**	0.0000	0.0000	**0.0001**	**0.0083**	**0.0015**	0.0000
65/225	**2**	**0**	6626	26	6	1	0	8	477	78	0
			0.1160	**0.0005**	**0.0001**	0.0000	0.0000	**0.0001**	**0.0083**	**0.0014**	0.0000
63/212	3	0	2049	1	1	0	0	0	25	11	0
			0.5568	0.0003	0.0003	0.0000	0.0000	0.0000	0.0068	0.0030	0.0000
65/224	4	0	1126	3	2	1275	0	241	19	6221	25
			0.5009	0.0013	0.0009	0.5672	0.0000	0.1072	0.0085	2.7675	0.0111
63/214	2	1	0	0	61	104	3	1	763	100	0
			0.0000	0.0000	0.0101	0.0172	0.0005	0.0002	0.1264	0.0166	0.0000
63/215	2	2	0	0	1084	50	0	1	396	3	0
			0.0000	0.0000	0.6139	0.0283	0.0000	0.0006	0.2243	0.0017	0.0000
63/216	2	3	1280	0	0	0	0	0	29	2	0
			0.6210	0.0000	0.0000	0.0000	0.0000	0.0000	0.0141	0.0010	0.0000
64/218	2	4	1035	0	0	0	0	0	0	20	0
			0.5879	0.0000	0.0000	0.0000	0.0000	0.0000	0.0000	0.0114	0.0000
64/219	2	5	1189	1	0	0	0	0	21	4	0
			0.6212	0.0005	0.0000	0.0000	0.0000	0.0000	0.0110	0.0021	0.0000
64/217	2	6	4089	9	2	0	1	0	76	10	0
			0.7714	0.0017	0.0004	0.0000	0.0002	0.0000	0.0143	0.0019	0.0000

With the SFS a second run was performed with a wall of 10 cm lead bricks placed between the RTG and the instrument to eliminate most of the directly incident γ's. We intended to measure the effect of the RTG produced neutron flux on the instrument.

As can be seen from the data in table 4-10, the number of RTG-induced events is low, but not negligible, when the instrument is in nominal mode. Only the E4 and the E12 channel show a sizeable number of events. The spectra of these events do not differ - within the limits imposed by the small number of events - from those obtained from 'real' electrons. Thus, it will not be possible to identify the RTG induced events by means of a suitable reduction technique. The expected 'quiet time cosmic radiation background countrate' as compiled by J. J. Engelmann (private communication) has been added to table 4-10 in column 7.

The SFS run with the lead brick shield indicates, however, that a number of background events are caused by γ-scattering from the walls of the hot cell, possibly even entering the instrument through the aperture. The introduction of the lead shield has significantly reduced the number of counts in the individual detectors, but the number of coincidence counts is the same as without the shield. We could not supply enough lead to completely shield the instrument from all sides, neither did we place an absorption layer in front of the aperture because we did not want to introduce a scattering surface close to the aperture. The result of this run suggests, however, that the room background was so large, that a number of events entered the instrument through the aperture. The other alternative would be to assume that all recorded events are caused by neutrons. To improve statistics especially for the E12 channel, a measuring time of approx. 100 hours would have been desirable, the low number of E12 events recorded precludes a precise identification of the events as to whether they are accidental coincidences or 'real' events caused by interactions in the instrument or by backscatter from the walls of the measuring cell.

During the final IST an RTG mating and functional test was scheduled. The KET instrument was switched on during this test to allow the collection of data in a configuration close to the actual situation in flight. Due to problems with

a thread in the RTG mounting flange, the device was never positioned right but instead was facing the instrument in a position in which the self-absorption in the source was reduced. The data recorded by KET (column 4 of table 4-10) shows, that although the rates for the individual detectors was higher by a factor of ≈2 than compared to the test at Mound, the E4 rate was lower by a factor of ≈2. No events were recorded in the other channels, therefore only an upper limit could be quoted. With the RTG mounted in the right position, the background is expected to be even lower and is not expected to cause any problems.

To aid in investigating this question, efforts are under way at the Universität Kiel to adapt the program package GEANT3 (Brun et al., 1986) to the KET detector arrangement and to probe the response of the instrument to incident γ's and neutrons with the help of model calculations.

Table 4-10 Response of KET - FM to SRTG, KET - SFS and KET - SFM to RTG Model F3, count rate data are given in counts/sec

KET	FM[1]	SFM[2]	SFM[3]	SFS[2]		COSMIC QUIET
CHANNEL	SRTG BACKGROUND	RTG BACKGROUND	RTG BACKGROUND	RTG BACKGROUND	RTG BACKGROUND WITH LEAD SHIELD	FLUX
D10	185.0	25.0	44.5	22.8	4.3	-
D20	76.0	9.9	22.8	10.5	2.7	-
C10	935.0	128.5	226.0	129.6	74.9	-
C20	3204.0	68.2	91.3	142.7	44.7	-
S20	6848.0	358.0	603.0	496.0	104.9	-
A0	4050.0	1134.0	1889.0	955.0	216.9	-
P1	6.7	0.6	1.4	0.6	0.1	0.1
P4	$<1.8 \cdot 10^{-5}$	$2.4 \cdot 10^{-3}$	$<1.0 \cdot 10^{-3}$	$8.8 \cdot 10^{-4}$	$4.2 \cdot 10^{-4}$	$5.0 \cdot 10^{-3}$
P32	$1.0 \cdot 10^{-3}$	$1.1 \cdot 10^{-4}$	$<3.0 \cdot 10^{-4}$	$1.8 \cdot 10^{-4}$	$1.1 \cdot 10^{-4}$	$1.0 \cdot 10^{-2}$
P116	$1.0 \cdot 10^{-3}$	$<1.9 \cdot 10^{-5}$	$<3.0 \cdot 10^{-4}$	$<1.8 \cdot 10^{-5}$	$1.8 \cdot 10^{-5}$	$3.0 \cdot 10^{-2}$
P190	$3.5 \cdot 10^{-4}$	$<1.9 \cdot 10^{-5}$	$<3.0 \cdot 10^{-4}$	$1.8 \cdot 10^{-5}$	$<1.8 \cdot 10^{-5}$	$3.0 \cdot 10^{-1}$
P4000	$<1.8 \cdot 10^{-5}$	$3.8 \cdot 10^{-5}$	$<3.0 \cdot 10^{-4}$	$9.2 \cdot 10^{-5}$	$1.4 \cdot 10^{-4}$	$1.0 \cdot 10^{-1}$
E4	$2.9 \cdot 10^{-3}$	$9.0 \cdot 10^{-3}$	$4.0 \cdot 10^{-3}$	$7.3 \cdot 10^{-3}$	$7.4 \cdot 10^{-3}$	$1.0 \cdot 10^{-2}$
E12	$<1.8 \cdot 10^{-5}$	$7.0 \cdot 10^{-4}$	$<3.0 \cdot 10^{-4}$	$1.5 \cdot 10^{-3}$	$1.4 \cdot 10^{-3}$	$3.0 \cdot 10^{-3}$
E300	$<1.8 \cdot 10^{-5}$	$<1.9 \cdot 10^{-5}$	$<3.0 \cdot 10^{-4}$	$<1.8 \cdot 10^{-5}$	$<1.8 \cdot 10^{-5}$	$5.0 \cdot 10^{-3}$

Note : 1. Measurements performed at JPL with FM prior to detector refurbishment on 10/13/1982

2. Measurement performed at Mound Laboratories from 3/11/1985 to 3/15/1985

3. Measurement performed at KSC on 2/12/1986

5 Energy Calibration and Spectrum Retrieval

The discussion of the calibration data in chapter 4 has shown, that it is not trivial to determine the energy spectra of the various particle species. For most of the nucleon channels, only very little additional information is contained in the pulse height data since only a very small fraction of the total energy loss in the sensor occurs in the detectors which can analyze it. The P116-channel registers not only protons with energies from 116 - 190 MeV (see table 2-2) but due to a false coincidence condition also α-particles with energies between 126 - 190 MeV/nuc are counted in this channel. In this case the energy losses in D1 and D2 can be used to separate the two particle species. The determination of energy spectra for nuclei is not the prime task for the KET instrument, however, the achievable energy resolution is given by the number of countrate channels only.

Electrons are counted in three coarse energy bands. The channels E4 and E12 are free of any contamination by other particle species with the exception of the RTG-induced events (see table 4-10). This background will be nearly constant with time, since the fuel composition changes only very slowly over the mission time, and is not expected to adversely influence the investigation of electron flux modulation. The level of this background is at least one order of magnitude below the cosmic quiet flux level.

The large body of data gathered during the calibration of the KET instrument will be used in preparing the programs necessary to retrieve the electron spectra from the flight data. The algorithms required for this task are being developed now and will consist of a 4-step approach.

1. Refine the model of the instrument for use with the GEANT3 (Brun et al., 1986) program. This process is iterative and aims at predicting the results of all the key calibration measurements.

2. With the model of the instrument perfected, compute the response for isotropically incident particles and predict the response for those particles and energies which could not be measured directly.

3. Using the model and a set of spectra with different shape and spectral indices as an input to the model calculations, the instrument will be predicted. This method will deliver a set of matrices for a limited number of different spectral parameters and can then be applied in a 'least-square-fit' technique to obtain a first estimate of the electron spectra.

4. The calibration data and the results of the model calculations will be used to construct a 3-dimensional response matrix. The identification as to particle type and energy centers around the pulse height information for the C2 and the S2 detector analyzed for a subset of the events registered in the countrate channels (on the C2 pulse height only in the case of the E12-type events). The signatures will be used to apply consistency checks and to identify different nuclei.

   For each bin of the C2-S2-matrix (penetration mode) a vector has to be constructed, of which each elements represents the probability for an event to be a specific particle having a definite energy (range) and which includes instrument characteristics as detection efficiency and geometrical factor as well. These vector elements have to be ordered in a certain way as to particle type and energy.

   For the E12 response matrix (absorption mode) this is a straight forward task, one has simply to order the calibration data (number of events) into suitable energy bins and assign probability values to each element as a function of the C2-response alone, on the basis of the number of events recorded in this bin at different energies. This response matrix is 1-dimensional since the signals in D1, C1 and D2 do not change with energy.

   For the E300 and the P4000 response matrices the task is more difficult since more vector elements have to be filled for each bin. The energy resolution required in this energy range, on the other hand, is low, so that only a small number of cells has to be evaluated.

A statistical analysis will have to be performed on the data of the instrument for each time period for which an electron spectrum has to be constructed to determine which method is best suited for the task.

6 References

Anderson, M. E., 'Neutron Flux, Spectrum, and Dose Equivalent Measurements for a 4500-W(th) PuO_2 General Purpose Heat Source', Mound Laboratories - Monsanto Research Corporation, **MLM-3248/UC-4**, National Technical Information Service, U.S. Department of Commerce, 1985

Bourdinand, M., J. B. Cheze, and J. C. Thevenin, 'Use of Silica Aerogel for Cerenkov Radiation Counter', Nucl. Instr. and Meth., **136**, 99-103, 1976

Brun, R., F. Bruyant, M. Maire, A. C. McPherson, and P. Zanarini, 'GEANT3 - Version 3.10.61 (Generation of Events and Tracks), CERN Data Handling Division, DD/EE/84-1, May 1986

Cantin, M., M. Casse, L. Koch, R. Jouan, P. Mestreau, D. Roussel, F. Bonnin, J. Moutel, and J. Teichner, 'Silica Aerogel used as Cerenkov Radiators', Nucl. Instr. and Meth., **118**, 177-182, 1974

Carlson, P. J., K. E. Johansson, J. Kesteman, J. Norrby, O. Pingot, S. Tavernier, F. Van Den Bogaert, and L. Van Ackeren, 'Increased Photoelectron Collection Efficiency of a Photomultiplier in an Aerogel Cerenkov Counter', Nucl. Instr. and Meth., **160**, 407-410, 1979

Decker R. B., S. M. Krimigis, and D. Venkatesan, 'Estimate of Cosmic-Ray Latitudinal Gradient in 1981-1982', Ap. J., **278**, L119, 1984

H. Fesefeldt, 'GHEISHA (Gamma-Hadroon-Electron Interaction and Shower Application), III. Physikalisches Institut RWTH Aachen, CERN Data Handling Division, PITHA 85/02)

Fulks G. J., 'Solar Modulation of Galactic Cosmic Ray Electrons, Protons, and Alphas', Journal of Geophysical Research, Vol. **80** , No. **13**, 1701-1714, 1975

Julliot C., 'Detection of Very High Energy Electrons, Results of Preliminary Calculations', Commissariat a L'Energie Atomique, Institut de Recherche Fondamentale, Division de la Physique, Servie d'Electronique Physique,

Centre d'Etudes Nucleaires de Saclay (internal report DPh/EP/Ap/80-7R/CJ), 1980

Julliot C., 'ISPM : Ensemble des donnees calculees par programme Monte Carlo Comparaison avec quelques resultats experimentaux', Commissariat a L'Energie Atomique, Institut de Recherche Fondamentale, Division de la Physique, Servie d'Electronique Physique, Centre d'Etudes Nucleaires de Saclay, (supplement to internal report DPh/EP/Ap/80-7R/CJ), 1985

Marsden, R. G., K.-P. Wenzel, and E. J. Smith, 'The Ulysses Mission', in: R. G. Marsden (ed.), The Sun and the Heliosphere in Three Dimensions, Proceedings of the XIXth ESLAB Symposium held at Les Diablerets, 477-490, D. Reidel Publishing Comp., 1986

McKibben, R. B., K. R. Pyle, and J. A. Simpson, 'The Solar Latitude and Radial Dependance of the Anomalous Cosmic-Ray Helium Component', Ap. J., 227, L147, 1979

Sierks, H., 'Auswertung der Eichmessungen des Kieler Elektronenteleskopes zur Erstellung von Energiespektren an Bord der Raumsonde ULYSSES (International Solar Polar Mission)', Experimentell-Physikalische Diplomarbeit, Institut für Reine und Angewandte Kernphysik, Christian - Albrechts - Universität Kiel, 1988

Simpson J. A.,J. D. Anglin, A. Balogh, M. Bercovitch, J. M. Bouman, E. E. Budzinski, J. R. Burrows, R. Carvell, J. Firth, M. Garcia-Munoz, J. Henrion, R. J. Hynds, B. Iwers, R. M. Jacquet, C. Julliot, H. Kunow, J. E. Lamport, G. A. Lentz, R. G. Marsden, R. B. McKibben, R. Müller-Mellin, M. A. Perkins, A. Raviart, E. Rode, T. R. Sanderson, R. J. Scheper, K. H. Stellmaschek, L. Treguer, M. Trischberger, A. J. Tuzzolino, and K.-P. Wenzel, 'The ISPM Cosmic-Ray and Solar-Particle Investigation', in: K.-P. Wenzel, R. G. Marsden, and B. Battrick (ed.), The International Solar Polar Mission - Its Scientific Investigations, ESA SP-1050, 155-183, Paris, 1983

Sullian, J. D., 'Geometrical Factor and Directional Response of Single and Multi-Element Particle Telescopes', Nuclear Instruments and Methods, 95, 5-11, 1971

Van Allen, J. A., 'Galactic Cosmic-Ray Intensity to a Heliocentric Distance of 18 AU', Ap. J., 238, 763-767, 1980

Webber W. R., A. C. Cummings, and E. C. Stone, 'Radial and Latitudinal Gradients of Anomalous Oxygen During 1977-1985', Proc. 19th Int'l Cosmic Ray Conf., La Jolla, 5, 172-175, 1985